Cellular prion protein in Alzheimer's disease: Molecular insights and behavior implications

Dissertation

for the award of the degree

"Doctor rerum naturalium (Dr. rer. nat.)"

of the Georg-August University Göttingen

within the doctoral Molecular Medicine

of the Georg-August University School of Science (GAUSS)

Submitted by

Ângela Patrícia da Silva Correia

from Chaves, Portugal

Göttingen, 2023

Thesis Committee

Prof. Dr. Inga Zerr

Department of Neurology, National Reference Center for TSE, University Medical Center Göttingen.

Prof. Dr. Tiago Outeiro

Department of Experimental Neurodegeneration, Outeiro Lab, University Medical Center Göttingen.

PD Dr. Roberto Goya-Maldonado

Department of Psychiatry and Psychotherapy, Laboratory of Systems Neuroscience and Imaging in Psychiatry (SNIPLab), University Medical Center Göttingen.

Members of the Examination Board

Prof. Dr. André Fischer

Dept. for Psychiatry and Psychotherapy, German Center for Neurodegenerative Diseases (DZNE), University Medical Center Göttingen.

Prof. Dr. Rubén Fernández-Busnadiego

Institute for Neuropathology, University Medical Center Göttingen

Prof. Dr. Oliver Wirths

Dept. for Psychiatry, Division of Molecular Psychiatry, University Medical Center Göttingen.

To my cherished daughter **Ariana**, *my loving mother* **Madalena**, *and my dear sister* **Susana**, *you are the pillars of my life, and I am endlessly grateful for the love and strength you bring into my world.*

Table of contents

List of figures

Table of tables

Abstract

Alzheimer's disease (AD) poses a substantial and increasing challenge, particularly due to our aging population, and its underlaying pathophysiology remains a topic of ongoing debate. Cellular prion protein (PrP^C) has surfaced as key player in Aβ induced toxicity in AD. Our research aimed to shed light on PrP^C's function in this context. I found a robust interaction between PrP^C and Aβ1-40, and Aβ1-42 via surface plasmon resonance (SPR). Further exploration in PrP^C overexpressing SH-SY5Y cells revealed its role as facilitator of Aβ internalization increasing the intracellular amount of oligomeric Aβ of more than 200%. *In vivo* studies using double transgenic 5xFADPrnp$^{+/+}$, 5xFADPrnp$^{+/-}$, and 5xFADPrnp$^{-/-}$ mice demonstrated a dose-dependent correlation between PrP^C levels and reduction of the lifespan of about 50%. A comprehensive battery of behavioral tests, encompassing cognitive and motor function assessments, revealed a significant impact of PrP^C levels on the onset and severity of cognitive and motoric impairments. However, PrP^C ablation did not fully restore Aβ provoked deficits and the observed deficits in behavior. The study also identified that PrP^C modulates the correlation between soluble Aβ levels and behavioral impairments. In the absence of PrP^C, the behavioral impairments were no longer directly linked to soluble Aβ levels, suggesting other conformations of Aβ, rather than its total levels, may play a crucial role in Aβ related toxicity. Moreover, using 3-D light sheet microscopy combined with QUINT analyses, our findings provided evidence that PrP^C may influence the overall burden of plaques but the distribution of Aβ in different brain regions. Additionally, a novel interaction between Aβ oligomers, PrP^C and Cav-1 was identified in cortical neurons, Cav-1 knockout cortical neurons reveled a significant reduction of intracellular Aβ oligomers in comparison with WT cortical neurons (reduction of ~ 25 to 50%), indicating Cav-1 role facilitating the internalization of Aβ-PrP^C complexes in neurons. Our research highlights PrP^C as promising candidate for future AD therapeutic strategies and introduces a novel mechanism perspective in AD pathogenesis.

I. Introduction

1. Dementia

Dementia is a broad term to describe a group of neurological disorders that cause a significant loss of cognitive functioning, including thinking, remembering, and reasoning, to a degree that significantly hinders a person's daily life and activities. In some cases, individuals with dementia may exhibit difficulties in emotional regulation, and their personalities may undergo notable changes. [1] Dementia affects a significant number of individuals worldwide, with approximately 50 million people currently living with this condition. The impact of dementia extends beyond individuals themselves, affecting their families and imposing a substantial economic burden.[2]

Dementia should be considered as an acquired syndrome resulting from a variety of potential causes, rather than being classified as specific disease itself. A conventional approach to conceptualize dementia involves categorizing it in two broad groups: neurodegenerative (non-reversible) and non-neurodegenerative (potentially reversible). [3] The most common causes of neurodegenerative dementia is Alzheimer's disease (AD), accounting approximately 60-80% of the cases, followed by vascular dementia, and Lewy body dementia (LBD).[4] These different diseases have relatively specific histological characterizations by varying degrees of neuronal loss, gliosis, and usually with abnormally misfolded protein depositions.[5]

2. Alzheimer's disease

Alöis Alzheimer firstly described AD in 1907 as an unusual illness of the cerebral cortex when he received the brain specimens of the patient that the clinical observations were so distinct that it could not be classified as one of the recognized illnesses at that time.[6]

The clinical features of AD encompass a range of cognitive impairments and behavioral changes that progressively worsen over time. One of the earliest and prominent cognitive signs of AD is the impairment of short-term memory (e.g., difficulties in remembering new information, conversations). While the memory deficit

is the traditional and common cognitive symptom, it is important to note that individuals with AD may present a varying pattern of cognitive impairment, such as, language problems (e.g., difficulties finding words), impaired reasoning and judgement (e.g., struggle with problem-solving tasks), decline of attention and concentration (e.g., difficulties staying focused on tasks). AD patients may present behavioral and psychological symptoms as personality changes (e.g., mood swings, depression, and exhibition of socially inappropriate behavior), disorientation and confusion (e.g., getting lost in familiar surroundings), agitation and aggression, and sleep disturbances. [7,8]

While aging is the primary risk factor for developing AD, it is important to note that AD is not a typical or inherent aspect of the aging process. Since AD is strongly related with age, it is expected that the burden of the disease will rise with the aging population and increased life expectancy, becoming acknowledge by the Word Health Organization as a critical global public health priority.[9,10] Additionally, other risk factors for the development of AD include among others, hypertension, diabetes, smoking, excessive alcohol intake, low level of education, air pollution, and brain damage.[11] Furthermore, family history and genetics are also important risk factors. [8]

Currently, there is no effective treatment to reverse or prevent the development of the disease.

2.1. Pathology of AD

The exact cause of AD is unknown, however, macroscopically, in the AD brain significant cortical atrophy is commonly observed, particularly in multimodal association cortices and limbic lobe structures. Frontal and temporal cortices frequently exhibit enlarged sulcal spaces accompanied by gyri atrophy. AD is commonly associated with medial temporal atrophy, which specifically affects the amygdala and hippocampus. This atrophy is often accompanied by enlargement of the temporal horns. However, these alterations alone are not specific to AD.[12]

Microscopically, the formation of two main protein aggregates in the extracellular (amyloid plaques) and intracellular (tau protein) compartments are AD hallmarks.[13] Amyloid plaques consist of aggregates of 4kDa 39-43 amino acid peptide called amyloid beta (Aβ) derived from the cleavage of the Amyloid Precursor Protein (APP).[14]

The intracellular aggregates consist in microtubule-associated protein tau leading to the neurofibrillary tangles (NTF) formation. Research has shown the formation of NFTs and neuronal cell loss typically occurs much later in the progression of AD compared to the deposition of extracellular Aβ.[15]

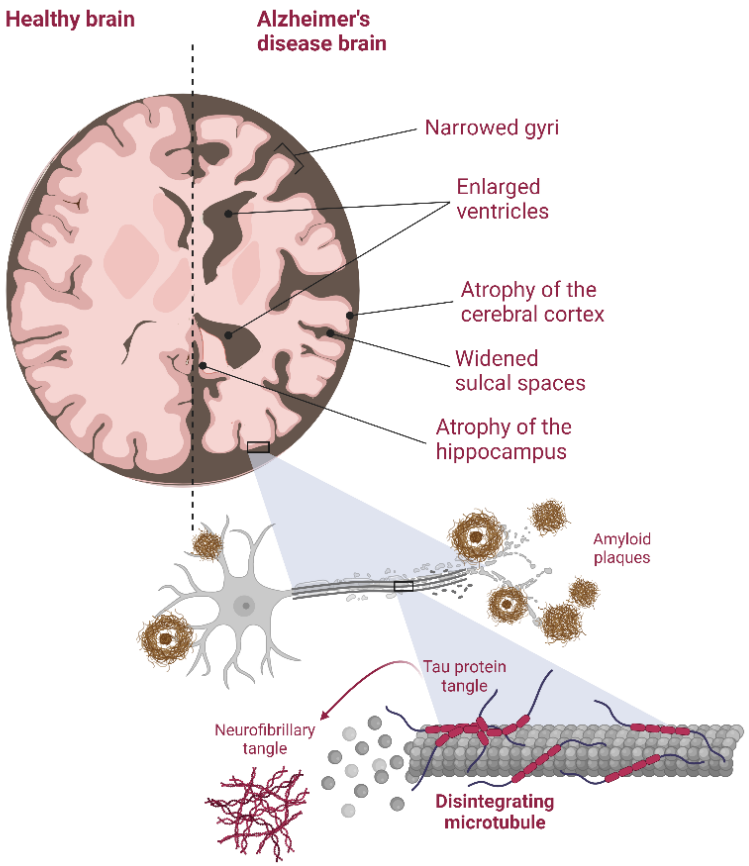

Figure 1 - Alzheimer's pathology. This image illustrates the dual perspective of Alzheimer's disease pathology, both macroscopic and microscopic. At macroscopic level, we see the structural changes, such a narrowed gyri, enlarged ventricles and widened sulcal spaces. Zooming in to the microscopic level, the neurons appear surrounded by clusters of Aβ deposits. Within the neuron, the hyperphosphorylated Tau leads to the disintegration of the microtubules and the formation of the neurofibrillary tangles. *Figure created with BioRender.com.*

2.2. Types of Alzheimer's disease

2.2.1. Sporadic Alzheimer's disease

The majority of AD patients, over 90%, are classified as sporadic cases, and typically have late-onset of the disease, occurring at the age of 65 or older, known as

late-onset Alzheimer's disease (LOAD). Approximately 40% of sporadic AD are associated with the epsilon 4 allele of the Apolipoprotein E (APOE) gene, which is considered a genetic risk factor in sporadic AD. [16,17] The APOE gene has three alleles (E2, E3, E4) that code for three distinct ApoE isoforms, which differ by only one single amino acid. APOE3 gene is the most prevalent in the Caucasian population. Individuals who carry a single copy of the APOE4 allele have a three to four-fold higher risk of developing AD compared with non-carriers. The risk for developing AD is further increased up to fifteen-fold for individuals who are homozygous for the E4 allele. [17] The remaining account of sporadic AD cases is believed to be a multifactorial combination of factors, including aging, genetic predisposition, and exposure to environmental agents such head trauma, toxins, and viruses. However, it is important to note that no specific environmental agents have been definitely proven to directly cause the pathogenesis of AD.[18]

2.2.2. Familiar Alzheimer's disease

Familiar AD is a rare form, representing 5-10% of the cases, and usually present an early disease onset. It is attributed to autosomal dominant mutations in three genes. These genes include APP gene located on chromosome 21q21.3, presenilin 1 (PSEN1) gene located on chromosome 14q24.2, and presenilin 2 (PSEN2) gene located on the chromosome 1q42.13. More than 230 mutations have been identified on these three genes as causative factor in familiar AD.[19–23]

These mutations are responsible for an alteration of the APP expression and processing leading to an increased production of Aβ peptides, including the more toxic Aβ1-40 and Aβ1-42 peptides. The excessive production of Aβ can result in accumulation and formation of amyloid plaques. Consequently, this sequence of events initiates a series of pathological processes.

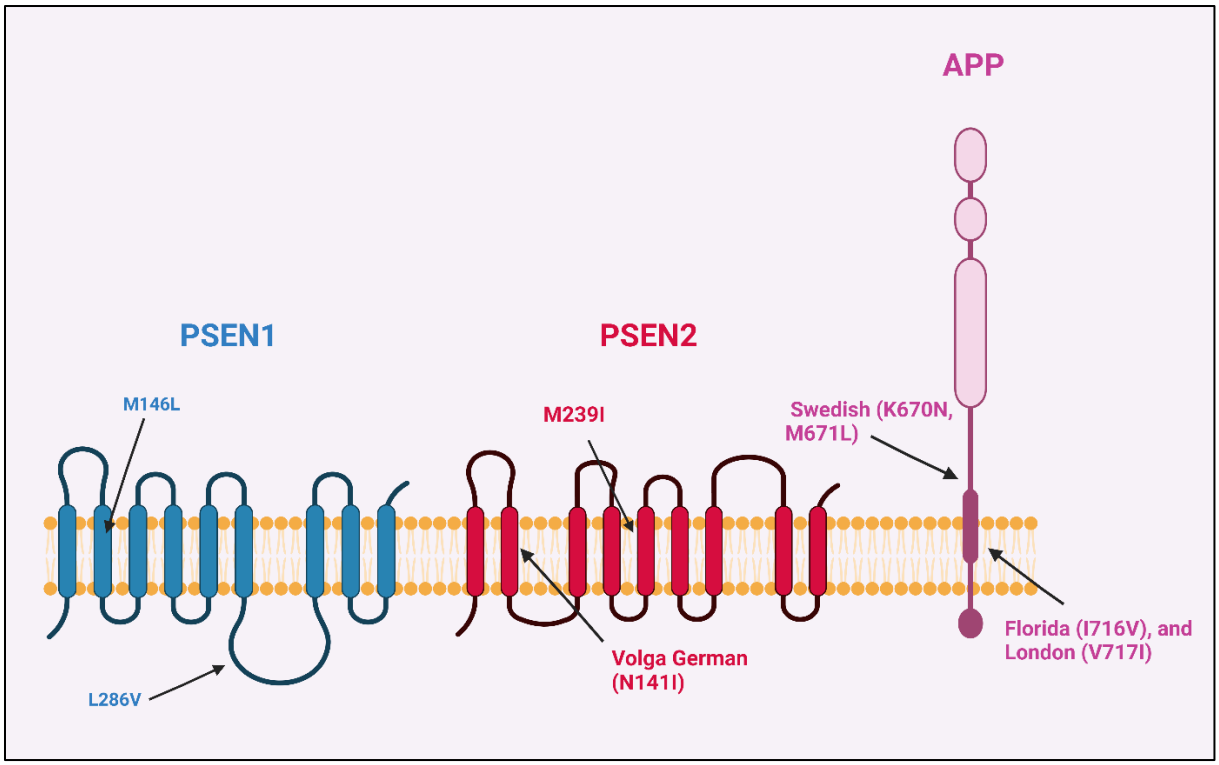

Figure 2 – Familiar Alzheimer's mutations in PSEN1, PSEN2 and APP genes. Representation of the mutated gene loci within PSEN1, PSEN2 and APP proteins known as causative of familiar Alzheimer's disease. Figure created with BioRender.com.

2.3. Amyloid cascade hypothesis

According to the amyloid cascade hypothesis, AD is caused by the pathological accumulation of Aβ plaques in different regions of the brain, leading to neuritic injury, the formation of neurofibrillary tangles through the aggregation of tau protein that ultimately leads to neuronal dysfunction and cell death.[24,25]

Numerous studies have provided substantial evidence the notion that the accumulation of Aβ peptides, particularly the Aβ1–42 isoform, which is hydrophobic in nature and aggregates faster than Aβ1–40, plays a pivotal role in pathogenesis of AD. These studies have highlighted the association between Aβ aggregation and the formation of amyloid plaques with cytokine release, multi-protein inflammatory response, microglial activation, and reactive astrocytosis. [26–29] Furthermore, the accumulation of Aβ oligomers not only triggers abnormal phosphorylation of tau protein, leading to NFT formation, but also neuroinflammation. APOE 4, the most significant genetic risk for sporadic AD, hinders Aβ clearance and facilitates its build up in the brain. [30–33] However, it is important to note that the extent of neuronal loss

and cognitive dysfunction in AD does not always align closely with the accumulation of Aβ. Additionally, demonstrating direct neurotoxicity of Aβ peptides has been difficult in many animal models. Moreover, many individuals that present robust plaque pathology show no signs of dementia.[15,34,35]

3. Proteins in Alzheimer's disease

3.1. Amyloid Precursor Protein (APP)

The amyloid precursor protein (APP) is a type I transmembrane glycoprotein and it is expressed in various mammalian cells. [36] While the precise physiological function of APP and its homologues is not fully understood, research suggest their involvement in several cellular processes. These processes include cell adhesion, neuronal protein trafficking along the axon, synaptogenesis, neurite outgrowth, and calcium metabolism.[37]

The processing of APP relies on activity of secretase enzymes, known as α-, β-, and γ-secretases, which produce different products that can be released into extracellular space or remain inside or associated with the cell. The process of APP can be broadly classified in two pathways: the non-amyloidogenic pathway and the amyloidogenic pathway.[38–40] The determination of whether APP follows the amyloidogenic or non-amyloidogenic pathway primarily depends on the co-localization of the protein and the respective secretases. [41,42]

In the non-amyloidogenic pathway, APP is cleaved by α-secretase, resulting in the release of soluble extracellular APP fragment (sAPPα), and a carboxyl terminal fragment containing 83 amino acids (C83), which is split by γ-secretase leading to the formation of a soluble extracellular p3 (3 kDa) and the APP intracellular domain (AICD), precluding the formation of Aβ toxic fragments. [42,43]

During the amyloidogenic APP processing, APP is cleaved by β-secretase (BACE1, β-site APP-cleaving enzyme 1), producing a soluble fragment called (sAPPβ), which is released into the extracellular space. The remaining fragment embedded in the cellular membrane is known as C99. Within the membrane, C99 is subsequently subjected to cleavage by the γ-secretase enzymatic complex. This process results in

the release of two distinct components: a cytoplasmatic polypeptide termed AICD (APP intracellular domain) on the luminal side of the membrane, and Aβ peptides on the opposite side of the membrane. The precise cleavage site of APP is variable, leading to a generation of Aβ peptides with varying lengths. These Aβ peptides typically range from 38 to 43 amino acids in length. Among these, Aβ1-40 is the most abundant species found in the healthy brain.[15,44–47]

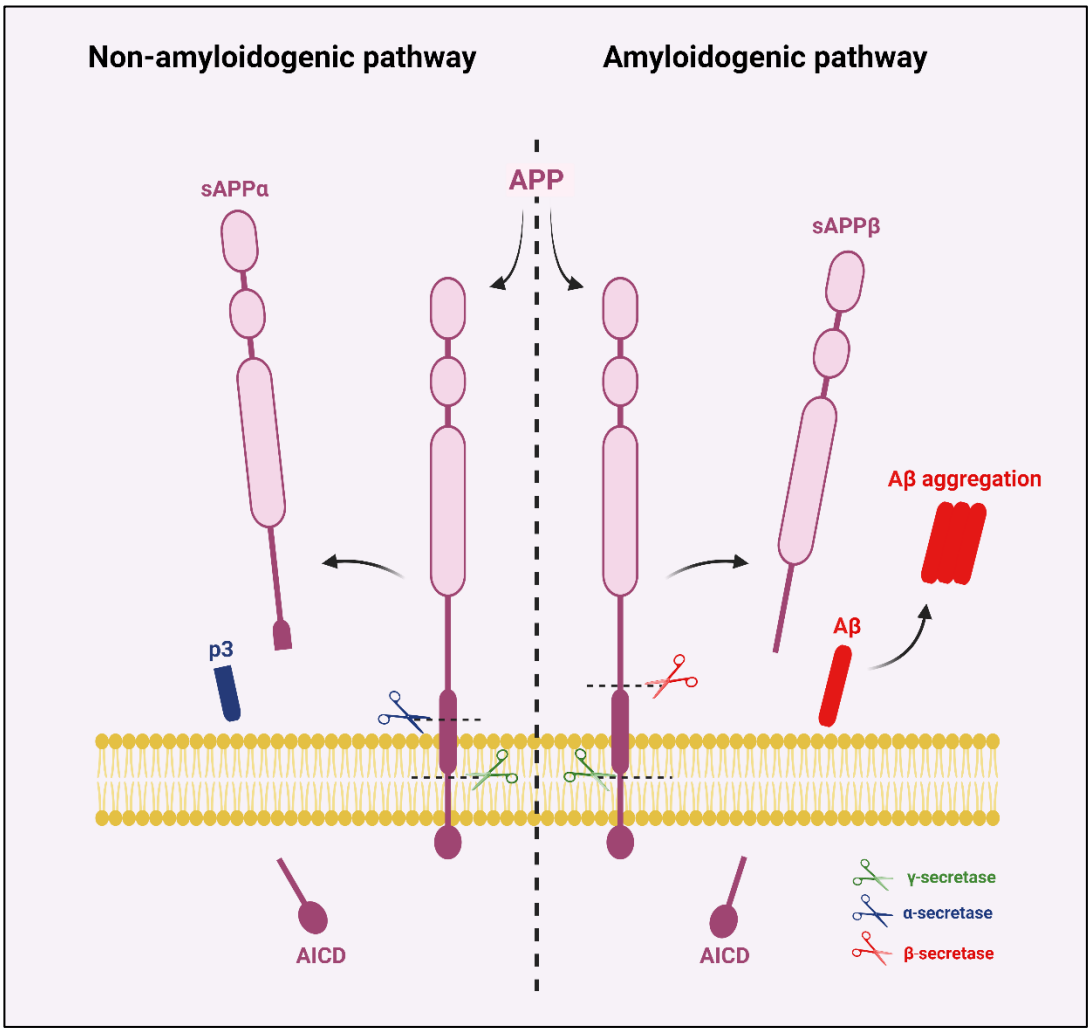

Figure 3 - APP processing pathways. The image shows the processing of APP in the non-amyloidogenic pathway (on the left), the physiologic favorable route, where APP is cleaved by α-secretase and γ-secretase generating non-pathologic fragments. The amyloidogenic pathway, depicted on the right side, shows the APP processed by β-secretase and γ-secretase, yielding Aβ fragments, these peptides have a propensity to aggregate. Figure created with BioRender.com.

3.2. Aβ monomers

The monomeric form of the Aβ peptide was widely considered as a functionless protein resulting from the breakdown of APP. In spite of that, various studies indicate that Aβ monomers have a non-pathological aspect and potential physiological function. [48] In vitro experiments have shown that inhibiting either α-secretase or β-secretase adversely affects the viability of cortical neurons. However, the addiction of picomolar concentrations of Aβ 1-40 and Aβ 1-42 monomers can rescue the viability of these neurons. [49,50] The monomeric Aβ was found to be protective by activating insulin/insulin like growth factor (IGF-1) receptor, that initiates a cascade of intracellular events that promote cell growth, survival and metabolic regulation. [51] Moreover, patients that suffered acute brain injury showed a strong correlation between the Aβ levels in the cerebral interstitial fluid and the patient neurological status. The Aβ concentrations increased as the neurological status improved. On the other hand, the Aβ concentrations fell when the neurological status declined. These observations suggested a potential role of Aβ in promoting neuroprotection. [52] However, the neuroprotective activity of Aβ is restricted to monomeric at low concentrations. These findings suggest that under normal physiological conditions, monomeric Aβ may play a beneficial role in neuronal maintenance and homeostasis.[50]

3.3. Aβ oligomers

Aβ monomers can assemble into various higher-order structures, encompassing a spectrum of sizes and complexities. [53] Aβ oligomers refer to any form of Aβ species that undergoes a structural transformation, leading to the formation of dimers or multimers. In healthy individuals, newly synthetized monomers of Aβ undergo a normal physiological processing. While the Aβ oligomers can interact with various proteins and receptors.[54,55] Previously, Aβ oligomers were considered as transitional forms leading to the formation of amyloid plaques, which were believed to be the pathogenic form of Aβ. However, the current understanding has shifted, and Aβ oligomers are now widely recognized as the most toxic and pathogenic form of Aβ. [55]

Aβ oligomers have been found in both extracellular and intracellular compartments within the brain tissue [56] and they can be classified into at least two categories: Type

1 and type 2, based on their relationship with amyloid fibrils. Type 1 Aβ oligomers (larger size, (~12 mers and above) appear to be unrelated with amyloid fibrils “off-pathway”, while type 2 Aβ oligomers (primarily dimers or trimers) exhibit a temporal, special, and structural association with amyloid fibrils “on-pathway”. [56,57]

Both type 1 and type 2 oligomers have an impact on neuronal signalling pathways, albeit likely through different sets of molecules. They contribute to varying levels of synaptic dysfunction, synaptic loss, and neuron death. Type 1 oligomers, even in small quantities, lead to a large-scale neurological dysfunction due to their disperse nature. In contrast, type 2 oligomers do not cause a broad neurological dysfunction, even in relatively large amounts, as they remain isolated or sequestered. [58]

3.4. Aβ aggregation and fibrils

Fibrils represent the predominant form of Aβ within the plaques. Amyloid fibrils are characterized by their repetitive, β-sheet-rich structures. These fibrils exhibit a high thermodynamic and kinetic stability, which arises from the association of multiple polypeptide molecules adopting a cross-β structure. [59] The specific mechanism and pathways leading to Aβ aggregation and fibril formation are still the subject of active research. However, several hypotheses have been proposed to explain the process of Aβ aggregation and formation of fibrillar assemblies. The nucleation-dependent polymerization model has traditionally explained the mechanism of Aβ assembly formation. This hypothesis suggests that the aggregation process begins with the formation of small aggregates, which act as template for further peptide assembly. [60–62] Some findings support the on/off-pathway hypothesis, indicating that some Aβ oligomers (type 1) may not directly serve as intermediates in the formation of fibrils. [57]

An alternative model is the fibril-seeded model. This hypothesis proposes that the presence of pre-existing fibrillar structures, referred as seeds, can trigger the aggregation. The presence of seeds act as catalyst for the aggregation, driving the formation and growth of fibrillar structures. [63]

Amyloid plaque buffering refers to the hypothesis where the amyloid plaques, composed of aggregated Aβ, function as storage or containment site for soluble Aβ species. The plaques act as a form of “buffer” by sequestering or binding soluble Aβ, thereby reducing its availability and potential toxicity. Over time, the storage of amyloid

plaque reaches saturation or lose its capacity, leading to the release and diffusion of toxic Aβ oligomers. [64]

4. Cellular receptors associated with Aβ

To fully comprehend the pathogenesis of AD, it is essential to understand the interaction between Aβ and neurons, as well as other cell types in the brain. The complexity of understanding the ligand Aβ lies in its existence in various forms, ranging from monomers, dimers, trimers, and oligomers to protofibrils and fibrils. [65]

Numerous studies provided evidence suggesting that specific receptors can exert a protective role, mitigating the harmful effects associated with the pathological process of AD. Receptors such as α7 nicotinic acetylcholine receptor (α7nAChR), low-density lipoprotein receptor-related protein 1 (LRP1), the insulin receptor, and the receptor for the neuropeptide Y (NPY) are involved in various cellular processes, including Aβ clearance and degradation, reducing the Aβ levels in the brain (reviewed in [65]).

Aβ oligomers have emerged as the most neurotoxic species, initiating a multitude of processes that underlie AD. Extensive investigation is being conducted to explore potential mechanisms by which Aβ oligomers interact with their targets, including the abnormal activation of signalling pathways. [66]

Purportedly, Aβ oligomers have the potential to directly damage neuronal membranes by forming pores. One specific effect is an increase in intracellular calcium (Ca2+) levels, which can have detrimental consequences for neuronal function and viability. [67]

Additionally, several cell-surface proteins have been identified as potential receptors for Aβ mediating their synaptotoxicity effect. Receptors, such as receptor for advanced glycation end products (RAGE), *N*-methyl-d-aspartate (NMDA), α-amino-3-hydroxy-5-methyl-4-isoxazolepropionic acid receptor (AMPAR), APO4 and cellular prion protein (PrP^C) are key-players in neurotoxicity through mechanisms of excitotoxicity, oxidative stress, inflammation, and impaired signalling [65,66].

To date, no single candidate receptor protein has been identified as being fully responsible for all aspects of Aβ toxicity. Many receptors may contribute to mediate

the Aβ activity; however, evidences indicate that PrP^C plays a relevant role in various systems in AD pathogenesis. [68]

4.1. PrP^C and Aβ

Evidences support the notion that the interaction between Aβ oligomers and PrP^C is crucial for a multitude of intracellular processes that mediate Aβ-induced synaptotoxic effects. Numerous studies have demonstrated that disrupting Aβ oligomers – PrP^C interaction can mitigate or attenuate downstream signalling events that contribute to synaptic dysfunction and neuronal damage.[68–70] Multiple studies provide evidence suggesting that specific regions of PrP^C, including N-terminal residues 23-27 and the 95-110 region, contain critical amino acid binding sequences for Aβ oligomer induced synaptic impairment and neuronal death[71]. [71] It has been reported that Aβ oligomers activate Fyn in a PrP^C dependent manner. The activated Fyn is known to hyperphosphorylate tau, leading to the detachment of tau from the microtubules and the formation of insoluble aggregates known as NFT.[72] A further evidence of the association of between PrP^C with amyloid beta has been demonstrated by their co-localization with amyloid plaques. [73]

It is important to note that the role of PrP^C as an Aβ oligomers receptor remains somewhat controversial, and there are reports that do not support this hypothesis. [74–76]

5. Cellular prion protein (PrP^C)

PrP^C is a protein encoded by *PRNP* gene, which can be located in the chromosome 20 in humans. [77] It is a membrane glycoprotein that is anchored to the lipid bilayer through a C-terminal glycosyl-phosphatidylinositol (GPI) anchor.[78] The three-dimensional structure of PrP^C includes a disordered N-terminal domain and a C-terminal globular region composed of three α-helices and two short β-strands. [79,80] The mature PrP^C consists of 210 amino acid residues, and its molecular weight can vary between 27-36 kDa due to different levels of glycosylation (unglycosylated, monoglycosylated, and diglycosylated). [81] PrP^C has been shown to be expressed at

high levels in the CNS, in particular in synapsis and spinal cord, and moderately expressed spleen, liver, heart and lungs. [82]

The PrP^{C} precise function on the cell surface remains uncertain. It is believed to play a crucial role in the nervous system, behavioural studies showed specific age-dependent differences between WT mice and $Prnp^{-/-}$ mice, which indicates an important function in the nervous system. [83] Moreover, $Prnp^{-/-}$ mice presented an altered circadian rhythm, and abnormal synaptic structure in the hippocampus. [84,85] The overexpression of PrP^{C} in seems to be protective against apoptotic stimuli in cell lines and primary neurons [86,87], human breast cancer [88], and oxidative stress. [89] Multiple studies suggest that PrP^{C} may be associated with multi-molecular complexes, which mediate different functions in various cellular compartments. [87]

Conformational changes of PrP^{C} into the pathogenic misfolded PrP^{Sc} conformer is responsible to cause a number of neurodegenerative diseases known as prion diseases.

II. Aims

The aims of this study are to conduct comprehensive investigation into the role of PrP^C in AD pathogenesis, addressing the ongoing debate surrounding its function. Given the divergent research outcomes in this topic, I employed a multifaceted approach to gain a deeper understanding of PrP^C's involvement in AD.

To achieve these goals, I conducted *in vitro* and *in vivo* investigations utilizing a diverse set of methodologies and models, contributing to a holistic understanding of PrP^C involvement in this complex neurodegenerative disorder:

1. Investigate PrP^C interaction with Aβ1-40 and Aβ1-42: Explore and characterize the binding affinity via surface plasmon resonance (SPR), shedding light on the molecular mechanism in AD.
2. Examine PrP^C impact on Aβ uptake: How levels of PrP^C influence the internalization of Aβ oligomers.
3. Assess PrP^C's effect on AD progression: generation of double transgenic 5xFADPrnp$^{-/+}$ and 5xFADPrnp$^{-/-}$ mice lines to study the effect of different PrP^C levels on lifespan and behavior.
4. Elucidating PrP^C's Influence on Aβ Plaque Load and Distribution via 3D imaging: Investigating the influence of PrP^C levels on the expression and distribution of Aβ plaques in different brain regions using light sheet microscopy and QUINT workflow analyses.
5. Investigation of further relevant proteins which are involved in the Aβ internalization via PrP^C in AD context.

III. Materials

This section provides the detailed lists of equipment, software and substances used in this project.

1. Equipment

Table 1 - Instruments used in this project.

Appliance and Model	Manufacturer
Balance LE6202S	Sartorius/ Goettingen, Germany
Bio-safety Cabinet Hera safe KS	Heraeus/ Osterode, Germany
Centrifuge 5415C	Eppendorf/Hamburg, Germany
Centrifuge Rotina 35R	Hettich/ Tuttlingen, Germany
ChemiDoc Imaging System XRS+	BioRad/ Munich, Germany
Electro blotting apparatus Mini Trans-Blot®	Bio-Rad /Munich, Germany
Electrophoresis apparatus Mini-Protean® III	Bio-Rad /Munich, Germany
Ice machine	Ziegra /Isernhagen, Germany
Incubator HERA Cell 150	Heraeus/ Osterode, Germany
Light microscope Axiovert 25	Zeiss / Göttingen, Germany
Lightsheet UltraMicroscope II	LaVision BioTec / Bielefeld, Germany
pH meter pH 526	WTW/ Weilheim, Germany
Shakers CERTOMAT R	Sartorius/ Goettingen, Germany
Spectrophotometers EL808	Bioteck instruments/Winooski-vermont, USA
Sterile filter pipette tips	Sarstedt / Sarstedt, Germany
Thermomixer 5436	Eppendorf/ Hamburg, Germany
Vortexer Genie 2™	Bender and Hobein /Zurich, Switzerland

2. Software

Table 2 - List of software.

Program	Use	References
Graphpad Prism 10	Statistical analysis	GraphPad Software / Inc. California, USA
Ilastik	Machine learning and pixel classification	European Molecular Biology Laboratory / Heidelberg, Germany
ImageJ 1.43u	Densitomatric analysis	National institutes of Health / USA
Imspector	*Image Acquisition*	Abberior Instruments / Göttingen, Germany
LabImage 2.7.1	Densitomatric analysis	Kapelan GmbH / Halle, Germany
MeshView	3D display	Neural Systems Laboratory, Institute of Basic Medical Sciences, Oslo, Norway
Nutil	Spatial analysis	Neural Systems Laboratory, Institute of Basic Medical Sciences, Oslo, Norway
QuickNII	Spatial registration	Neural Systems Laboratory, Institute of Basic Medical Sciences, Oslo, Norway
VisuAlign	Nonlinear refinements	Neural Systems Laboratory, Institute of Basic Medical Sciences, Oslo, Norway
Zeiss LSM 4.2.0.121	Immunofluorescence	MicroImaging GmbH, Göttingen, Germany

3. Consumables and reagents

3.1. General consumables

Table 3 - List of general consumables.

Product	Manufacturer
X-well cell culture chambers	Sarstedt / Sarstedt, Germany
6-Multiwell-plates	Sarstedt / Sarstedt, Germany
Cell culture flask	Sarstedt / Sarstedt, Germany
Cell scraper	Sarstedt / Sarstedt, Germany
Falcon tubes 15 and 50ml	Sarstedt / Sarstedt, Germany
PVDF-Membrane	GE H. Life Science / Solingen, Germany
Safe-Lock tubes 0.2, 0.5, 1.5 and 2ml	Sarstedt / Sarstedt, Germany
Serological pipettes 2, 5, 10, 25ml	Sarstedt / Sarstedt, Germany

3.2. Chemicals and Reagents

Table 4 - Chemicals and reagents.

Product	Manufacturer
100bp Standard DNA marker	New England Biolabs / Frankfurt am Main, Germany
1,1,1,3,3,3-Hexafluoro-2-Propanol	Sigma-Aldrich / Steinheim, Germany
Acrylamid	Roth / Karlsruhe, Germany
Ammoniumperoxidsulfat (APS)	BioRad / Munich, Germany
B27	Thermo-Fischer / Schwerte, Germany
Bradford’s reagent	BioRad / Munich, Germany
BSA (1000 µg/ml)	Sigma-Aldrich / Steinheim, Germany
CaCl2	Sigma-Aldrich / Steinheim, Germany
Cysteine	Sigma-Aldrich / Steinheim, Germany
DBE dibasic ester	Sigma-Aldrich / Steinheim, Germany
Dichloromethane	Sigma-Aldrich / Steinheim, Germany
Dimethyl sulfoxide	Sigma-Aldrich / Steinheim, Germany

DNase I (1mg/ml)	Roche / Mannheim, Germany
Donkey serum	Merck / Darmstadt, Germany
Dulbecco's Modified Eagle Medium DMEM	Thermo-Fischer / Schwerte, Germany
Ethylenediaminetetraacetic acid	Sigma-Aldrich / Steinheim, Germany
Fetal Bovine Serum	Thermo-Fischer / Schwerte, Germany
Glimepiride	Sigma-Aldrich / Steinheim, Germany
Glutamax (100x)	Thermo-Fischer / Schwerte, Germany
Glutaraldehyde	Science Services / Munich, Germany
Glycine	Thermo-Fischer / Schwerte, Germany
HBSS medium	Gibco/Thermo-Fischer / Schwerte, Germany
Heparin sodium salt	Thermo-Fischer / Schwerte, Germany
HEPES	Thermo-Fischer / Schwerte, Germany
Human beta Amyloid (1-40) Recombinant	Thermo-Fischer / Schwerte, Germany
Human beta Amyloid (1-42) Recombinant	Thermo-Fischer / Schwerte, Germany
Human beta-Amyloid Peptide (1-40)	Abcam / Cambridge, UK
Human beta-Amyloid Peptide (1-42)	Abcam / Cambridge, UK
Hydrogen peroxide 30%	Merck / Darmstadt, Germany
Laminin	Sigma-Aldrich / Steinheim, Germany
Milk powder	Roth / Karlsruhe, Germany
Neurobasal	Thermo-Fischer / Schwerte, Germany
Papain	Roth / Karlsruhe, Germany
Paraformaldehyde	Roth / Karlsruhe, Germany
PBS Dulbecco	Merck / Darmstadt, Germany
Penicillin-Streptomycin	Thermo-Fischer / Schwerte, Germany
Phosphatase inhibitor	Roche / Mannheim, Germany
Poly-L-ornithine hydrobromide	Sigma-Aldrich / Steinheim, Germany
Precision Plus Protein standards	BioRad / Munich, Germany
Precision Plus Protein Standards (dual color)	Bio-Rad / München, Germany
Primocin	Invivogen / San Diego, USA

Protease inhibitor	Roche / Mannheim, Germany
Pyruvic Acid	Thermo-Fischer / Schwerte, Germany
SDS	Roth / Karlsruhe, Germany
TEMED	Roth / Karlsruhe, Germany
Triton x-100	Sigma-Aldrich / Steinheim, Germany
Trypsin/EDTA	Biochrom / Berlin, Germany
Tween	Roth / Karlsruhe, Germany
Uranyl acetate	Merck / Darmstadt, Germany

3.3. Antibodies

Table 5 – List of antibodies.

Antibody	Dilution	Supplier
Alexa Flour 488, Donkey Anti-Mouse	1:1000	Abcam, Cambridge, UK
Alexa Flour 555, Donkey Anti-Rabbit	1:1000	Abcam, Cambridge, UK
Alexa Flour 750, Donkey Anti-Goat	1:1000	Abcam, Cambridge, UK
Anti-Amyloid Oligomers antibody	1:1000	Abcam, Cambridge, UK
Anti-Amyloid βA4, clone 1E8	1:1000	Merck / Darmstadt, Germany
Anti-Caveolin 1	1:1000	Abcam, Cambridge, UK
Anti-Fyn	1:1000	Abcam, Cambridge, UK
Anti--Fyn	1:1000	Abcam, Cambridge, UK
Anti-GAPDH	1:1000	Abcam, Cambridge, UK
Anti-SAF-32	1:1000	Abcam, Cambridge, UK
Anti-β-actin-antibody	1:1000	Abcam, Cambridge, UK
AP-conjugated anti-mouse IgG	1:10000	Santa Cruz Biotechnology, Santa Cruz, USA
AP-conjugated anti-rabbit IgG	1:10000	Santa Cruz Biotechnology, Santa Cruz, USA
APP	1:1000	Abcam, Cambridge, UK

3.4. Kits

Table 6 – Kits.

Name	Company
DNeasy Blood & Tissue kit	Qiagen / Hilden, Germany
Elisa essay Aβ1-40	IBL / International
Elisa essay Aβ1-42	IBL / International
Elisa Prion Protein (PRNP)	Cloud-clone corp. / Katy, USA
Pierce™ BCA Protein Assay Kits	Thermo-Fischer / Schwerte, Germany

3.5. Oligonucleotides

Table 7 – Oligonucleotides.

Primer	Sequence in 5' – 3' orientation	Supplier
Mu_PrP_WT_for ($Prnp^{+/+}$ allele)	ATGGCGAACCTTGGCTACTGGGCTG	TIB Molbiol / Berlin, Germany
Mu_PrP_WT_Rev ($Prnp^{+/+}$ allele)	CATCCCACGATCAGGAAGATG	TIB Molbiol / Berlin, Germany
oIMR3611_For 5xFAD	CGGGGGTCTAGTTCTGCA	TIB Molbiol / Berlin, Germany
oIMR3610_Rev 5xFAD	AGGACTGACCACTCGACCAG	TIB Molbiol / Berlin, Germany
P3 ($Prnp^{-/-}$ allele)	ATTCGCAGCGCATCGCCTTCTATCGCC	TIB Molbiol / Berlin, Germany
P4 ($Prnp^{-/-}$ allele)	CATCCCACGATCAGGAAGATG	TIB Molbiol / Berlin, Germany

4. Buffers composition

4.1. General buffers

Table 8 - General buffers composition.

Transfer solution (10x)	**Transfer buffer**
58,2 g Tris	100 ml transfer solution (10x)
29,3 g Glycine	200 ml Methanol
3,75 g SDS	700 ml of water
add 1 L on VE-H2O	
Upper gel buffer	**Bottom gel buffer**
0.5 M Tris/HCl	80.38 g Tris-HCl
0.4 % SDS	119.93 g Tris
pH 6.8	4 g SDS
	add 1 L on VE-H2O
	pH = 8.8
TBST (10x)	**Blocking solution**
200 mM Tris	5 % milk powder
1.5 M NaCl	TBST
1% Tween	
Running buffer	**Extraction buffer**
0.1 SDS	50 mM Tris-HCL (pH 7.5)
192 mM Glycine	150 mM NaCl
25 mM Tris/HCL pH 8.3	2 mM EDTA
	1 % Triton
	Protease and Phosphatase Inhibitor

Enhanced chemiluminescence solution (ECL)	
Solution 1 (10 ml):	**Solution 2 (10 ml):**
2.5 mM Luminol	18% H_2O_2
0.4 mM p-coumaric acid	0.1 M Tris/HCl pH 8.5
0.1 M Tris/HCl pH 8.5	

Immunofluorescence buffers	
Permeabilization Solution	**Blocking Solution**
PBS	PBST
0.2% Triton X-100	2% BSA

4.2. PCR master mix

Table 8 - Master mix composition.

Reagent	Final concentration
10X Standard Taq Reaction Buffer	1x
10 mM dNTPs	200 µM
10 µM Forward Primer	0.2 µM
10 µM Reverse Primer	0.2 µM
Template DNA	<1,000 ng
Taq DNA Polymerase	1.25 units/50 µl PCR
Nuclease-free water	

4.3. Clearing protocol buffers

Table 9 - Clearing iDISCO+ protocol buffers composition.

PTwH (1L)	**PTx.2 (1L)**
100ml PBS 10x	100ml PBS 10x
2ml Tween-20	2ml tritonX-100
1ml of 10mg/ml Heparin stock solution	
Permeabilization Solution (500ml)	**Blocking Solution**
400ml PTx.2	42ml PTx.2
11,5g of Glycine	3ml of Donkey serum

4.4. Cell culture buffers

Table 10 - Cell Culture buffers composition.

HBSS buffer	**Enzyme Solution**
HBSS medium	HBSS buffer
1 mM HEPES	25 units/mL Papain
0.2% Primocin	10 µg/mL DNAse
1 mM pyruvic acid	1.5 mM Cysteine
15% ddH2O	0.75 mM EDTA 7.5 pH
	1.5 mM CaCl2
Plating Medium	**Neuronal buffer**
Neurobasal	Neurobasal
5% FBS	1% Glutamax
1% Glutamax (100x)	2% B27

2% B27

0.2% Primocin

0.2% Primocin

SH SY5Y-Medium

Dulbecco’s Modified Eagle Medium

10 % fetal bovine serum (FBS)

1 % Glutamax

1.5 mM Cysteine

0.75 mM EDTA 7.5 pH

IV. Methods

1. Extraction of genomic DNA

The was extracted from tail biopsys using the DNeasy Blood & Tissue kit following the manufacturer's instructions. Briefly, tail samples were lysed overnight at 56ºC, and the lysate was processed using the DNeasy Mini spin column method. After centrifugation and washing steps, the DNA was eluted from the column. The elution step was repeated twice for thorough DNA recovery.

2. Genotyping of mice

For genotyping, the DNA extracted from the tail biopsy was combined with the master mix (see material). For the PCR, the following programs were used:

Table 11 - PCR programs.

Mutation	**5xFAD**		**Prnp+/+**		**Prnp$^{-/-}$**	
	Temperature	**Time**	**Temperature**	**Time**	**Temperature**	**Time**
Initial denaturation	95°C	3 min.	95°C	3 min.	95°C	1 min.
30 cycles	95°C	30 sec.	95°C	30 sec.	95°C	30 sec.
	56°C		56°C		62°C	2 min.
	72°C	60 sec.	72°C	45 sec.	72°C	1 min.
		1 min.		1 min. and 15 sec.		
Final extension	72°C	6 min.	72°C	10 min.	72°C	5 min.
Hold	4°C	-	4°C	-	4°C	-

3. Animals

The mice used in this study were cared for by Central Animal Facility of Medical School Göttingen. They were housed under constant conditions, including 12/12 hours light/dark cycle and a temperature range of 21-21°C. The mice had unrestricted access to food and water. The mice strains used in this project were the following:

WT - 129B6 wild-type (mixed 129Sv and C57BL/6 background);

5xFADPrnp$^{+/+}$ - 129B6/5xFAD mice express five AD-linked mutations: the K670N/M671L (Swedish), I716V (Florida), and V717I (London) mutations in human APP (695) and M146L and L286V mutations in PS1. These mice are wild-type for the *Prnp* gene;

Prnp$^{-/-}$ - 129B6/Prnp$^{-/-}$ mice lacking the neuronal cell-surface PrP^{C} protein;

5xFADPrnp$^{-/-}$ - 129B6/5xFAD/Prnp$^{-/-}$ double transgenic mice exhibiting AD-linked mutations and the lack of cell-surface PrPC protein;

Prnp$^{-/+}$ - 129B6/Prnp$^{+/-}$ (PrP^{C} heterozygous mice) were obtained crossing 129B6 with 129B6/Prnp$^{-/-}$ mice;

5xFADPrnp$^{-/+}$ - 129B6/5xFAD/Prnp$^{+/-}$ carried AD-linked mutations and heterozygosity for PrP^{C} protein.

The Genotyping was performed through PCR from the tail biopsy.

3.1. Ethics

All the animal procedures have been approved by the ethics committee of German Federal state of Niedersachsen and are in accordance with the ethic permission number 13/1232.

4. Behavioral testing

The behavioral testing involved mice of different ages, specifically at 3, 9, 12, and 14 months old. Seven days prior the tests the animals were individually housed. On the test days, the mice were transported in their individual cage to the testing room, allowing them a 30 min. of adaptation period. The tests were conducted during the light cycle. These procedures were identical for all tested mice.

4.1. Open Field (OP)

The OP test was conducted in a single testing session in a dimly square apparatus measuring 72 by 72 cm. The apparatus was virtually divided into sixteen 18 by 18 cm squares, with squares six, seven, ten, and eleven designated as the imaginary central zone, and the remaining twelve squares representing the peripheral zone. The mice were positioned in one of the four corners of the OF and allowed to explore the apparatus for a duration of 5 min. The mice's activity was recorded using video motility system (Video-Mot II, TSE, Bad Homburg, Germany). The number of squares crossed and the locomotion in the center squares were quantified. Following the test, the apparatus was cleaned with 70% ethanol and left to dry.

4.2. Elevated Plus Maze test (EPM)

The EPM test was conducted using an apparatus consisting in two open arms (60 cm) and two closed arms (60 cm). The open arms, positioned opposed to each other, had no walls. The closed arms, also positioned opposed to each other, were equipped with high walls measuring 20 cm to enclose the arms. A central platform, measuring 10 cm by 10 cm, connected the arms. The entire apparatus was elevated 50 cm above the floor and placed within an empty square measuring 70 cm by 70 cm to prevent fallen mice from escaping during the experiment. To initiate the test, the mice were placed in the center of the platform and allowed to freely explore the apparatus for 5 min. Throughout this period, the behavior of the mice was recorded using a video tracking system (Video-Mot II, TSE, Bad Hamburg, Germany). Following each session, the apparatus was thoroughly cleaned using 70% ethanol and left to dry.

Subsequently, the recorded data were analyzed to determine the time spend by the mice in the open arms, closed arms, and central platform of the EPM.

4.3. Rotarod (RR)

The RR apparatus used in this study consisted of a horizontal rotating bar that rotated along its long axis. During the training phase, each mouse was placed on the RR at a constant speed of 5 rpm for a maximum duration of 280 seconds. This training phase spanned over 5 consecutive days, allowing mice to familiarize themselves the RR apparatus. The testing day involved two trials, with a 5 min. interval between them. Foe each trial, the mice were placed on an accelerating RR that gradually increased in speed from 4.0 rpm to 40 rpm over a duration of 280 seconds. The latency to fall, which measured the time taken by the mouse to fall from the RR, was recorded. The best trial out of the two conducted during testing day was evaluated.

4.4. Fear conditioning (CFC)

The CFC test involved and acrylic square chamber measured 31.8 cm x 25.4 cm x 26.7 cm. The chamber was equipped with an electrifiable metal grid floor, a calibrated shock generator, a sound source, and a video system (VFC system, Med Associates). The conditioning phase began by placing the mouse inside the chamber and allowing it to freely explore it for 180 seconds. During this exploration period, a background sound was continuously present. Following this, a tone was presented as the conditioned stimulus, and during the final 2 seconds of the tone, a 0.5 mA foot shock was administered to the mouse as the unconditioned stimulus. The mice were then left in the chamber for an additional 30 seconds after the foot shock. On the following day, the cued test was conducted. In this test, the mice were placed in a different context, which included a smooth white floor covering the metal grids and curved white walls covering the chamber walls providing a new context that was unrelated to the conditioning chamber. The mouse was allowed to explore the chamber for 210 seconds, and during the last 180 seconds, the auditory cue that was present during conditioning was reintroduced. The freezing behavior, defined as the absence of

motion excluding respiration, was measured using the video system (VFC system, Med Associates).

4.5. Preparation of mice brain samples and protein extraction

Following the completion of behavioral experiments, the mice were sacrificed using CO_2 asphyxiation, followed by cervical dislocation. Dissection was performed, and the brains hemisphere were bilaterally separated. The cortex was isolated and utilized as the sample for the subsequent molecular experiments.

To initiate protein extraction, the cortex tissue was homogenized in a lysis buffer (see materials) for 30 min. Subsequently, the lysed tissue was subjected to centrifugation at 13000 rpm for 20 min at 4°C. The supernatant was collected, aliquoted and stored at -80°C and used for further experimental procedures.

5. Immunoblotting

For protein quantification, the BCA assay was used, ensuring the determination of the sample's protein concentration. Equal protein amounts were loaded into SDS-PAGE gels (see material). Following protein separation, the proteins were transferred from the gels to PVDF membranes. To prevent non-specific binding, the membranes were blocked in 5% non-fat milk in TBST for 1 hour. Next, the membranes were incubated at 4°C with the primary antibodies diluted in bocking buffer. Following primary antibody incubation, the membranes were washed 3 times for 5 min. with TBST at room temperature. Subsequently, a secondary antibody, diluted in 5% non-fat milk in TBST was incubated in the membranes at RT for 1 hour. Following secondary antibody incubation, the membranes were washed 3 times for 5 min. After the final washing step, the enzymatic reaction was initiated by ECL solution. The resulting protein bands were visualized using Molecular Imager ChemiDoc XRS+ with Image Lab software. Densiometric analysis of the bands intensities was performed using Lab Image 2.7.1 data analyzer.

6. Enzyme Linked Immuno-Sorbent Assay (ELISA)

The levels of Aβ1-40 and Aβ1-42 in the mouse cortex were quantified using Aβ1-40 and Aβ1-42 ELISAs. Additionally, the quantification of PrP^C was achieved through prion protein ELISA. The ELISA assays were performed following the recommendations provided by the respective suppliers.

7. Aβ peptides preparation

The generation of oligomeric Aβ followed a method previously described by other authors. [90,91] Lyophilized Aβ1-40 and Aβ1-42 were initially suspended in 1,1,1,3,3,3-Hexafluoro-2-Propanol to create a 1 mM solution. The suspension was then incubated for 2 hours at RT, followed by aliquoting and subsequent lyophilization via a Speed-Vac. The resulting films were stored at -80°C until further use. To prepare the Aβ oligomers, the films were re-suspended in DMSO to achieve a final concentration of 5 mM. The suspension was then sonicated for 10 min. in water bath to ensure proper dissolution and dispersion of the Aβ. Subsequently, the Aβ/DMSO mixture was diluted in sterile PBS and incubated overnight at 4°C, allowing the oligomerization to occur.

8. Cell culture and Aβ treatment

Human neuroblastoma cells wild type (SH-SY5Y WT) and human neuroblastoma cells stably expressing full-length human PrP^C (SH-SY5Y PrP^C) were cultured in SH SY5Y-Medium (see material). The cells were maintained at a temperature of 37 °C, with a CO2 supply of 5%. For the Aβ treatment, the cells were treated separately overnight with a final concentration of 10 µM of these peptides. The treatment was conducted in SH SY5Y-Medium. Following the treatment, the cells were lysed, collected and stored at -80°C until further experiments.

9. Preparation of primary cortical neurons

Primary cortical neurons were prepared using brains obtained from post-natal day 0 (P0) pups. The meninges were removed, the cortex tissue was isolated and subjected to digestion in enzyme buffer (see material) at 37°C for 20-30 min. After digestion, the cells were incubated in plating medium (see material) at 37°C for 5 min. Subsequently, the cells were washed twice with HBSS buffer (see material). The cells were re-suspended in plating medium, counted and plated on poly-L-ornithine and Laminin coated plates. The plating medium was replaced in the following day with neuronal buffer (see material). Half of the medium was replaced with fresh medium every 3-4 days.

10. Cleavage of PrP^C

To induce cleavage of PrP^C from the cell membrane, the cells were exposed to glimepiride at final concentration of 25 µM. This incubation was carried out for a duration of 2 hours. Subsequently, cells were washed to remove the drug. Following the drug washout, the cells were treated.

11. Immunofluorescence

For immunofluorescence analysis, cells were cultures in x-well cell culture chambers and the desired protocol was followed. Subsequently, the cells were fixated in freshly prepared 4% PFA for 10 min. After fixation, the cells were washed 3 times in PBS and subsequently permeabilized (see materials) for 10 min. Following the permeabilization, the cells were blocked (see materials) for 30 min. After blocking step, the cells were incubated with the desired primary antibodies with their suitable dilution for 1 hour at room temperature. Next, the cells were washed 3 times with PBS and incubated with their suitable fluorescent antibodies at RT for 1 hour. After incubation, the cells were washed 3 times with PBS, the chambers were sealed and observed under the microscope.

12. Transmission Electron Microscopy (TEM)

Transmission electron microscopy was performed to examine the solutions with 300 µM oligomerized Aβ1-40 and Aβ1-42. A Formvar-coated copper EM-grid was floated on 10µL of sample followed by the addition of 10 µl of 0.25% glutaraldehyde. After 1 min., the grid was washed in 3 drops of water. For the contrast, the grid was incubated with 2% aqueous uranyl acetate solution for 30 – 60 seconds. Excess uranyl acetate solution was removed by gently touching the grid vertically with a piece of filter paper. The negative stained samples were imaged with TEM and the digital micrographs were obtained with on-axis 2048*2048-CCD camera (TRS, Moorenweis, Germany).

13. Surface-Plasmon Resonance (SPR) measurements

Protein interaction analysis was conducted using through ProteOn XPR36 Protein Interaction Array system. To immobilize human recombinant PrP^C, a GLH sensor chip was utilized, resulting in a final immobilization level of 2200 RU. A ligand surface, lacking any bound protein, served as blank. Measurements were carried out at 25°C, the analytes were diluted in PBST. Aβ1-40, Aβ1-42 and CAV-1 were tested at concentrations of 15 µg/mL and 20 µg/mL. The signal obtained from the blank was subtracted from the protein bound signal. The ProteOn analysis software utilized the Langmuir 1:1 interaction model to calculate the corresponding association and dissociation rate constants.

14. Production of recombinant human PrP^C

The human recombinant PrP^C was purified following a previously described method.[92]

Briefly, the pET41a (+) vectors containing the gene encoding Human PrP^C 23-230 (Biocat) were introduced into E. coli Rosetta cells (DE3) (Merck Millipore). The transformed cells were then cultured on Luria-Bertani agar (LB) medium supplemented with kanamycin (50µg/mL) and chloramphenicol (34µg/mL) in petri dishes. The cultures were incubated overnight at 37°C. A single colony from the transformed cells

was selected and added to LB medium containing kanamycin (50µg/mL) and chloramphenicol (34µg/mL). The culture was then incubated at 37°C with shaking at 250 rpm for 6 hours. After incubation, Overnight Express Autoinduction system 1 (Sigma-Aldrich) was added and the cells were further incubated at 37°C with shaking at 250 rpm for 20 hours. Following the incubation, the cells were harvested by centrifugation, and the supernatant was discarded. To purify the inclusion bodies, the cell pellet was re-suspended and homogenized using 1X Bug Buster Mix (Merck Millipore). The suspension was incubated at room temperature for 20 minutes, and then 0.1X Bug Buster Master Mix (Merck Millipore) was added. The mixture was centrifuged at 13,000 x g for 15 minutes at 4°C. The pellet containing the inclusion bodies was dissolved in a solution of 8M guanidine (38g guanidine in 0.1M NaPO4 at pH 8). The suspension was then incubated for 50 minutes at room temperature on a rotating mixer. After the incubation, the mixture was centrifuged at 13,000 x g for 5 minutes at 4°C to separate the soluble fraction from the insoluble components. The collected supernatant was combined with equilibrated Ni-NTA beads in denaturing buffer (6M GdnHCl, 0.1M NaPO4 at pH 8) and incubated for 40 minutes. Following the incubation period, the Ni-NTA beads were loaded into the Äkta #XK16 column for purification. The tubes with the eluted proteins were collected from the largest UV 280 peak from the FPLC and submitted to dialysis.

.

15. Heart perfusion

In order to remove the blood from the brains of the mice, heart perfusion was conducted. Before the surgical procedure, the mice were anesthetized intraperitoneally (IP) using a combination of ketamine (100 mg/kg) + medetomidine (1 mg/Kg). In order to confirm the adequacy of anesthesia, the mouse's level of sedation was assessed by testing its response to tail and toe pinches. Subsequently, the skin and the diaphragm were opened to expose the chest cavity and the heart. A needle was inserted into the left ventricle and a small cut was made in the right atrium. PBS + 1% heparin was pumped into the heart for 3 min at a rate of 4 mL/min, followed by 4% PFA solution for 5 min. Next, the brain was collected and placed in 4% PFA at 4°C overnight. In the following day, the brains were washed in PBS and stored at 4°C.

16. Tissue clearing and immunolabeling through iDISCO+ protocol

In this study, the iDISCO+ method was employed. [93,94] Succinctly, the washed samples underwent dehydration using a series of methanol/H_2O solutions (ranging from 20% to 100%). Each solution was incubated with the sample for 1h. Following dehydration, the samples were washed in 100% methanol for 1h and then chilled at 4°C. Then, the samples were incubated overnight with shaking at room temperature in a solution consisting of 66% DCM and 33% methanol. The next day, the samples were washed twice in 100% methanol at RT, and then chilled at 4°C. The samples were bleached in 5%H2O2 in methanol, overnight at 4°C. On the following day, the samples were rehydrated using a series of methanol/H_2O solutions (ranging from 100% to 0%). Each solution was incubated with the sample for 1h. In the end, the samples were washed 2 times at RT in PTx.2 (see material). After the methanol treatments, the samples proceeded to immunolabeling process. Firstly, they were incubated in permeabilization solution for 2 days at 37°C and then transferred to blocking buffer and incubated for another 2 days at 37°C. The primary antibody was diluted in PTwH / 5%DMSO / 3% Donkey serum (see material) and incubated with the samples for 5 days at 37°C, and then, the samples were washed 4 – 5 times in PTwH for 1 day. The secondary antibody was diluted in PTwH / 3% Donkey Serum and incubated with the samples for 5 days at 37°C. In the end, the samples were washed 4 – 5 times in PTwH for one day. Following immunolabeling, the clearance was achieved through a series of methanol/H2O (ranging from 20% to 100%), each solution was incubated with the sample for 1h. Subsequently, they were incubated in 66%DCM / 33%Methanol, at RT with shacking for 3h. Next, the samples were washed twice in 100%DCM for 15 min. with shacking. Finally, the samples were immersed in DBE and stored in the darkness until imaging. The brain hemispheres were horizontally imaged using LaVision Ultramicroscope II and Imspector Microscope controller software.

17. Lightsheet image analysis (QUINT)

The images acquired from the light sheet microscope were pre-processed, registered and analyzed using the QUINT workflow.[95] In summary, ImageJ software was utilized to convert images into the desired formats. The spatial registration of the

mouse brain was performed using QuickNII with Allen mouse brain atlas version 3 2017 reference atlas. Subsequently, the images were processed with VisuAlign for fine-tunning of the images registered in QuickNII. Ilastik software was used for pixel classification of the images. The spatial analysis was performed using Nutil software.

18. Statistical Analysis

Statistical analyses were performed using GraphPad prism 10 software. For normally distributed data, t-test was employed. The life span of mice was analyzed using Mantel-Cox test and the Gehan-Breslow- Wilcoxon test. Significant results were accepted as *$p < 0.05$, **$p < 0.01$ and ***$p < 0.001$. Pearson's correlation analysis was performed to analyze the correlation between variables of interest.

V. Results

1. Analyses of PrP^C interaction with Aβ via SPR

To explore the possible direct binding of PrP^C and Aβ1-40 and Aβ1-42, surface plasmon resonance was employed. Full-length recombinant human PrP^C was immobilized as ligand on GLC at a concentration of 870 nM. Subsequently, recombinant Aβ1-40 (10µg/mL and 25µg/mL) and Aβ1-42 (10µg/mL and 20µg/mL) were run over the immobilized PrP^C. To assess the binding affinity, I employed the 1:1 Langmuir model for evaluation, which allowed to calculate the equilibrium dissociation constant (KD) (Figure 4). This value is indicative of the characteristic binding affinity between the molecules. A low KD value indicates a strong binding affinity between the molecules, meaning a small concentration of the dissociated complex at equilibrium. The sensorgrams displayed a clear association and dissociation phase between PrP^C - Aβ1-40, and PrP^C - Aβ1-42. The KD was calculated from the sensorgram data revealing a notably low KD values in both interactions. These results showed a high affinity interaction between PrP^C and both Aβ peptides. The binding affinity of PrP^C with Aβ1-42 (KD =1.13E-08) is higher than its binding affinity with Aβ1-40 (KD = 2.88E-08).

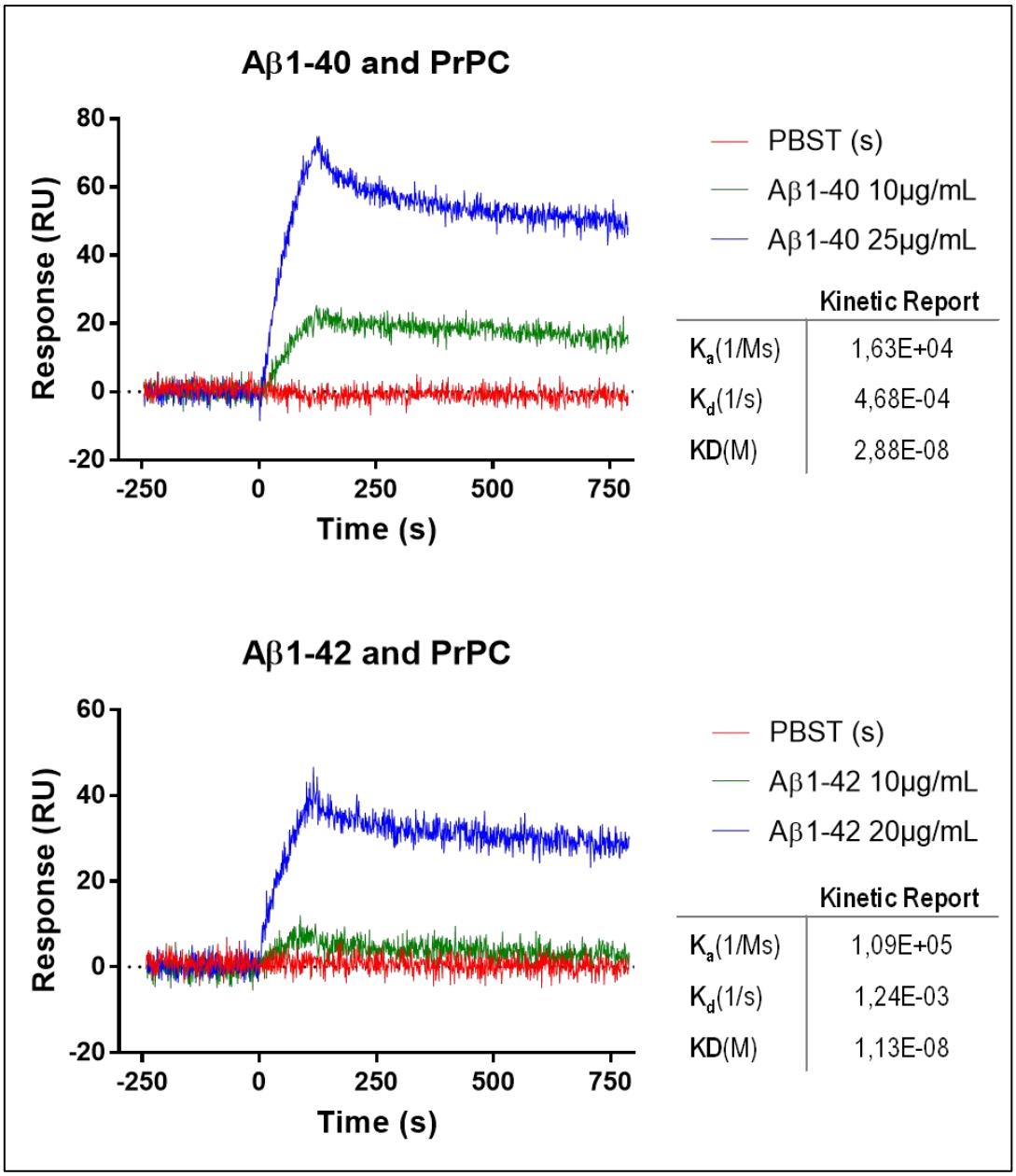

Figure 4 – SPR sensorgram analysis of PrP^C interactions with Aβ1-40 and Aβ1-42. The graphs display the results obtained from the SPR experiments measuring the binding affinity between the PrP^C and the two amyloid-beta peptides, Aβ1-40 and Aβ1-42. The KD for each interaction was calculated, revealing a KD of 2.88E-8 for PrP^C - Aβ1-40 binding and a KD of 1.13E-08 for for PrP^C - Aβ1-42 binding.

2. Morphological analysis of aggregated Aβ via TEM

TEM imaging was conducted to analyse the morphology and state of the Aβ peptides aggregation used to treat the cells. Two separated aliquots of Aβ1-40 and Aβ1-42 were incubated 12h and 24h before imaging (see methods). After 12h incubation (A and C), the presence of Aβ1-40 and Aβ1-42 oligomers is visible, with an

average area size of 170 nm and 136 nm, respectively (Figure 5). At this specific time point, the protofibrils and higher-order fibrillar structures were not visible. The 24h incubation condition revealed a presence of slightly bigger oligomers size, with and average area size of 197 nm for of Aβ1-40 and 253 nm for Aβ1-42 (B and D) when compared with the oligomers area size at 12h incubation condition. Additionally, at 24h incubation, it is possible to visualize the assembly of protofibrils by Aβ oligomers incorporation

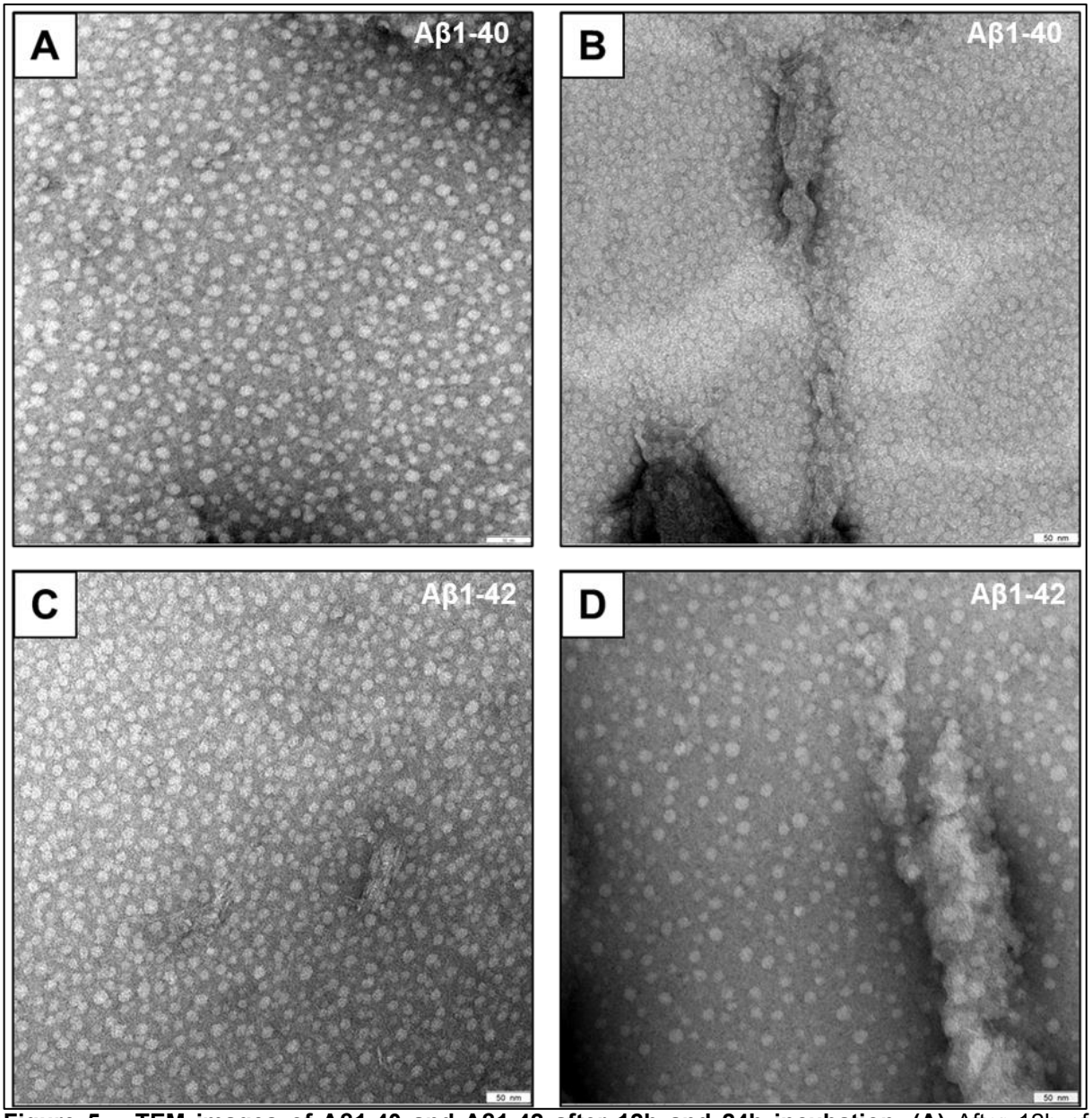

Figure 5 – TEM images of Aβ1-40 and Aβ1-42 after 12h and 24h incubation. (A) After 12h of incubation time, Aβ1-40 formed oligomers with an average area size of 170 nm. **(B)** Following 24h incubation of Aβ1-40, oligomers with an average size of 197 nm were observed, and protofibrils were formed. **(C)** After 12h of incubation time, Aβ1-42 formed oligomers with an average area size of 136 nm.

(D) After 24h incubation of Aβ1-42, the oligomers displayed an average area size of 253 nm, and protofibril were also observed being formed. The scale bar represents 50 nm.

3. Co-localization of PrP^C with Aβ1-40 and Aβ1-42

To investigate the potential co-localization of PrP^C with Aβ1-40 (Figure 6) and Aβ1-42 (Figure 7) oligomers, SH-SY5Y^{WT} cells (normal physiological PrP^C cells) and SH-SY5Y^{PrPC} (PrP^C overexpressing cells) cells were subjected to overnight treatment with Aβ1-40 and Aβ1-42 oligomers at a concentration of 10 μM. Following fixation, cells underwent immunostaining using SAF32 antibody for PrP^C, and anti-amyloid beta oligomers antibody for Aβ1-40 and Aβ1-42 oligomers. Cells that overexpress exhibit distinct characteristics compared to cell with normal PrP^C expression levels. The protein flourescence of PrP^C, Aβ1-40 and Aβ1-42 were determined by measuring the mean intensity within the cell region, and to measure the intensity of co-localization between PrP^C and Aβ oligomers, the Mander's coefficient was calculated. Cells with higher PrP^C expression demonstrate an enhanced signal intensity for PrP^C staining. This heightened expression is visually represented by a more prominent and widespread distribution of PrP^C throughout the plasm membrane. Also, cells that overexpress PrP^C, exhibit an increased fluorescence signal for Aβ oligomers compared with cells with normal PrP^C expression. Furthermore, in PrP^C overexpressing cells, PrP^C-enriched regions exhibit an intensified staining signal for Aβ oligomers, represented by overlapping fluorescence signals. The co-localization analysis (Figure 8) revealed similar levels of overlap between PrP^C and Aβ oligomers; the relative amount of specific co-localization between these protein remains comparable between both cell lines.

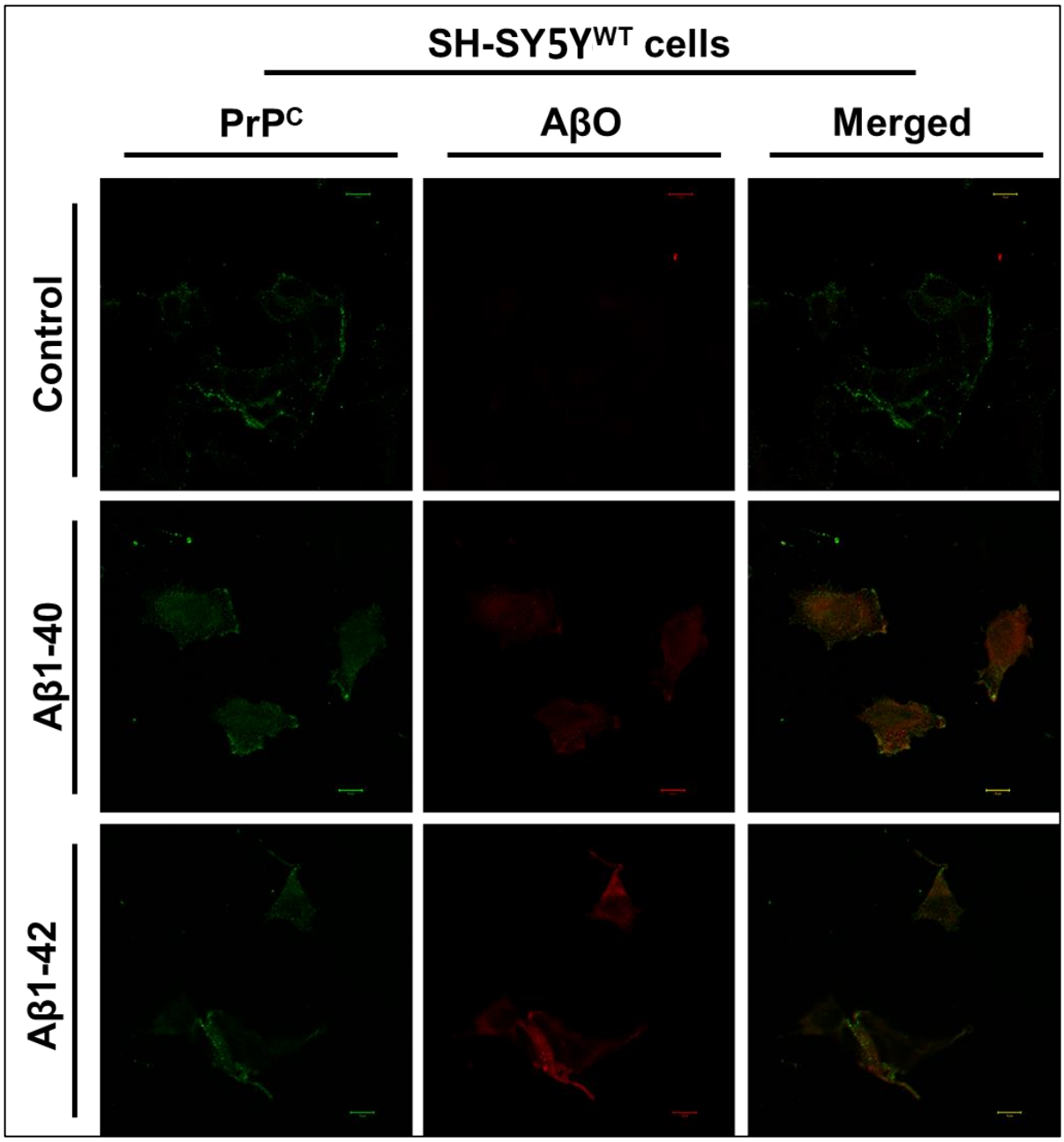

Figure 6 - PrP^C and Aβ1-40/ Aβ1-42 oligomers in SH-SY5Y^{WT} cells. Double immunostaining using SAF32 antibody against PrP^C (green), and anti- Aβ antibody against Aβ1-40 and Aβ1-42 (red) in SH-SYS5^{WT} cells. The areas of colocalization between these two proteins appear as yellow in the merged image. The scale bars represent 10 μm.

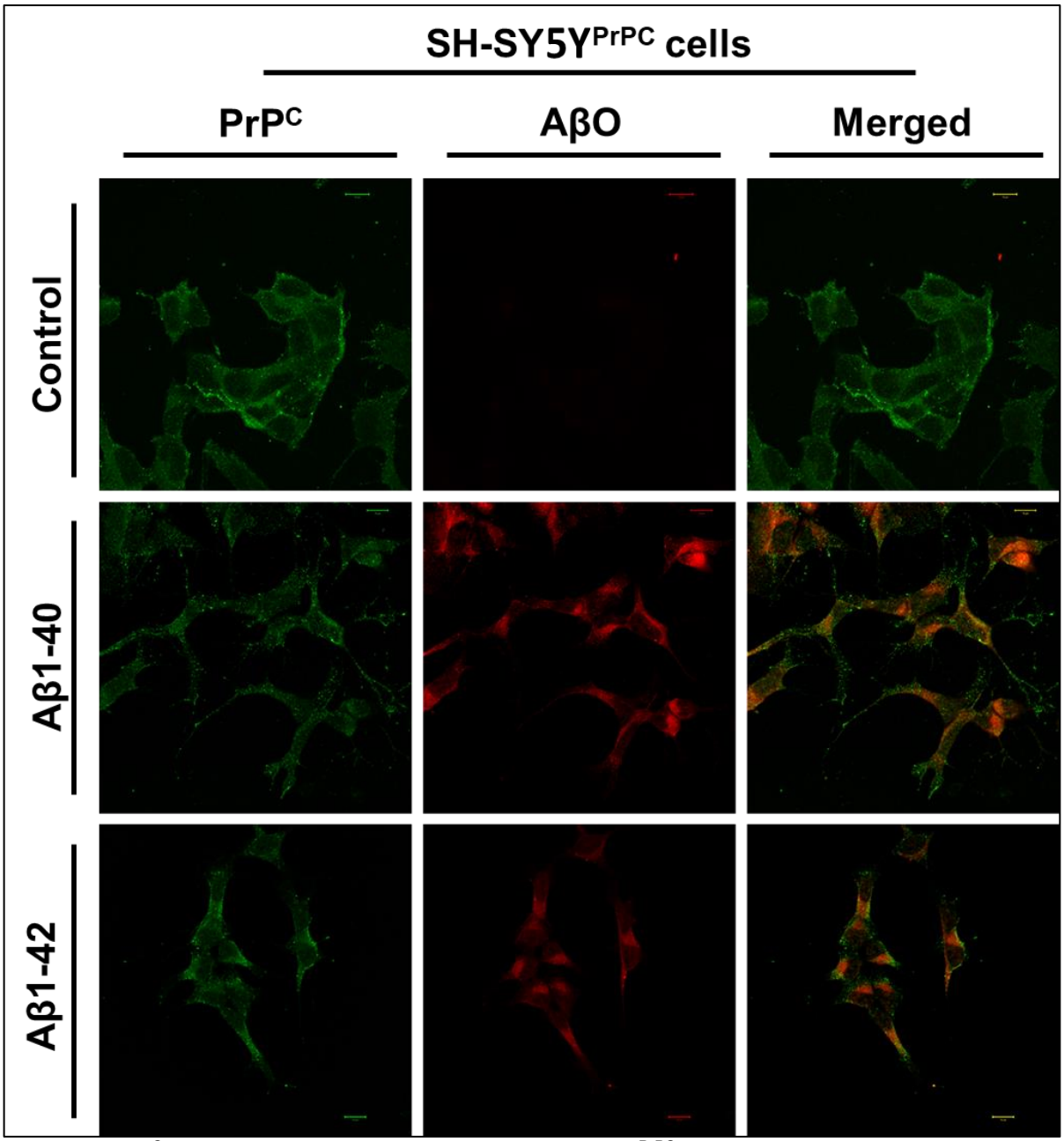

Figure 7 - PrP^C and Aβ1-40/Aβ1-42 oligomers in SH-SY5Y^{PrPC} cells. Double Immunostaining using SAF32 antibody against PrP^C (green), and anti-amyloid beta antibody against Aβ1-40 and Aβ1-42 (red) in SH-SY5Y^{PrPC} cells. The areas of colocalization between these two proteins appear as yellow in the merged image. The scale bars represent 10 μm.

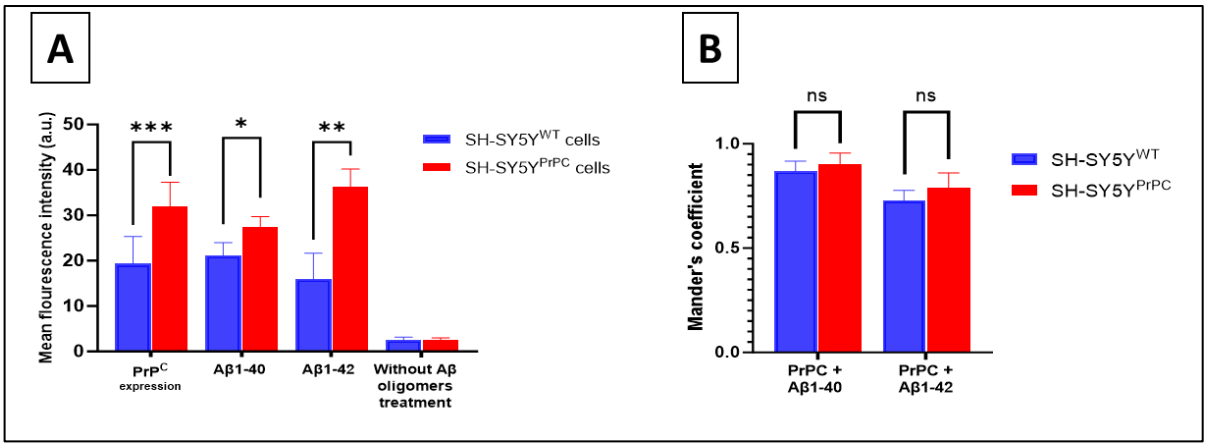

Figure 8 – Aβ levels and co-localization with PrP^C. (A) Mean fluorescence intensity was conducted to assess the difference in the proteins levels in both cell lines (n=20). The results demonstrate a significant increased mean fluorescence intensity of PrP^C in SH-SY5Y^{PrPC} compared with SH-SYS5^{WT}(***p<0.001). Additionally, there are significant differences in the mean fluorescence intensity of Aβ1-40 and Aβ1-42 between SH-SYS5^{WT} and SH-SY5Y^{PrPC}. SH-SY5Y^{PrPC} revealed higher intensity of Aβ1-40 (*p<0.05) and Aβ1-42 (**p<0.01) compared with SH-SYS5^{WT}. **(B)** Manders coefficient analysis was performed to quantify the co-localization between PrP^C with Aβ1-40 / Aβ1-42 in SH-SY5Y^{WT} and SH-SY5Y^{PrPC} cells (n=20). The results revealed no statistically significance differences in colocalization, both cell lines indicate a comparable degree of colocalization.

After obtaining the data from the confocal microscope, I proceeded with ELISA assays for Aβ1-40 and Aβ1-42 (Figure 9). These assays were utilized to measure and quantify the level of Aβ in both cell lines. Our data revealed a substantial increase of Aβ1-40 and Aβ1-42 levels in both cell types lines after Aβ1-40 and Aβ1-42 oligomers treatment, in comparison with their not treated controls. When comparing SH-SY5Y^{WT} and SH-SY5Y^{PrPC}, SH-SY5Y^{PrPC} displayed a significantly higher levels of Aβ1-40 and Aβ1-42 than SH-SY5Y^{WT}.

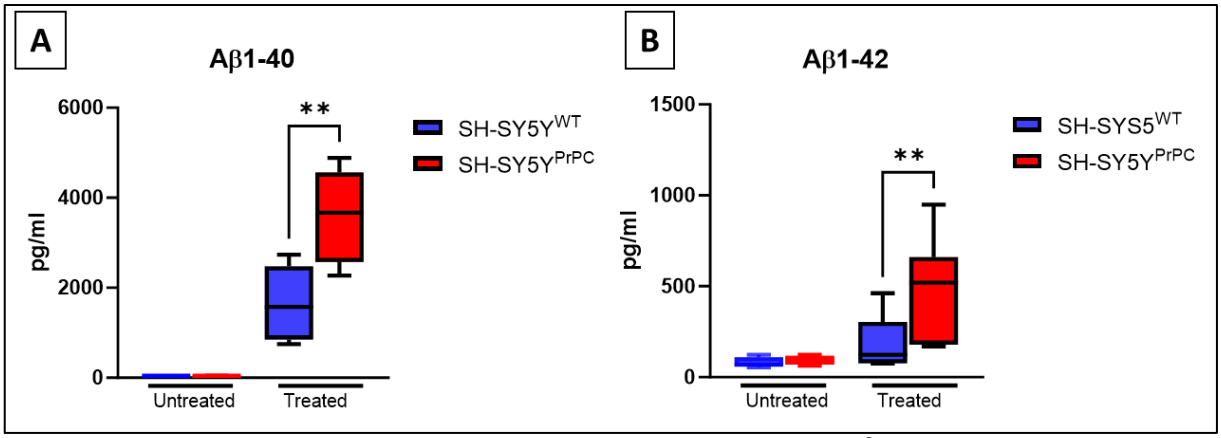

Figure 9 – Detection of Aβ1-40 and Aβ1-42 levels depending on PrP^C level via ELISA (measured via ELISA). (A) Aβ1-40 quantification in treated and untreated SH-SY5Y^{WT} and SH-SY5Y^{PrPC} cell lines (n=20). The treated cells demonstrate a noticeable increase in Aβ1-40 levels to the untreated cells. Additionally, SH-SY5Y^{PrPC} show a significant increase of Aβ1-40 levels (**p<0.01) when compared with SH-SY5Y^{WT} cells. **(B)** Quantification of Aβ1-42 in both treated and untreated SH-SY5Y^{WT} and SH-SY5Y^{PrPC} cell lines (n=20). The treated cells exhibit a prominent increase in Aβ1-42 levels compared to untreated cells. When comparing the two cell lines, SH-SY5Y^{PrPC} shows a significant higher level of Aβ1-42 (**p<0.01) than SH-SY5Y^{WT} cells.

4. *In vivo* experiments

Following *in vitro* experiments, I transitioned to *in vivo* investigations using different lines of AD mice models, namely, WT, 5xFADPrnp^{+}/$^{+}$, Prnp^{-}/$^{+}$, 5xFADPrnp^{-}/$^{+}$, Prnp^{-}/$^{-}$, and 5xFADPrnp^{-}/$^{-}$, from 3 to 14 months, to gain further insights into the behavioural and molecular implications of different levels of PrP^C expression in 5xFAD mice model.

4.1. Mice characterization by WB

The WB analyses served to confirm the generation of the specific mice models (Figure 10), at the protein expression level, used in this study, including WT, 5xFADPrnp^{+}/$^{+}$, Prnp^{-}/$^{+}$, 5xFADPrnp^{-}/$^{+}$, Prnp^{-}/$^{-}$, and 5xFADPrnp^{-}/$^{-}$. For WB the mice brains homogenates were used. GAPDH was utilized as a loading control in the WB experiments. The result shows a relatively constant expression across all samples confirming equal protein loading and gel transfer efficiency. Increased expression patterns of APP were observed in the three different mouse groups carrying the 5xFAD

mutations, namely 5xFADPrnp$^{+/+}$, 5xFADPrnp$^{-/+}$, and 5xFADPrnp$^{-/-}$. In contrast, mice without 5xFAD mutations (WT, Prnp$^{-/+}$ and Prnp$^{-/-}$) exhibited a low APP expression. The PrP^{C} bands displayed a strong signal in the animals that have a normal physiological expression of PrP^{C}, namely, WT and 5xFADPrnp$^{+/+}$. Animals' heterozygotes for PrP^{C}, containing only one allele for PrP^{C} expression (Prnp$^{-/+}$ and 5xFADPrnp$^{-/+}$), present an evident band signal decrease in comparison with the previous groups. PrP^{C} knockout mice (PrP$^{-/-}$ and 5xFADPrnp$^{-/-}$) displayed a total absence of bands.

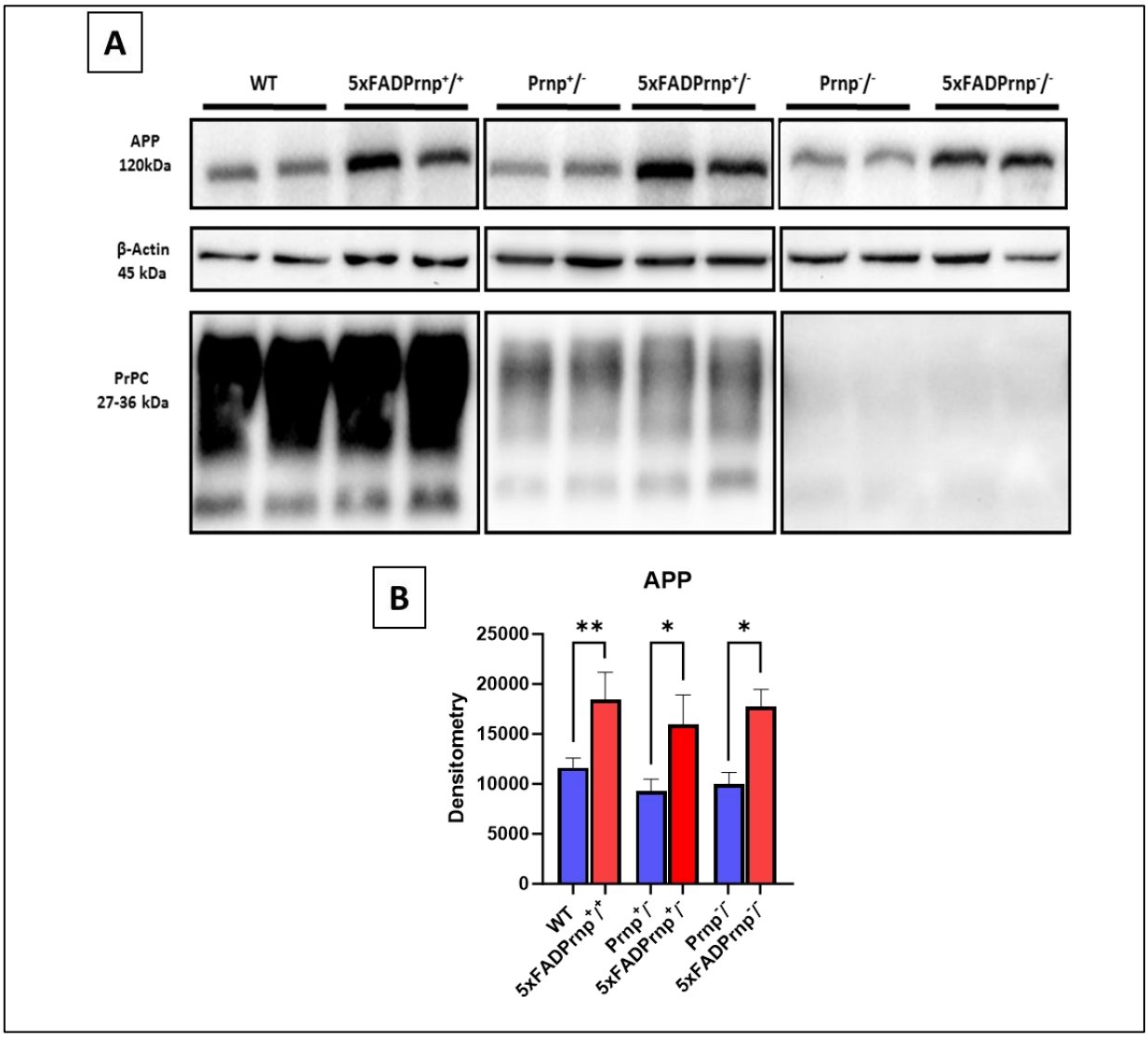

Figure 10 - Western blot of the mice brains homogenates. **(A)** The expression levels of APP, PrP^{C} in brain homogenates from the different mice groups. **(B)** APP densitometry (n=5). GAPDH was used as loading control.

4.2. PrP^C expression depending on the amount of Aβ pathology and PrP^C expression during aging

To quantify the PrP^C expression differences between animals that have a normal physiological expression of PrP^C and animals' heterozygotes for PrP^C Iutilized PrP^C ELISA. For the ELISA experiment I used the mice brain homogenates. The ELISA analysis demonstrates a significant decrease of PrP^C expression in heterozygotes groups ($Prnp^{-/+}$ and $5xFADPrnp^{-/+}$) in comparison with mice groups that are WT for PrP^C (WT and $5xFADPrnp^{+/+}$) (Figure 11). No significante PrP^C expression was observed between WT and $5xFADPrnp^{+/+}$, and between $PrP^{-/+}$ and $5xFADPrnp^{-/+}$ at 9 months.

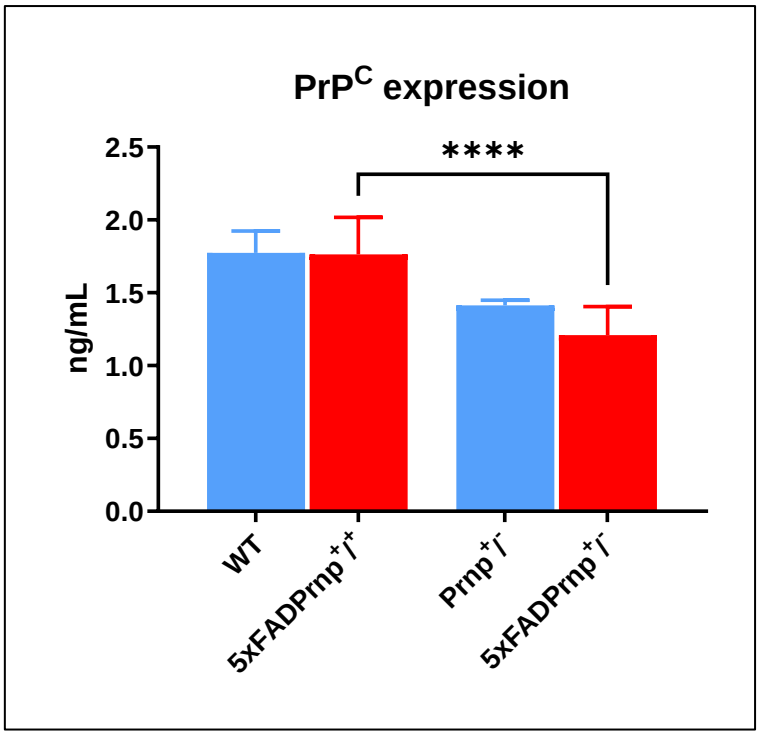

Figure 11- PrP^C ELISA of mice brains homogenates. PrP^C ELISA results reveal significant (****p<0.0001) decreased expression in heterozygous mice groups ($Prnp^{-/+}$ and $5xFADPrnp^{-/+}$) compared to WT mice for PrP^C (WT and $5xFADPrnp^{+/+}$) at 9 months of age (n=5). The analysis didn't show differences of PrP^C expression between WT and $5xFADPrnp^{+/+}$, and between $Prnp^{-/+}$ and $5xFADPrnp^{-/+}$.

To investigate whether there exists a correlation between PrP^C abundance and the age of the mice, PrP^C ELISA was performed in mice from 3 to 16 months (Figure

12). The ELISA quantification reveals no significance correlation between PrP^C levels and aging in 5xFADPrnp$^{+/+}$ mice. Similarly, in 5xFADPrnp$^{-/+}$, there was also no significant association between PrP^C levels and aging. In both groups, there was no statistical variation in PrP^C levels with increasing age, the PrP^C levels remain constant during aging.

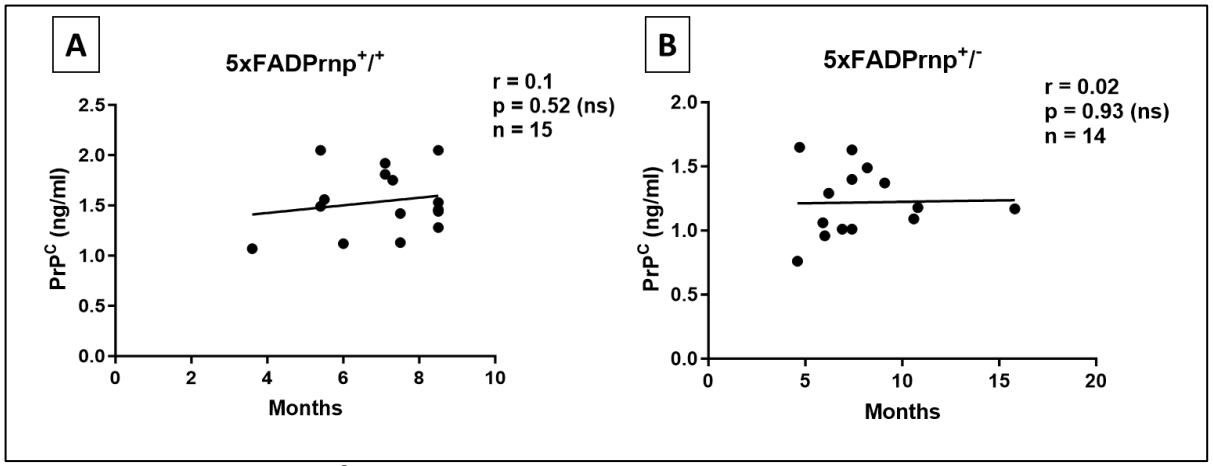

Figure 12 - Analysis of PrP^C levels during aging in 5xFAD mice. 5xFADPrnp$^{+/+}$ **(A)** and 5xFADPrnp$^{-/+}$ **(B)** showing no significant correlation between PrP^C levels and aging in both cases. There is a consistent PrP^C abundance throughout the aging process in these mice lines.

4.3. Aβ levels throughout the aging process in mice

The Aβ1-40 and Aβ1-42 ELISAs was conducted on mice brain homogenates to investigate the relationship between age and Aβ accumulation in the brains of the mice models (Figure 13). The correlation analysis between levels of Aβ1-40 and Aβ1-42 and the age was performed in three different mice groups: 5xFADPrnp$^{+/+}$, 5xFADPrnp$^{-/+}$ and 5xFADPrnp$^{-/-}$. In the 5xFADPrnp$^{+/+}$ mice group (3 to 16 months), a strong positive correlation was observed between the levels of Aβ1-40 and the age (r = 0.73, p = 0.002). Similarly, there was a positive correlation between Aβ1-42 levels and aging (r = 0.65, p = 0.009) in this group. In the 5xFADPrnp$^{-/+}$ group, there is a significant positive correlation between the Aβ1-40 levels and aging (r = 0.7, p = 0.006). Also, a positive correlation was observed between Aβ1-42 and aging (r = 0.54, p = 0.04) within the same group. Similarly, to the other two mice groups, 5xFADPrnp$^{-/-}$ mice showed a

significant positive correlation between amyloid-beta levels and aging, Aβ1-40 (r = 0.55, *p* = 0.015) and Aβ1-42 (r = 0.58, *p* = 0.008). These results showed an increase of Aβ1-40 and Aβ1-42 correlated with aging in the three mice groups carrying the 5xFAD mutations.

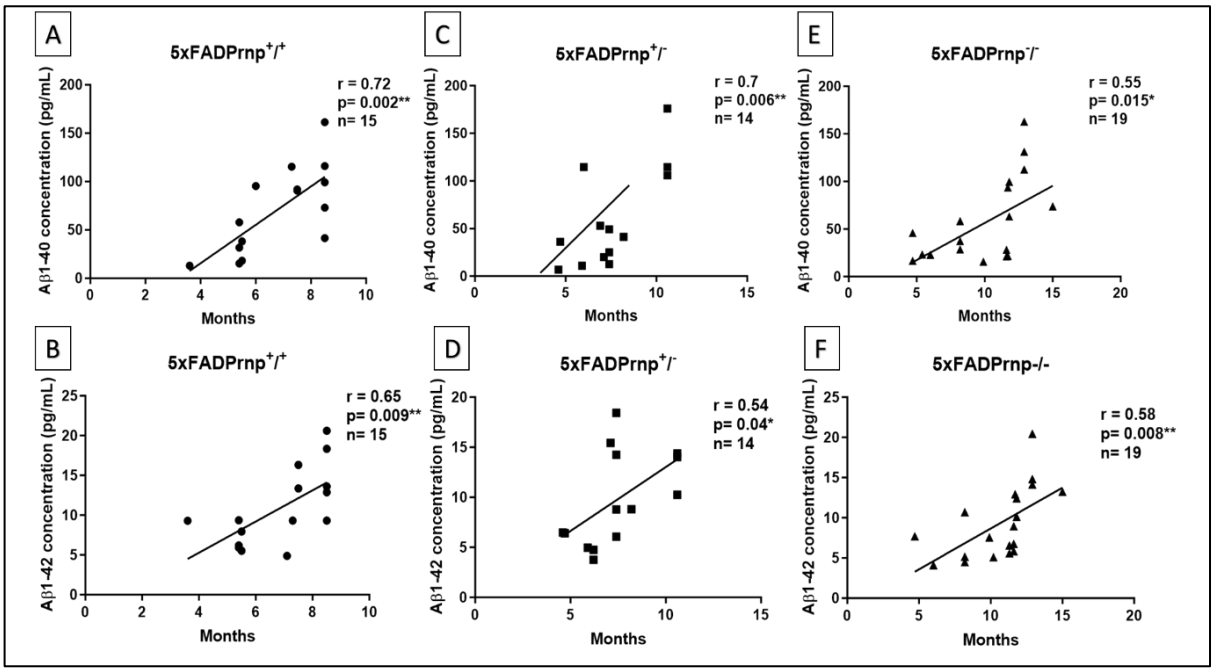

Figure 13 - Correlation of amyloid-beta levels with aging in 5xFADPrnp$^{+/+}$, 5xFADPrnp$^{-/+}$, and 5xFADPrnp$^{-/-}$. (A) In 5xFADPrnp$^{+/+}$ mice is observed a positive correlation for Aβ1-40 (r = 0.73, p = 0.002) and Aβ1-42 (r = 0.65, p =0.009) **(B)**. For 5xFADPrnp$^{-/+}$ mice **(C-D)**, a positive correlation was found for Aβ1-40 (r = 0.7, p = 0.006) and Aβ1-42 (r = 0.54, p =0.04). The 5xFADPrnp$^{-/-}$ mice group **(E-F)**, displayed a positive correlation for Aβ1-40 (r = 0.55, p = 0.015) and Aβ1-42 (r = 0.58, p = 0.008). The p-values indicate statistical significance in all cases.

When I examined the Aβ1-40 and Aβ1-42 levels in the three different mice models at 9 months of age (n=5), significant differences in Aβ accumulation in these mice brains were observed (Figure 14). Statistical analyses revealed a significant decrease of Aβ1-40 in 5xFADPrnp$^{-/-}$ compared to 5xFADPrnp$^{+/+}$ mice. No significant statistical differences were found in Aβ1-40 levels when comparing 5xFADPrnp$^{+/+}$ with 5xFADPrnp$^{-/+}$ or 5xFADPrnp$^{-/+}$ with 5xFADPrnp$^{-/-}$. Similarly, the statistical analyses of Aβ1-42 demonstrated a significant decrease in 5xFADPrnp$^{-/-}$ compared to both 5xFADPrnp$^{+/+}$ and 5xFADPrnp$^{-/+}$. There was no statistical difference in Aβ1-42 levels between 5xFADPrnp$^{+/+}$ and 5xFADPrnp$^{-/+}$.

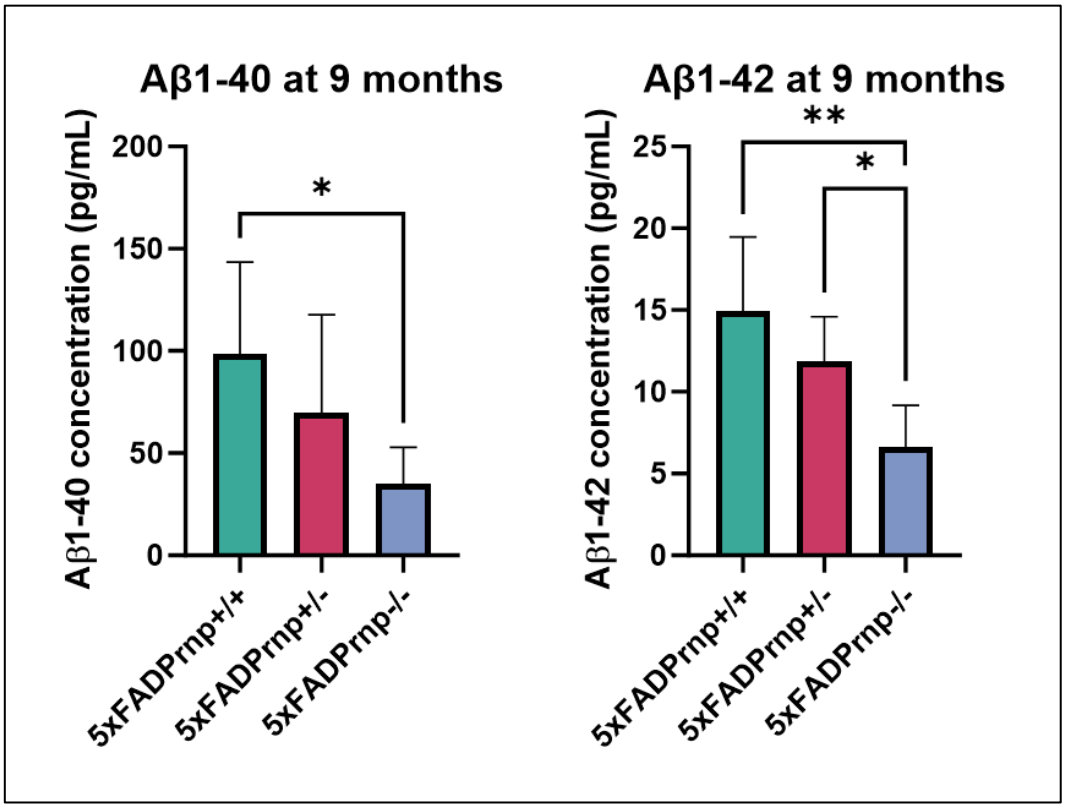

Figure 14 - Aβ1-40 and Aβ1-42 levels in the different mice models. Aβ1-40 levels exhibit a statistically significant decrease in 5xFADPrnp$^{-/-}$ when compared to 5xFADPrnp$^{+/+}$ (*p= 0.03). No statistically significant differences were observed in Aβ1-40 levels when comparing 5xFADPrnp$^{+/+}$ with 5xFADPrnp$^{-/+}$ or 5xFADPrnp$^{-/+}$ with 5xFADPrnp$^{-/-}$. The analyses of Aβ1-42 levels revealed significant decrease in 5xFADPrnp$^{-/-}$ compared to both 5xFADPrnp$^{+/+}$ (**p= 0.007) and 5xFADPrnp$^{-/+}$ (*p= 0.02). No significant statistical differences were found in Aβ1-42 levels between 5xFADPrnp$^{+/+}$ and 5xFADPrnp$^{-/+}$.

4.4. Influence of PrP^{C} on 5xFAD mice lifespan

In this part, I conducted an investigation to assess the influence of PrP^{C} on mice lifespan (Figure 15). To accomplish this, I measured the lifespans of mice different genetic backgrounds, including WT, 5xFADPrnp$^{+/+}$, Prnp$^{-/+}$, 5xFADPrnp$^{-/+}$, Prnp$^{-/-}$, and 5xFADPrnp$^{-/-}$. Lifespan measurements were conducted by closely monitoring the mice from birth until their natural death. The lifespan analysis revealed that WT mice displayed a median lifespan of 826 days. In contrast, 5xFADPrnp$^{+/+}$ exhibit a notably reduced median lifespan of 350 days. The median lifespan of 5xFADPrnp$^{+/+}$ mice decreased by approximately 57% compared to WT mice. In Prnp$^{-/+}$, I obtain a median

of 738 days and a median of 476 days for 5xFADPrP$^{-/+}$. 5xFADPrP$^{-/+}$ median lifespan is approximately reduced in 35% in comparison with Prnp$^{-/+}$ mice. Prnp$^{-/-}$ mice presented a median lifespan of 724 days and 5xFADPrnp$^{-/-}$ showed a lifespan median of 609 days. The 5xFADPrnp$^{-/-}$ mice exhibit a 16% shorter median lifespan of than Prnp$^{-/-}$ mice.

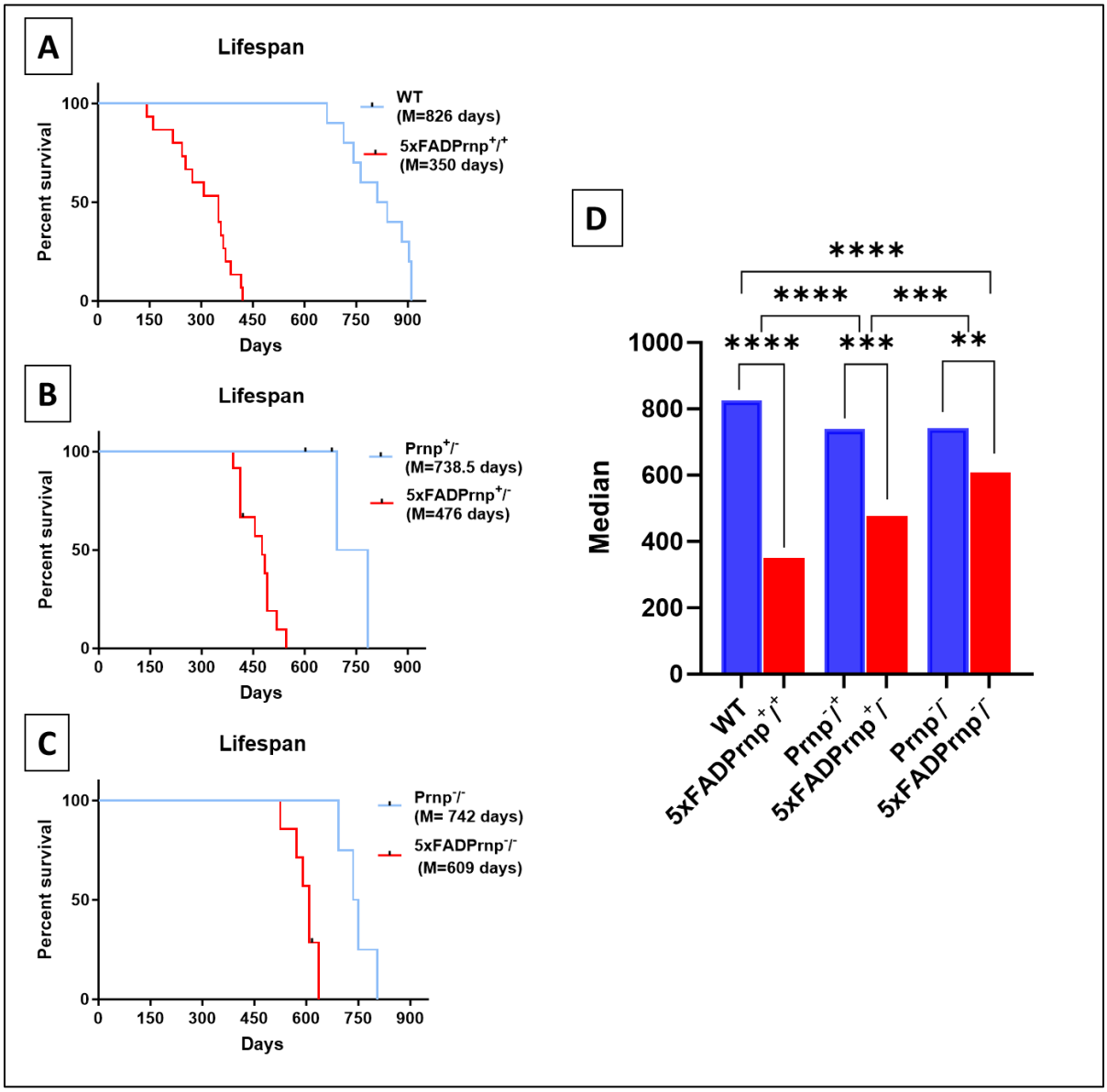

Figure 15 – Effect of PrPC on mice Lifespan. (A) Lifespan comparison between WT mice (M = 826 days) and 5xFADPrnp$^{+/+}$ (M = 350 days), **(B)** Prnp$^{-/+}$ (M = 738 days) and 5xFADPrP$^{-/+}$ (M = 476 days), and **(C)** between Prnp$^{-/-}$ (M = 742 days) and 5xFADPrnp$^{-/-}$ (M = 609 days). **(D)** Comparison of the median lifespans among the six groups. Where exhibit a statistical significance of (****p<0.0001) between WT and 5xFADPrnp$^{+/+}$, (***p= 0.0005) between Prnp$^{-/+}$ and 5xFADPrP$^{-/+}$, and (**p= 0.008) between Prnp$^{-/-}$ and 5xFADPrnp$^{-/-}$. The comparison between 5xFADPrnp$^{+/+}$ and 5xFADPrP$^{-/+}$ presented a significance

of (****p<0.0001), (***p= 0.0001) between 5xFADPrP$^{-/+}$ and 5xFADPrnp$^{-/-}$, and (****p<0.0001) between 5xFADPrnp$^{+/+}$ and 5xFADPrnp$^{-/-}$.

4.5. PrP^{C} influence on 5xFAD locomotor activity in open field

The open field test was utilized to evaluate the locomotor activity of different mice genotypes at various ages (Figure 16). The distance travelled by the mice was measured. At 3 months of age, there was no significant difference in anxiety-related behaviour between WT and 5xFADPrnp$^{+/+}$ in the locomotor activity of the mice. At 9 months, 5xFADPrnp$^{+/+}$ mice displayed significant decrease on their locomotor activity compared with WT. In the comparison between Prnp$^{-/+}$ and 5xFADPrnp$^{-/+}$ mice, at 3 and 9 months, there were no significant differences in the locomotor activity performance. In opposite, at 12 months, 5xFADPrnp$^{-/+}$ mice showed a significant decrease in their locomotor activity when compared with Prnp$^{-/+}$. The comparison between Prnp$^{-/-}$ and 5xFADPrnp$^{-/-}$ mice, revealed no significant differences in locomotor activity performance across all the tested ages (3, 9, 12, and 14 months of age).

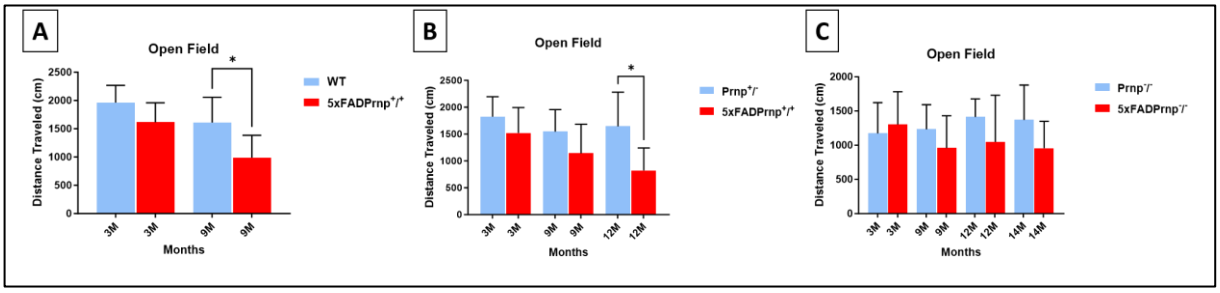

Figure 16 – Distance travelled on the open field. Distance travelled (cm) in the open field test (n= 6). **(A)** The graph depicts the comparison of distance travelled between WT and 5xFADPrnp$^{+/+}$ at different ages. At 3 months, there was no statistical differences in the distance travelled. At 9 months, 5xFADPrnp$^{+/+}$ showed a significant reduction in the distance travelled compared with WT mice (*p=0.04). **(B)** The graph illustrates the comparison between Prnp$^{-/+}$ and 5xFADPrP$^{-/+}$ mice at different ages. At both 3 and 9 months of age, there was no significant difference in the distance travelled. At 12 months of age, 5xFADPrP$^{-/+}$ mice exhibit a significant decrease in the distance travelled compared to Prnp$^{-/+}$ (*p=0.03). **(C)** The graph shows the comparison between Prnp$^{-/-}$ and 5xFADPrnp$^{-/-}$ at different ages. No significant differences in the distance travelled were observed across all tested ages (3, 9, 12, and 14 months).

4.6. Influence of PrP^C on motor performance in 5xFAD mice

Rotarod test was conducted to assess the motor function in the different mouse groups: WT, 5xFADPrnp^{+}/$^{+}$, Prnp^{-}/$^{+}$, 5xFADPrP^{-}/$^{+}$, Prnp^{-}/$^{-}$, and 5xFADPrnp^{-}/$^{-}$ (Figure 17). The mice were tested at different ages groups to evaluate the progression of motor deficits over time. For the comparison between WT and 5xFADPrnp^{+}/$^{+}$, the results revealed that at 3 months of age, there was no statistically significant difference in motor performance between the two groups. In contrast, at 9 months of age, the 5xFADPrnp^{+}/$^{+}$ mice demonstrated a significant decline in motor function compared with WT mice group. Next, the comparison between Prnp^{-}/$^{+}$ and 5xFADPrP^{-}/$^{+}$ revealed no significant difference in motor performance at both 3 and 9 months of age. At 12 months of age, the 5xFADPrP^{-}/$^{+}$ mice exhibit a significant decline in motor function compered to Prnp^{-}/$^{+}$ mice. The comparison between Prnp^{-}/$^{-}$ and 5xFADPrnp^{-}/$^{-}$ at 3, 9, and 12 months of age showed no significant differences in motor performance between the two groups. When compared the performance between the two groups at 14 months of age, it is observed a significant decline of the motor function in 5xFADPrnp^{-}/$^{-}$ in comparison with Prnp^{-}/$^{-}$.

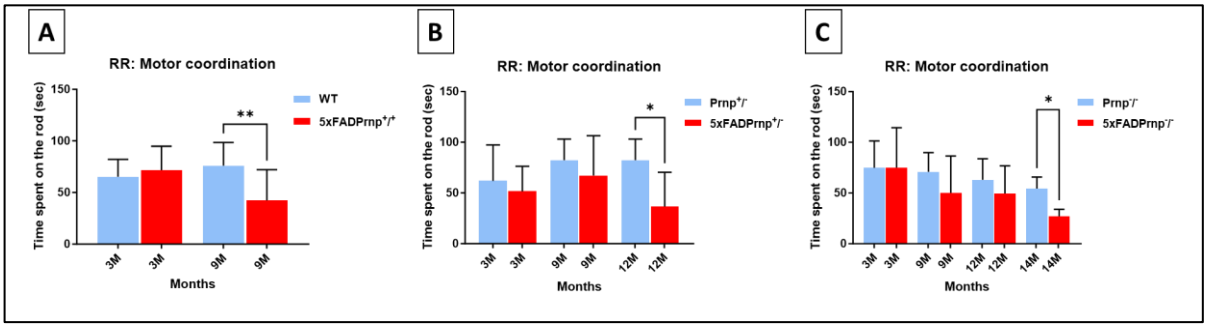

Figure 17- Motor function. All the graphs display the time spent by the mice on the rotarod apparatus at different ages (n= 6). **(A)** Motor function comparison between WT and 5xFADPrnp^{+}/$^{+}$ mice: No statistical difference at 3 months, 5xFADPrnp^{+}/$^{+}$ mice showed a significant (**p= 0.004) decline of motor function at 9 months. **(B)** Motor function comparison between Prnp^{-}/$^{+}$ and 5xFADPrP^{-}/$^{+}$ mice: No statistical difference at 3 and 9 months. At 12 months 5xFADPrP^{-}/$^{+}$ showed a significant decline of the motor functions when compared with Prnp^{-}/$^{+}$ mice (*p= 0.01). **(C)** Motor function comparison between Prnp^{-}/$^{-}$ and 5xFADPrnp^{-}/$^{-}$ no significant differences at 3, 9, and 12 months. At 14 months, 5xFADPrnp^{-}/$^{-}$ mice performed significantly worse in comparison with Prnp^{-}/$^{-}$ (*p= 0.02).

4.7. PrP^C influence in anxiety-related behaviour in 5xFAD mice

The elevated plus maze was conducted to assess general anxiety-related behaviour in the different mice groups with different ages (Figure 18). At 3 months of age, there was no significant difference in anxiety-related behaviour between WT and 5xFADPrnp$^{+/+}$ in the percentage of time spent in the open arms. At 9 months, 5xFADPrnp$^{+/+}$ mice exhibit a significant decrease in anxiety behaviour, spending more time in the open arms in comparison with WT mice. Similarly, at both 3 and 9 months of age, there were no significant differences in anxiety-behaviour between Prnp$^{-/+}$ and 5xFADPrP$^{-/+}$ mice groups in the time spent on the open arms. At 12 months of age, 5xFADPrP$^{-/+}$ exhibit a significant decrease in anxiety-behaviour, spending significantly more time in the open arms compared to Prnp$^{-/+}$ mice. Likewise, at 3 and 9 months of age, Prnp$^{-/-}$ and 5xFADPrnp$^{-/-}$ presented no significant differences in anxiety-behaviour, spending relatively the same time in the open arms. At 12 and 14 months of age, 5xFADPrnp$^{-/-}$ mice showed a significant decrease of anxiety-behaviour, exhibiting a notably increased time in the open arms compared with Prnp$^{-/-}$.

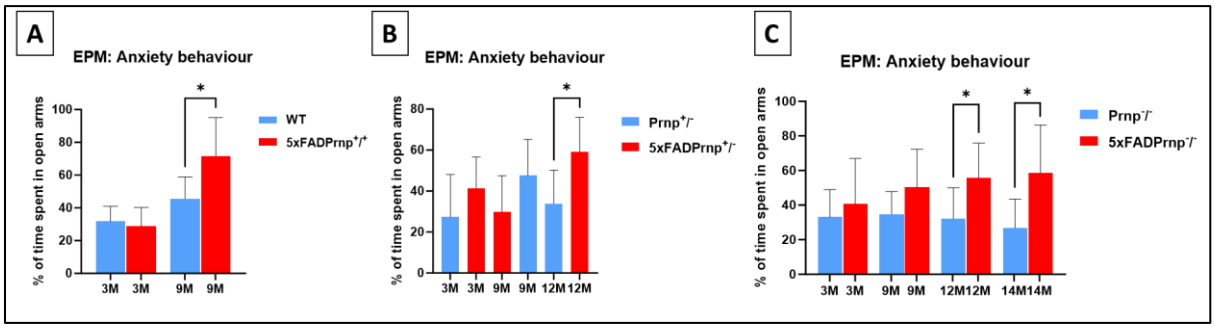

Figure 18 - Anxiety-behavior. Each graph displays the percentage of time spent by the mice in open arms of the maze at different ages (n=6). In **(A)**, at 3 months old, there was no statistical difference between WT and 5xFADPrnp$^{+/+}$ in the time spent in the open arms. At 9 months of age, 5xFADPrnp$^{+/+}$ mice showed a significant increase in the time spent in the open arms when compared with WT mice (*p= 0.03). **(B)** At 3 and 9 months of age, there was no significant difference between Prnp$^{-/+}$ and 5xFADPrP$^{-/+}$ mice. At 12 months of age, 5xFADPrP$^{-/+}$ mice exhibit a significant increase of the time spent in the open arms in comparison with Prnp$^{-/+}$ (*p= 0.033). In **(C)**, at 3 and 9 months, there was no difference between Prnp$^{-/-}$ and 5xFADPrnp$^{-/-}$ mice groups in the time spent in the open arms. The significant increase of time spent in the open arms in 5xFADPrnp$^{-/-}$ compared to Prnp$^{-/-}$ is observed at 12 (*p= 0.04) and 14 (*p= 0.02) months of age.

4.8. PrP^C effect in associative learning of 5xFAD mice

Fear conditioning test was conducted to assess the associative learning in the different mice groups. The freezing time was measured as an indicator of the associative learning (Figure 19). At 3 months of age, no significant differences in associative learning were found, as indicated by the freezing time, between WT and 5xFADPrnp^{+}/$^{+}$, as well as between Prnp^{-}/$^{+}$ and 5xFADPrP^{-}/$^{+}$ mice. At 9 months of age, the 5xFADPrnp^{+}/$^{+}$ group exhibited a significant decline in associative learning, freezing less time compared to WT. Likewise, 5xFADPrP^{-}/$^{+}$ displayed a significant decrease of the associative learning when compared with Prnp^{-}/$^{+}$ at 9 and 12 months of age. When comparing Prnp^{-}/$^{-}$ and 5xFADPrnp^{-}/$^{-}$, no significant differences were observed at 3 and 9 months of age. In contrast, at 12 and 14 months of age, significant differences emerged between 5xFADPrnp^{-}/$^{-}$ and Prnp^{-}/$^{-}$ mice, with 5xFADPrnp^{-}/$^{-}$ mice exhibiting impaired associative learning compared to Prnp^{-}/$^{-}$.

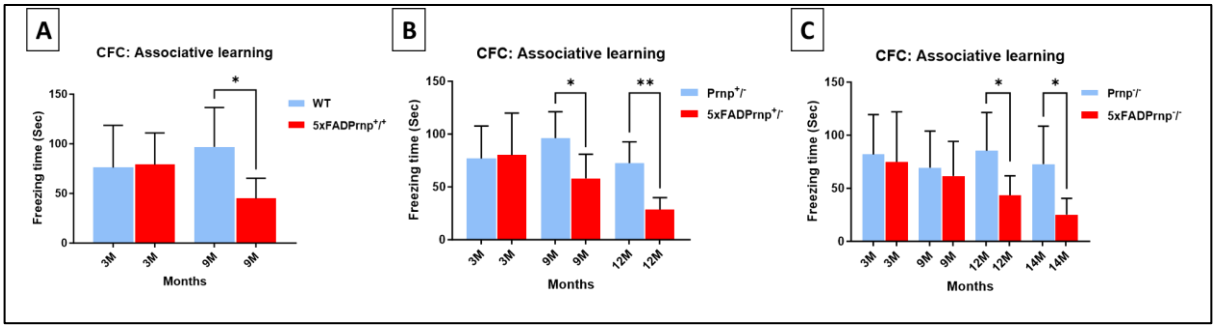

Figure 19 – Freezing time on the cued fear conditioning test. Freezing time was measured in different mouse groups at different ages (n= 6). In **(A)**, at 3 months of age, there was no statistical difference in the freezing time between WT and 5xFADPrnp^{+}/$^{+}$. 5xFADPrnp^{+}/$^{+}$ displayed a decreased freezing time at 9 months of age in comparison with WT mice (*p= 0.04). **(B)** Comparison between Prnp^{-}/$^{+}$ and 5xFADPrP^{-}/$^{+}$ mice. At 3 months, no significant difference in freezing time was found. At 9 and 12 months of age, 5xFADPrP^{-}/$^{+}$ exhibit a significant reduction of the freezing time compared to Prnp^{-}/$^{+}$, (*p= 0.04) and (**p= 0.004), respectively. In **(C)**, at 3 and 9 months, there was no significant differences in the freezing time between Prnp^{-}/$^{-}$ and 5xFADPrnp^{-}/$^{-}$ mice. At 12 and 14 months of age, significant differences emerged between Prnp^{-}/$^{-}$ and 5xFADPrnp^{-}/$^{-}$ groups, with 5xFADPrnp^{-}/$^{-}$ mice displaying a reduced freezing time, (*p= 0.04) and (*p= 0.03), respectively, compared to Prnp^{-}/$^{-}$.

5. Correlation between amyloid-beta levels and behaviour performance

In this study, I investigated the potential correlation between Aβ1-40 and Aβ1-42 levels and mice's performance in behaviour tests. Following the behavioural tests, the animals were sacrificed, and the brain homogenate was utilized to measure the Aβ1-40 and Aβ1-42 levels using ELISAs.

5.1. Locomotor activity and Aβ1-40 and Aβ1-42 levels

I investigated the potential correlation between Aβ1-40 and Aβ1-42 levels and the mice's performance in the distance travelled in the open field test from the different genetic background mice, including 5xFADPrnp$^{+/+}$, 5xFADPrP$^{-/+}$ and 5xFADPrnp$^{-/-}$ (Figure 20). For the 5xFADPrnp$^{+/+}$ there was no significant correlation observed between Aβ1-40 levels and their locomotor activity. Similarly, for Aβ1-42 levels in 5xFADPrnp$^{+/+}$ mice there was no significant correlation with their locomotor activity performance. In the 5xFADPrP$^{-/+}$ the correlation analysis revealed no significant correlation between Aβ1-40 levels and their locomotor activity in the open field test. Likewise, for Aβ1-42 levels in 5xFADPrnp$^{+/+}$ mice, there was no significant correlation with their performance. For 5xFADPrnp$^{-/-}$ mice, the correlation analysis between Aβ1-40 levels and their locomotor activity performance in the open field test showed no significant correlation. Similarly, for Aβ1-42 levels in the 5xFADPrnp$^{-/-}$ mice, there was no significant correlation observed with their performance in the open field.

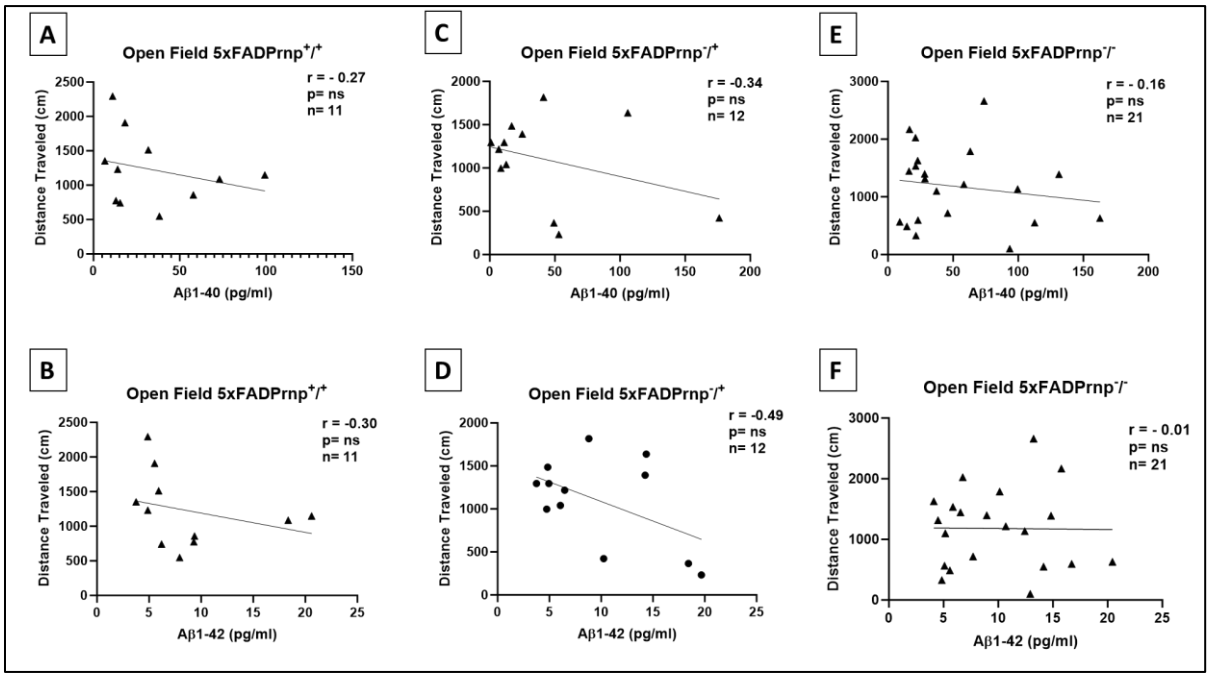

Figure 20 - Correlation analysis between amyloid beta levels and locomotor activity performance. **(A)** The graph shows the correlation analysis between Aβ1-40 levels and distance traveled in the open field test in the 5xFADPrnp^{+}/$^{+}$ mice. No significant correlation was observed. **(B)** Correlation analysis between Aβ1-42 levels and distance traveled. The results reveal no signification correlation between them. **(C)** For the 5xFADPrP^{-}/$^{+}$ mice, the graph illustrates the correlation analysis between Aβ1-40 levels and the distance traveled in the open field apparatus. No significant correlation was found. **(D)** The graph represents the correlation analysis between Aβ1-42 levels and distance traveled in the open field test. **(E)** In the 5xFADPrnp^{-}/$^{-}$ mice, the graph depicts the correlation analysis between Aβ1-40 levels and distance traveled in the open field test. No significant correlation was observed. **(F)** Correlation analysis between Aβ1-42 levels and distance traveled in 5xFADPrnp^{-}/$^{-}$ mice. The results reveal no significant correlation between Aβ1-42 levels and distance traveled in the open field test.

5.2. Anxiety-related behaviour and Aβ1-40 and Aβ1-42 levels

In this study, I examined the potential correlation between Aβ1-40 and Aβ1-42 levels and anxiety-like behavior in mice in the elevated plus maze. I conducted our analysis using the three different mice groups: 5xFADPrnp^{+}/$^{+}$, 5xFADPrP^{-}/$^{+}$ and 5xFADPrnp^{-}/$^{-}$ (Figure 21). For each group, I examined the relationship between Aβ1-40 and Aβ1-42 and the percentage of time spent in the open arms during the test. In 5xFADPrnp^{+}/$^{+}$ mice, I found a significant negative correlation between Aβ1-40 and anxiety levels. The graph shows that the higher levels of Aβ1-40 were associated with

the decrease of anxiety-like behavior. Similarly, there was a significant negative correlation between Aβ1-42 levels the anxiety levels, higher levels of Aβ1-42 were correlated with the decrease of anxiety-like behavior. In 5xFADPrP$^{-/+}$ mice, I observed a significant negative correlation between Aβ1-40 and anxiety levels, the higher levels of Aβ1-40 were significantly correlated with the decrease of anxiety-like behavior. The correlation between Aβ1-42 and anxiety levels in 5xFADPrP$^{-/+}$ was not statistically significant. In 5xFADPrnp$^{-/-}$ mice group, I found no significant correlation between Aβ1-40 and anxiety-levels. Likewise, there was no significant correlation between Aβ1-42 and anxiety levels.

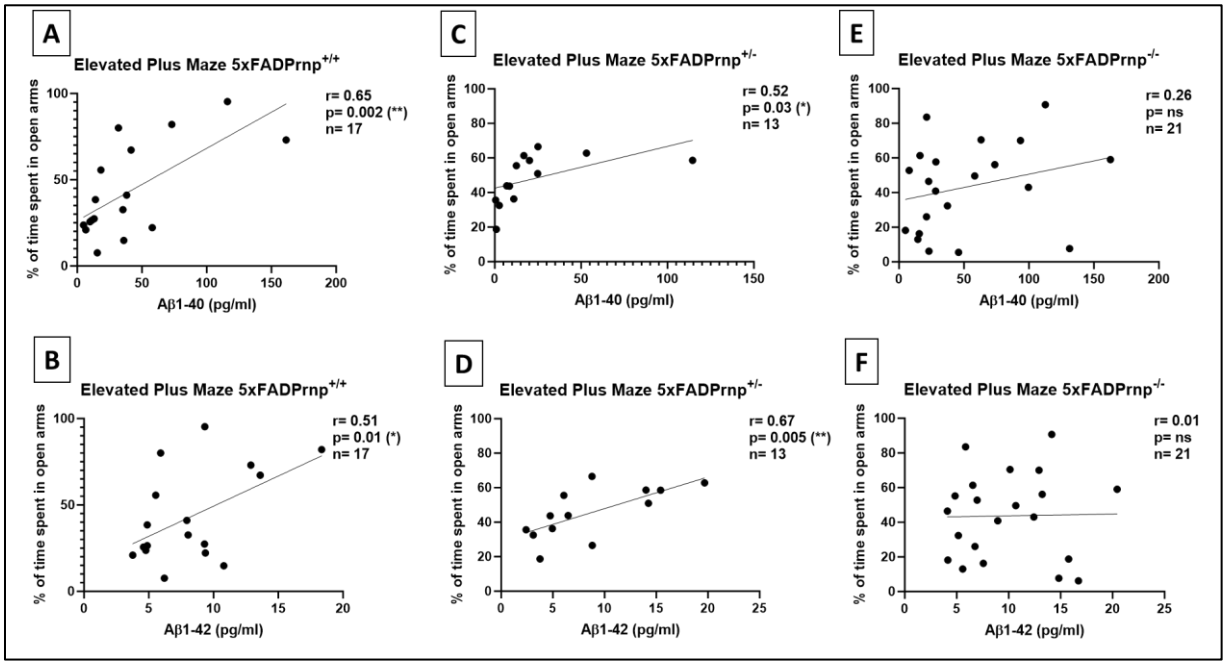

Figure 21 - Correlation between Aβ1-40 and Aβ1-42 levels and the percentage of time spent in the open arms. (A) Correlation between Aβ1-40 and the percentage of time spent in the open arms in 5xFADPrnp$^{+/+}$ mice. The graph shows a significant positive correlation (r= 0.65) between Aβ1-40 levels and the time spent in the open arms(*p=0.016). **(B)** Correlation between Aβ1-42 and the percentage of time spent in the open arms in 5xFADPrnp$^{+/+}$ mice. The result reveals a significant positive correlation (r= 0.51) between Aβ1-42 levels and the time spent in the open arms (*p=0.01). **(C)** The graph depicts the correlation between Aβ1-40 levels and the time spent in the open arms. A significant positive correlation is observed (r= 0.52, *p=0.03). **(D)** Correlation between Aβ1-42 levels and the time spent in the open arms arms, a significant positive correlation was observed (r=0.67, **p=0.005). **(E-F)** The graphs represent the correlation between Aβ1-42 levels and the time spent in the open arms. In both cases, there was no significant correlation between the Aβ1-42 levels and the time spent in the open arms.

5.3. Motor performance and Aβ1-40 and Aβ1-42 levels

To evaluate the potential correlation between Aβ1-40 and Aβ1-42 levels and motor performance, I conducted our analysis using the rotarod test in the different transgenic mice groups and their Aβ levels measured by ELISAs (Figure 22). Our findings revealed a significant and negative correlation between Aβ1-40 levels and motor performance in the 5xFADPrnp^{+}/$^{+}$, 5xFADPrP^{-}/$^{+}$ and 5xFADPrnp^{-}/$^{-}$ mice models. In these mice, higher levels of Aβ1-40 were significantly correlated with impaired motor performance on rotarod task. Similarly, Aβ1-42 levels in the 5xFADPrnp^{+}/$^{+}$ and 5xFADPrP^{-}/$^{+}$ mouse models also showed significant negative correlation with the motor performance. The elevated Aβ1-42 levels were significantly correlated with to poorer motor performance. In 5xFADPrnp^{-}/$^{-}$ mouse, I did not find a significant correlation between Aβ1-42 levels and the motor performance.

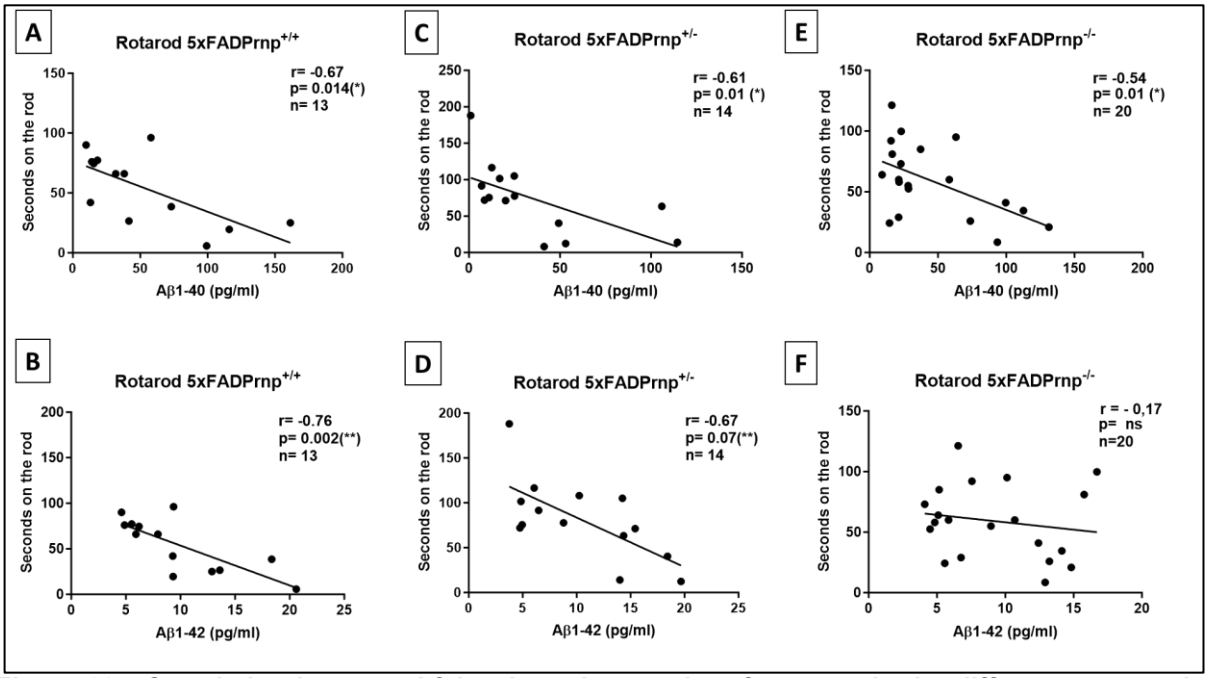

Figure 22 - Correlation between Aβ levels and rotarod performance in the different transgenic mice models. The graph **(A)** shows the correlation between Aβ1-40 and the time spent on the rod in 5xFADPrnp^{+}/$^{+}$. There is a significant negative correlation between Aβ1-40 levels and the time spent on the rod (r= -0.67, **p*=0.014). Higher levels of Aβ1-40 correlate with less time on the rod. **(B)** correlation between Aβ1-42 and the time spent on the rod in 5xFADPrnp^{+}/$^{+}$. The results show a significant negative correlation between the Aβ1-42 and the time spent on the rod (r= -0.76, ***p*=0.002). The higher levels of Aβ1-42 are associated with less time spent on the rod. **(C)** The graph depicts a significant negative correlation between Aβ1-40 levels and time on the spent performing on the rod (r= -0.61, **p*= 0.01) in 5xFADPrP^{-}/$^{+}$. Higher levels of Aβ1-40 correlate with less time performing on the rod. **(D)** The graph presents a significant negative correlation between Aβ1-42 and the time spent on the rod (r= -0.54,

*p=0.0.) in 5xFADPrP$^{-/+}$. **(E)** The graph displays a significant negative correlation between Aβ1-40 levels and the time that the mice spent performing on the rod (r= -0.54, *p=0.01) in 5xFADPrnp$^{-/-}$. Higher levels of Aβ1-40 are associated with reduced time on the rod. **(F)** The graph shows no significant correlation between Aβ1-42 and the time spent on the rod in 5xFADPrnp$^{-/-}$ mice.

5.4. Associative learning and Aβ1-40 and Aβ1-42 levels

In this study, I evaluated the correlation between Aβ1-40 and Aβ1-42 levels and the associative learning skills in different mice models (Figure 23). In 5xFADPrnp$^{+/+}$, the analysis between Aβ1-40 levels and the associative learning showed a significant negative correlation, the higher level of Aβ1-40 was associated with impaired associative learning skills of the animals. Similarly, in 5xFADPrnp$^{+/+}$, the correlation between Aβ1-42 levels and the associative learning was also significantly negative, higher levels of Aβ1-42 were linked with the associative learning impairment. In opposite, in 5xFADPrP$^{-/+}$ and 5xFADPrnp$^{-/-}$, I did not find any significant correlation between Aβ1-40 and Aβ1-42 levels and their associative learning skills. The Aβ levels were not correlated with their associative learning performance.

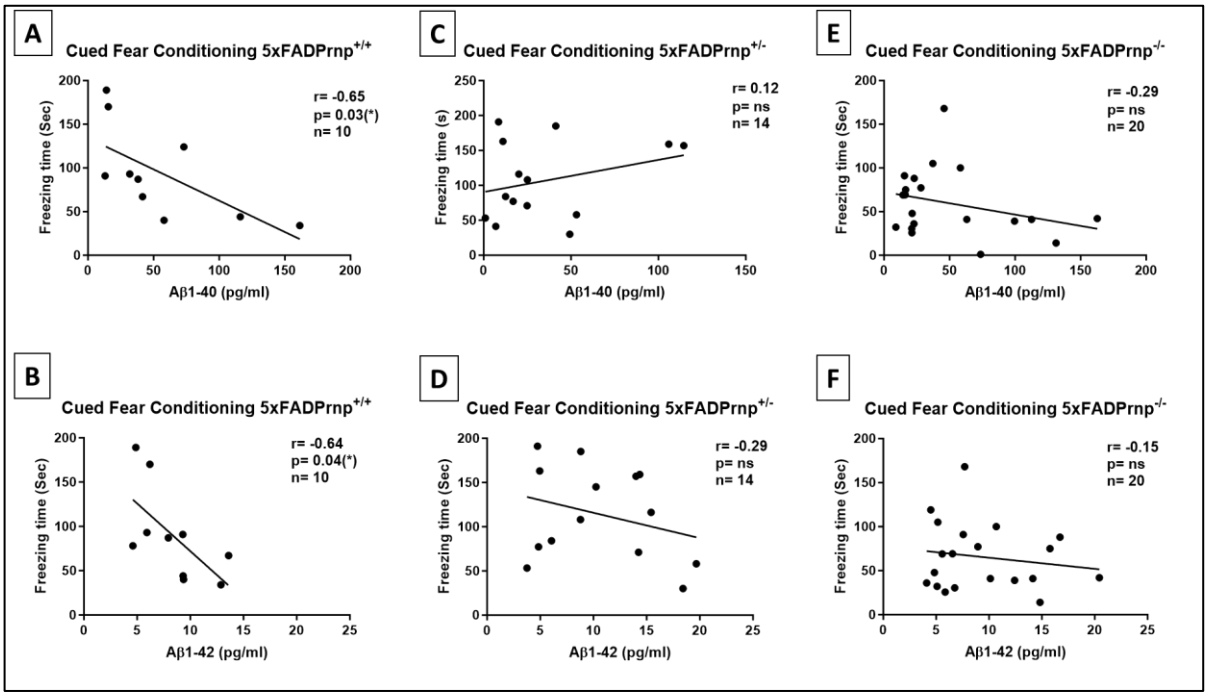

Figure 23 – Correlation between Aβ levels and freezing time in the cued fear conditioning. (A) This graph shows a significant correlation between Aβ1-40 and the freezing time in 5xFADPrnp$^{+/+}$ (r= -0.65, *p= 0.03). The higher amount of Aβ1-40 the reduced freezing time. **(B)** This graph demonstrates the significant negative correlation between Aβ1-42 and the freezing time in the cued fear conditioning

test in 5xFADPrnp$^{+/+}$ (r= -0.64, *p=0.04). **(C)** In this graph, there is no significant correlation between Aβ1-40 levels and the mice freezing time in 5xFADPrP$^{-/+}$. **(D)** This graph depicts no significant correlation between Aβ1-42 levels and the freezing time in in 5xFADPrP$^{-/+}$. **(E)** In this graph, there is no significant correlation between Aβ1-40 levels and the freezing time in 5xFADPrnp$^{-/-}$. **(F)** This graph reveals no significant correlation between Aβ1-42 levels and the freezing time in 5xFADPrnp$^{-/-}$.

6. Detection and quantification of Aβ plaques in different brain regions via 3D-microscopy

The present study employed the light sheet microscopy in combination with QUINT workflow to investigate the Aβ deposition in the different structures of the brain. This approached allowed the visualization and quantitative analyses of Aβ plaques in different brain regions in a three-dimension-context in both 5xFADPrnp$^{+/+}$ (Figure 24) and 5xFADPrnp$^{-/-}$ (Figure 25) mice models at 8 months of age.

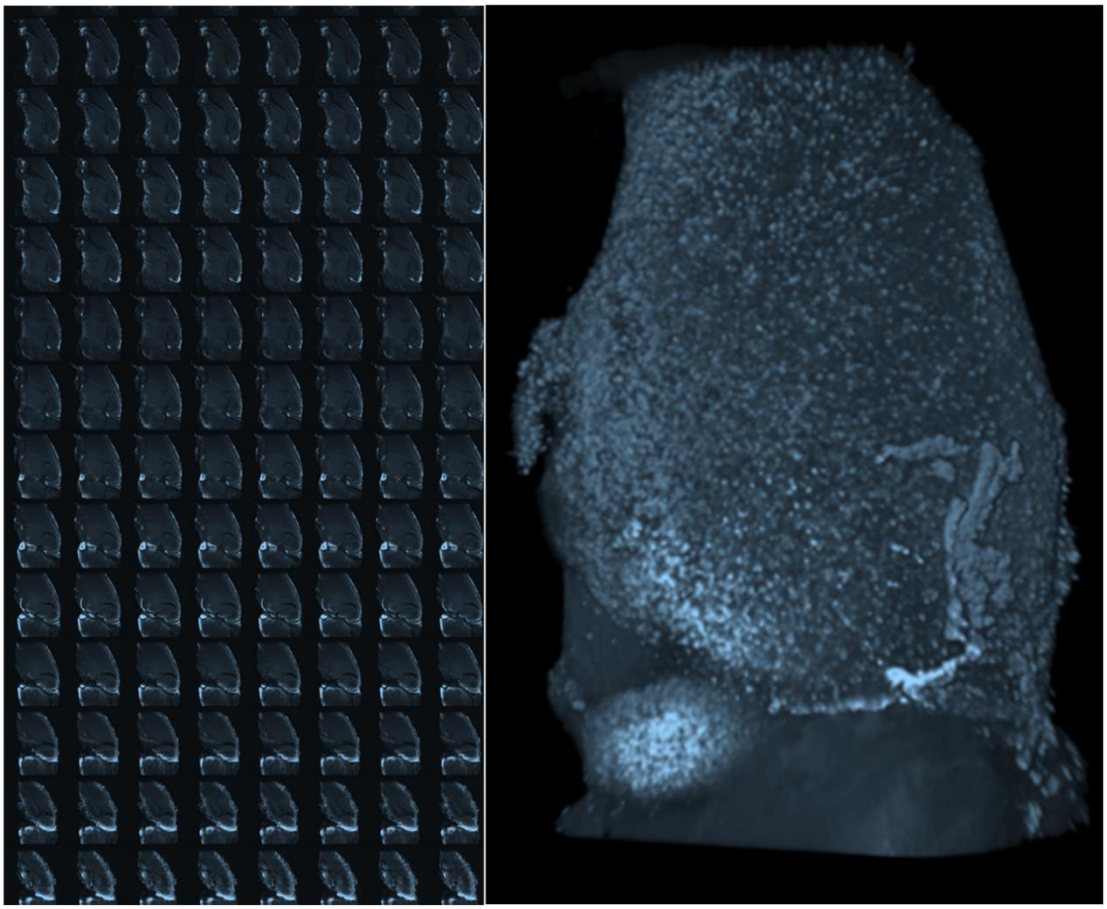

Figure 24 - Serie of images from a 5xFADPrnp$^{+/+}$ mouse brain and 3D reconstruction. Series of images acquired through Ultramicroscope II and 3D reconstruction of the image series through Fiji.

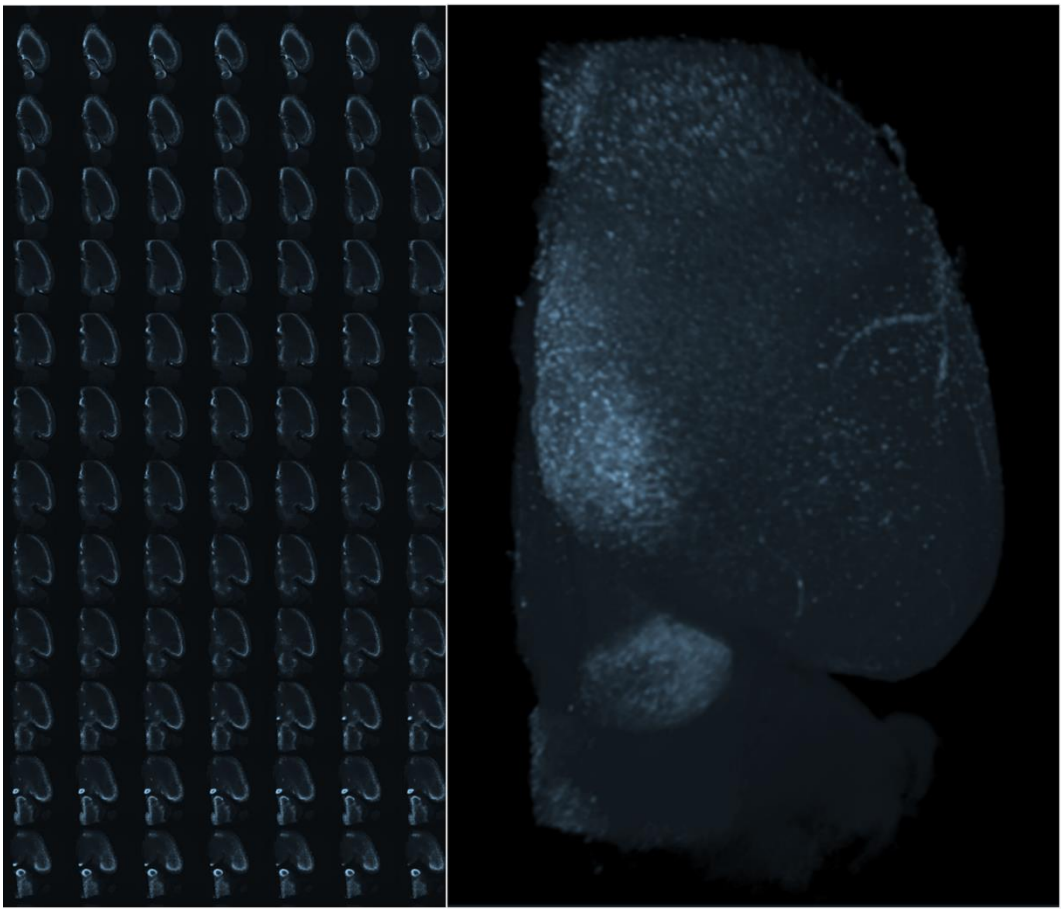

Figure 25 - Serie of images from a 5xFADPrnp$^{-/-}$ mouse brain and 3D reconstruction. Series of images acquired through Ultramicroscope II and 3D reconstruction of the image series through Fiji.

6.1.3-D imaging of Aβ plaque distributions load in different brain regions of 5xFADPrnp$^{+/+}$

In the 5xFADPrnp$^{+/+}$ mice brains, the analyses of Aβ plaques load across different regions revealed distinctive patterns (Figure 26). A widespread deposition of Aβ plaques is evident across diverse brain areas. Among these regions, the cortex, olfactory area, and hippocampus stand out with the higher Aβ plaques load (Figure 27). Following these very high-load-regions, hypothalamus, thalamus and mid-hind-medulla exhibit a notable high load of Aβ plaques. The brain regions such as fibre tracts, striatum and palladium, and ventricular system displayed lower plaque load comparatively to the previous described regions.

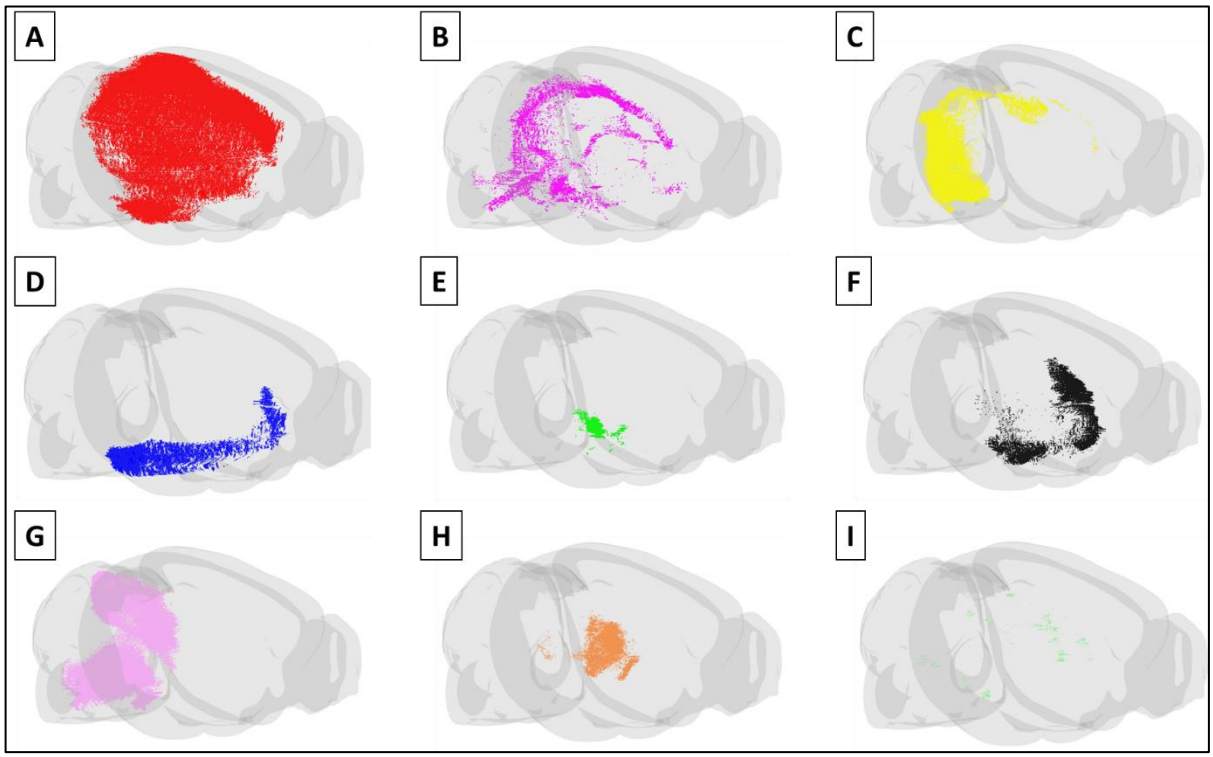

Figure 26 - 3-D imaging of Aβ -–plaque distribution in different brain regions of 5xFADPrnp^{+}/$^{+}$ mice brains. In this figure, the distribution of Aβ -plaques in 5xFADPrnp^{+}/$^{+}$ mice brains is depicted. Each labelled region corresponds to a specific brain area analysed for Aβ -plaque load: **(A)** Cortex, **(B)** Fibre tracts, **(C)** Hippocampus, **(D)** Olfactory areas, **(E)** Hypothalamus, **(F)** Striatum and Palladium, **(G)** Mid-Hind Medulla, **(H)** Thalamus and **(I)** Ventricular system.

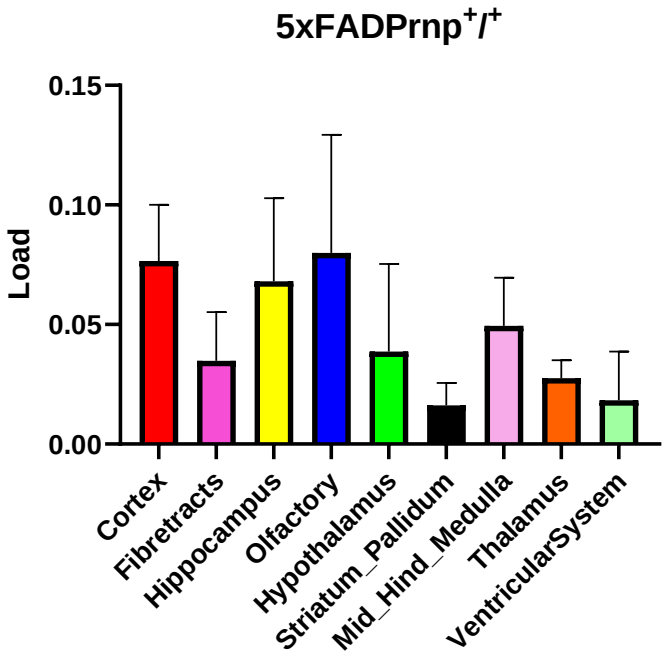

Figure 27 – Quantitative Aβ -plaque load in 5xFADPrnp^{+}/$^{+}$ mice brain regions. The graph presents the Aβ -plaque load measurements for the different brain regions. The following values present an

average Aβ-plaques load for each region: cortex (0.076), fibre tracts (0.034), hippocampus (0.068), olfactory bulb (0.07999), hypothalamus (0.038), striatum and palladium (0.016), mid-hind medulla (0.049), thalamus (0.0275), and ventricular system (0.0182).

6.2.3 3-D imaging of Aβ plaque distribution in different brain regions of 5xFADPrnp$^{-/-}$

The analyses of Aβ plaques revealed a widespread distribution throughout the 5xFADPrnp$^{-/-}$ mice brains after 8 months (Figure 28). Predominant Aβ-plaques deposition was observed in cortex, followed by the olfactory areas and hippocampus. Subsequently, the hypothalamus and mid-hind medulla manifested moderate plaque load. The fibre tracts, ventricular system, thalamus, and striatum and pallidum presented the areas with lower load of Aβ-plaques in comparison with the previous described areas (Figure 29).

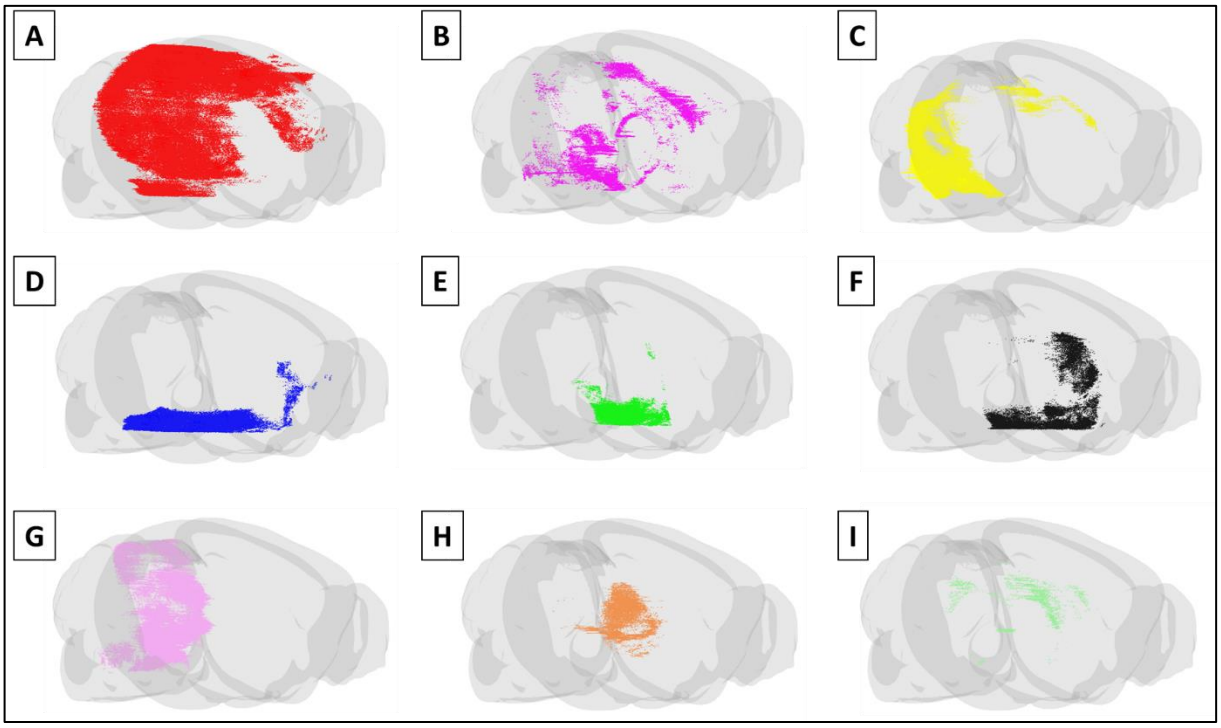

Figure 28 – 3-D imaging of Aβ-plaques in 8 months old 5xFADPrnp$^{-/-}$ mice brains. In this figure, the distribution of Aβ -plaques in 5xFADPrnp$^{-/-}$ mice brains is depicted (n=3). Each labelled region corresponds to a specific brain area analysed for Aβ -plaque load: **(A)** Cortex, **(B)** Fibre tracts, **(C)** Hippocampus, **(D)** Olfactory areas, **(E)** Hypothalamus, **(F)** Striatum and Palladium, **(G)** Mid-Hind Medulla, **(H)** Thalamus and **(I)** Ventricular system.

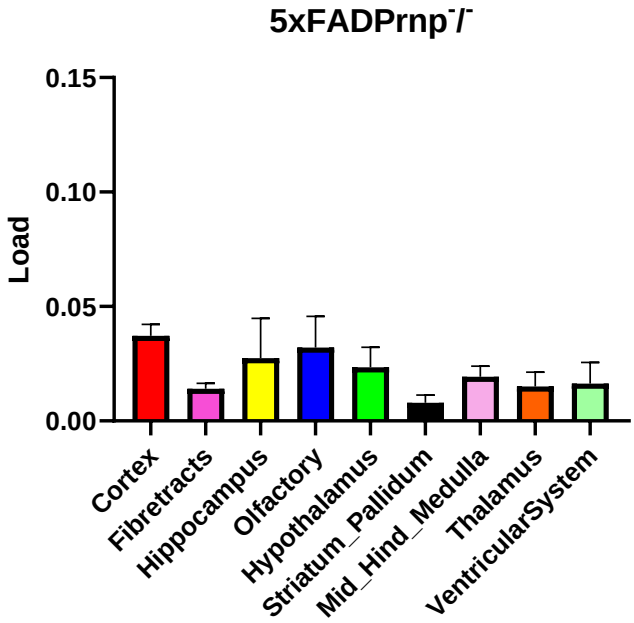

Figure 29 - **Quantitative Aβ-plaques load in 5xFADPrnp$^{-/-}$ mice brain regions.** The graph presents the Aβ-plaque load measurements for the different brain regions (n=3). The following values present an average Aβ-plaques load for each region: cortex (0.037), fibre tracts (0.014), hippocampus (0.027), olfactory areas (0.032), hypothalamus (0.023), striatum and palladium (0.007), mid-hind medulla (0.019), thalamus (0.015), and ventricular system (0.0163).

6.3. Comparison of Aβ-plaque load in different brain region of 5xFADPrnp$^{+/+}$ and 5xFADPrnp$^{-/-}$

In order to discern potential differences in the Aβ-plaque load between 5xFADPrnp$^{+/+}$ and 5xFADPrnp$^{-/-}$ mice brains at 8 months of age, Aβ-plaque load in the different brain regions were statistically analyzed (Figure 30). In the 5xFADPrnp$^{+/+}$ mice, the cortex exhibits a statistically significant higher load of Aβ-plaques in comparison with the cortex load of Aβ-plaques in 5xFADPrnp$^{-/-}$. Similar trend continues in the fibre tracts, hippocampus, olfactory areas, hypothalamus, mid-hind medulla, thalamus, and striatum and pallidum, where 5xFADPrnp$^{+/+}$ mice present a higher load of Aβ-plaques in comparison with the same regions in 5xFADPrnp$^{-/-}$, albeit without statistical significance. 5xFADPrnp$^{+/+}$ and 5xFADPrnp$^{-/-}$ mice present a relatively similar Aβ-plaques load in the ventricular system.

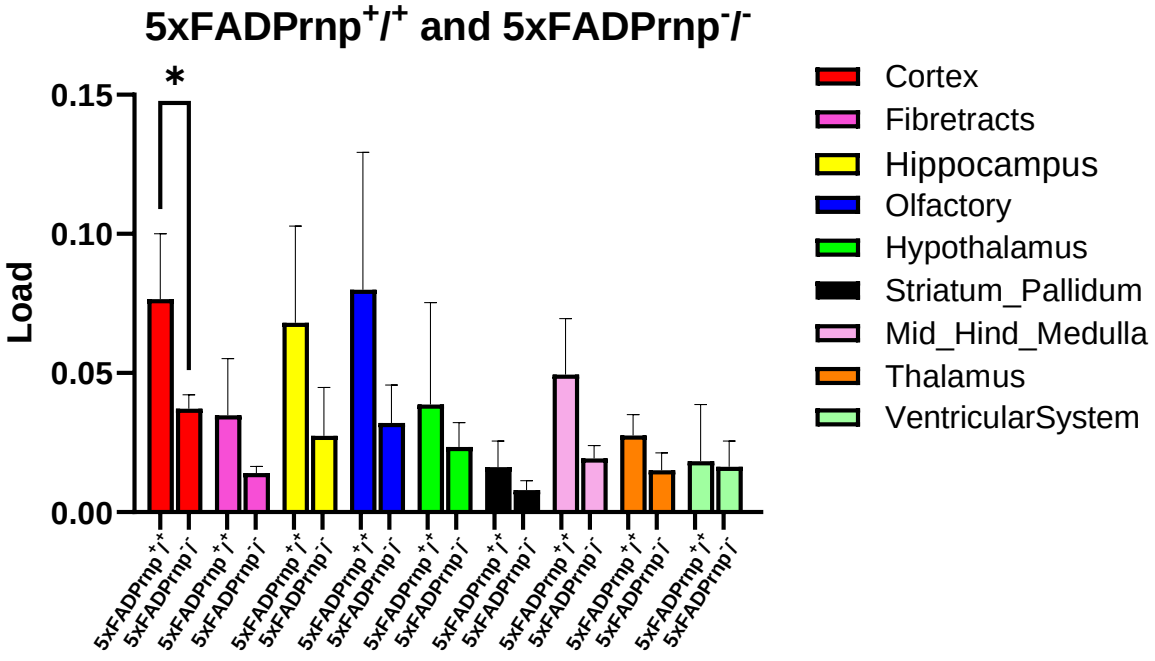

Figure 30 – Comparison of Aβ-plaque distribution in the different brain regions of 5xFADPrnp$^{+/+}$ and 5xFADPrnp$^{-/-}$. The graph depicts the Aβ-plaques load comparison across distinct brain regions in two different mouse lines (n=3): 5xFADPrnp$^{+/+}$ and 5xFADPrnp$^{-/-}$. In the cortex, 5xFADPrnp$^{+/+}$ demonstrate a significant higher load of Aβ-plaques in comparison with 5xFADPrnp$^{-/-}$ (*p= 0.04). The other brain regions do not show statistically significant differences in terms of Aβ-plaques load.

7. Exploration of a putative interaction partner of PrP^{C} relevant in AD

To better understand the mechanism of PrP^{C}-Aβ oligomers internalization by the cells, I search for proteins closely co-located with PrP^{C}. PrP^{C} is enriched within caveolae [96], where Cav-1 serves as the predominant protein component, contributing to processes such as signaling transduction, lipid trafficking, and endocytosis.[97] This prompted an exploration of potential association between PrP^{C} and Cav-1.

7.1. Caveolin-1 interaction with PrP^{C} and Aβ

In this study, I employed the SPR to investigate the potential interactions between Caveolin-1 (Cav-1) and Aβ1-40, and Aβ1-42 (Figure 31). Through SPR analysis, I

quantitatively assessed the binding characteristics of these interactions by calculating the equilibrium dissociation constant (KD). Our SPR analysis revealed a specific and stable direct-interaction between Cav-1 and Aβ1-40 at both concentrations tested (10µg/mL and 20µg/mL). The sensorgrams obtained from these experiments displayed concentration-dependent binding, indicating stronger interaction with higher concentrations of Aβ1-40. Similarly, the SPR analysis between Cav-1 and Aβ1-42 demonstrated a robust and specific interaction at both Aβ1-42 concentrations (10µg/mL and 20µg/mL), also displaying concentration-dependent binding responses.

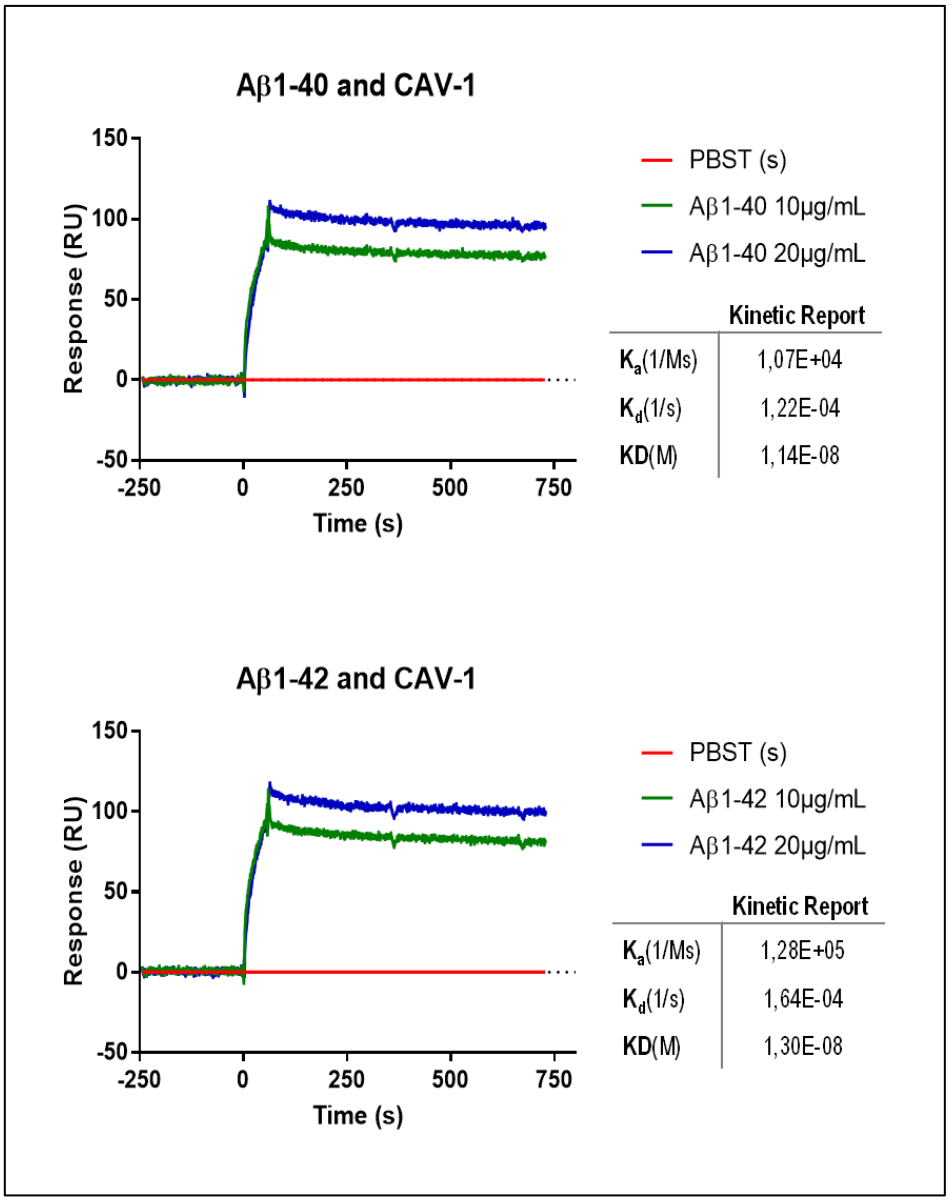

Figure 31 – SPR sensorgrams of Cav-1 and Aβ1-40 and Cav-1 and Aβ1-42. The SPR sensorgrams display the results of the binding affinity experiments between Cav-1 and Aβ1-40 and Cav-1 and Aβ1-42. The determined equilibrium dissociation constants of these interactions were 1.14E-08 for Aβ1-40 and 1.30E-08 for Aβ1-42.

Additionally, I wanted to investigate the potential interaction between Cav-1 and PrP^C by SPR. The SPR analysis revealed a significant and strong interaction between Cav-1 and PrP^C at both tested concentrations (10µg/mL and 20µg/mL). The binding response displayed a concentration-dependent behaviour, with more pronounced interaction observed at higher PrP^C concentration (Figure 32).

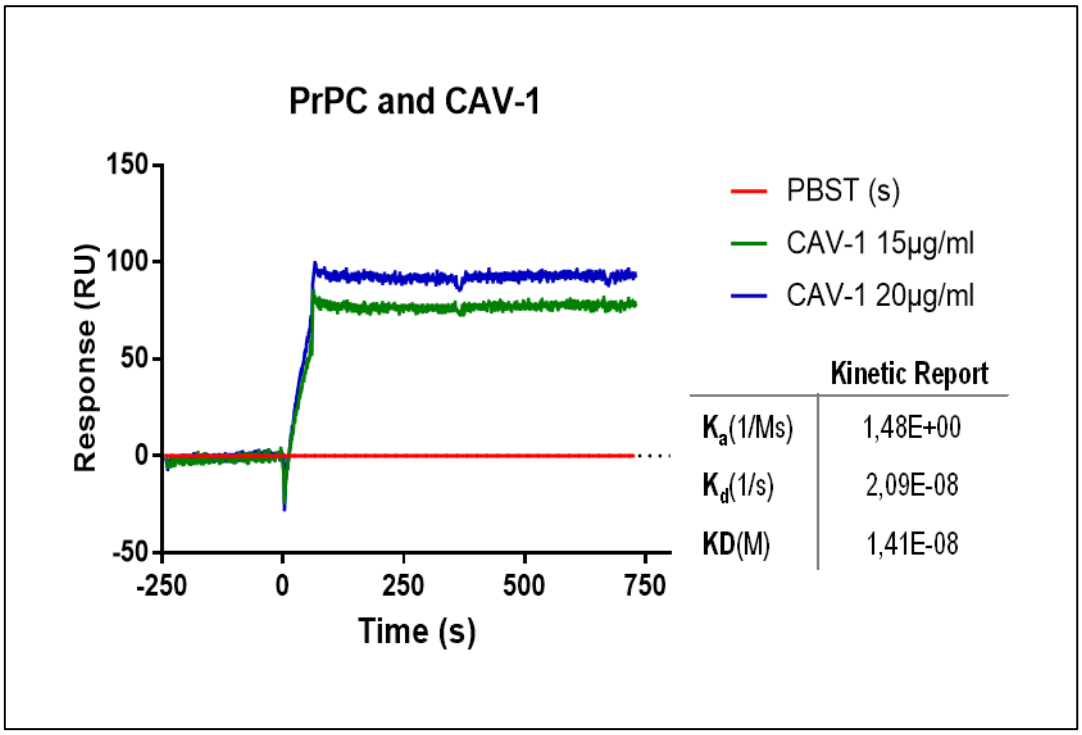

Figure 32 – SPR of Cav-1 and PrP^C. The SPR sensorgram illustrates the binding response between Cav-1 and PrPC with an equilibrium dissociation constant of 1.41E-08.

7.2. Caveolin-1 influence on Aβ uptake on primary neurons

Following the SPR interaction confirmation between Cav-1 with PrP^C, Aβ1-40, and Aβ1-42, I treated WT and Cav-1 knockout primary neurons with Aβ1-40, and Aβ1-42 oligomers overnight. Using Aβ1-40 and Aβ1-42 ELISAs, I quantified the levels of Aβ1-40, and Aβ1-42, respectively, on the neuron's lysates. The analyses revealed a significant reduction in Aβ1-40 (65% less) and Aβ1-42 (25% less) levels in Cav-1 knockout neurons compared to WT neurons (Figure 33).

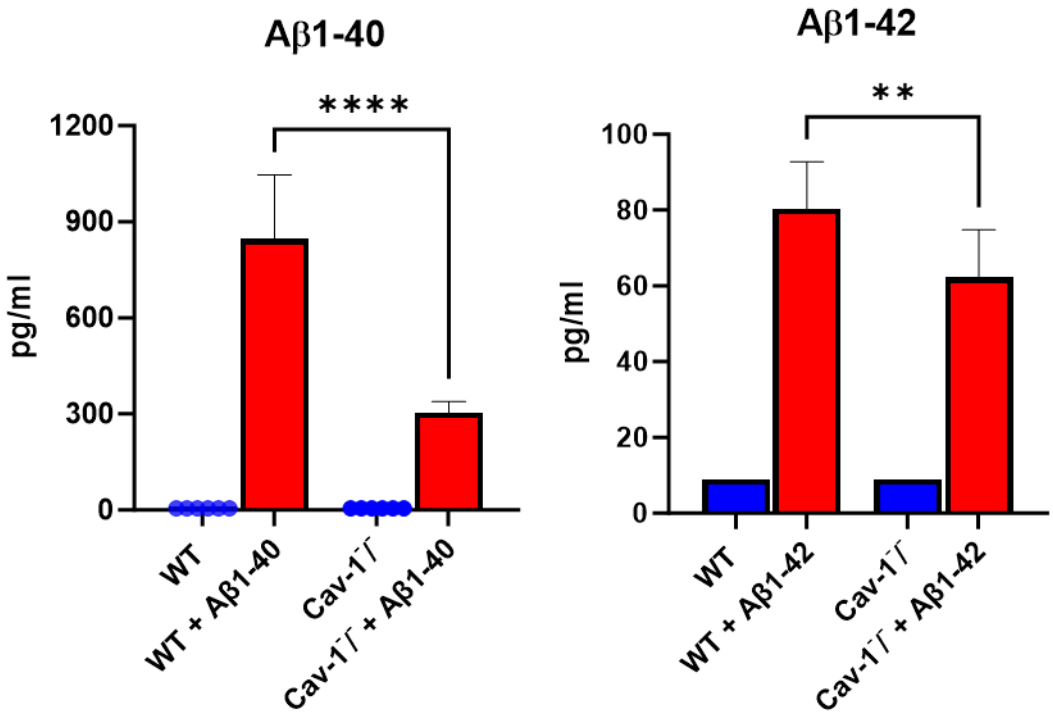

Figure 33 -Analyses of Aβ levels in WT and Cav-1 KO primary neurons. ELISA Quantification of Aβ1-40 and Aβ1-42 in WT and Cav-1 primary neurons (n=12). **(A)** The Aβ1-40 quantification revealed a significant decrease of Aβ1-40 levels in Cav-1 KO neurons in comparison with WT neurons (****p<0.0001). **(B) The statistical analyses of** Aβ1-42 levels showed a significant decrease of the Aβ1-42 levels in Cav-1 KO neurons compared to WT neurons (**p= 0.0017).

VI. Discussion

Alzheimer's disease is the leading cause of dementia and is rapidly becoming one of the most expensive, deadly, and challenging disease of this century. Since age is the main risk factor of dementia, the ongoing rise in life expectancy and the aging of the population also raise the chances of individuals developing this condition.[98,99] The pathophysiological mechanisms of AD continue to be a topic of debate. The primary theory places Aβ accumulation as the central event in this process, commonly known as the "amyloid cascade hypothesis". [25] Aβ oligomers are thought to exert harmful effects on the synapses, in part, through their interaction with cell surface receptors.[55] PrP^C emerged as the kye receptor for the Aβ oligomers induced toxicity.[68] However, the role of PrP^C in AD remains a subject of debate and ongoing research.

The aim of this thesis is to conduct a comparative analysis to discern the effects of the presence and absence of PrP^C on the progression and pathology of AD, with a specific focus on Aβ uptake and deposition, and cognitive impairment, through behavioral, biochemical and histological analysis to provide valuable insights into the complex interplay between PrP^C and Aβ.

1. In *vitro* studies of PrP^C-mediated toxicity of Aβ

1.1. Interaction studies: PrP^C has higher binding affinity with Aβ1-42 than with Aβ1-40

The SPR analyses enables the determination of the binding-characteristics of the interactions between PrP^C and two Aβ peptides, Aβ1-40 and Aβ1-42, both implicated in AD pathology. [100] The results obtained from the experiments demonstrated a stable and direct interaction between PrP^C and Aβ1-40 and Aβ1-42, at different concentrations. Moreover, in our analyses, the calculated KD value revealed a stronger binding affinity between PrP^C and Aβ1-42 (KD= 1.13E-08 M) compared to PrP^C and Aβ1-40 (KD= 2.88E-08 M). These interaction distinctions may have functional implications, as Aβ1-42 is known to me potentially more neurotoxic than Aβ1-40 [101], suggesting that PrP^C may be a contribute to a great neurotoxicity in AD. Our findings are confirmed by previous researchers, suggesting PrP^C as high-affinity receptor for

Aβ oligomers, demonstrated through different methods, including co-immunoprecipitation, SPR (KD ≤ 2.0E-8 M) and immunochemistry.[68,75,102–105] These studies provided the indication that the critical amino acid binding sequence for Aβ1-42 oligomers is found in the N-terminal residues 23-27 and the 95-110 region of PrP^C , using cells with deleted regions of PrP^C and targeting PrP^C with epitope specific antibodies. [68,102–104]

While these previous studies have been primarily focused on examining the interaction between PrP^C and Aβ1-42 oligomers, often referred as ADDL (Aβ-derived diffusible ligands), our research incorporated Aβ1-40 into the investigation of the PrP^C – Aβ interaction. I aimed to explore whether both Aβ1-40 and Aβ1-42 oligomers share the same receptor, PrP^C, and discern their binding characteristics, shedding light on their similarities and common mechanisms in AD pathology.

1.2. Establishment of a cell model to explore the uptake of Aβ

1.2.1. Aggregation protocol for Aβ: Exploration of protofibril formation through oligomer incorporation

Following the Aβ oligomerization protocol (see material), I proceeded with TEM imaging that provides high-resolution images, allowing to visualize the detailed structure of Aβ aggregates, this level of detail is important for understanding their morphology and arrangement. I conducted this experiment with the primary objective of controlling the aggregation state of Aβ prior administering it to the cells (primary and secondary cell lines). Controlling the aggregation state of Aβ is crucial for ensuring precise and controlled conditions during our cell treatments. The results obtained following the incubation of Aβ peptides Aβ1-40 and Aβ1-42 in two different time points provided insights into the oligomerization and protofibril formation. At 12 hours of incubation at 4°C, Aβ1-40 oligomers had an average size of approximately 170 nm, while Aβ1-42 oligomers were slightly smaller, around 136 nm. With extended incubation of 24 hours at 4°C, both Aβ1-40 and Aβ1-42 oligomers increased in size. Aβ1-40 oligomers reached an average size of approximately 197 nm, while Aβ1-42 oligomers grew to approximately 253 nm. These observations are consistent with the existing literature, which portrays that Aβ1-42 has a greater propensity for aggregation.

[106] Importantly, the 24 hours incubation revealed the formation of protofibrils by oligomer incorporation in both Aβ1-40 and Aβ1-42 incubations. These findings support the nucleation-dependent polymerization mechanism. This mechanism requires seeding to gradually build up larger structures through incorporation of additional Aβ molecules. [107] These finding emphasize the significance of the oligomer's incorporation on the formation of protofibrils.

To further investigate the mutual interactions between PrP^C and oligomeric Aβ, I treated two different cell lines, SH-SY5Y^{WT}, characterized by low endogenous PrP^C expression, and stable transfected SH-SY5Y^{PrPC} cells, which exhibit approximately a 5-fold higher level of PrP^C expression. Following treatment with Aβ1-40 and Aβ1-42 oligomers, I observed a significant increase in fluorescence signal in cell overexpressing PrP^C for both Aβ1-40 and Aβ1-42 oligomers, compared to cells with normal PrP^C expression. Moreover, our co-localization analysis revealed that the extend of overlap between PrP^C and both Aβ oligomers remained consistent between both cell lines. These findings suggest a high-affinity and specific binding between PrP^C and Aβ1-40 and Aβ1-42 oligomers, in line with our results from SPR experiments, and that PrP^C involvement in Aβ oligomer binding is consistent, regardless of whether PrP^C is overexpressed or expressed at normal levels. In prior study using hippocampal neurons and COS-7 cells that express PrP^C, the researchers found the PrP^C and Aβ1-42 oligomers interaction through immunostaining.[108] However, our study builds upon prior research by providing more comprehensive examination of the PrP^C-Aβ oligomers interaction, using distinct PrP^C expression cell lines with the focus on PrP^C levels, the inclusion of Aβ1-40, and the consistency of PrP^C-Aβ oligomers binding.

To gain insights into PrP^C-Aβ oligomers binding and potential uptake, I proceeded with ELISAs assays to quantify the Aβ1-40 and Aβ1-42 levels in the cell's lysates. When comparing the two cell lines, cells overexpressing PrP^C exhibited significantly higher levels of both Aβs (>200% more) compared with cells with normal physiological expression of PrP^C. Indicating that PrP^C may play a pivotal role in the Aβ oligomers internalization by the cell. Our findings are in accordance with prior research that found PrP^C and Aβ1-42 co-internalize in SH-SY5Y cell line, detected by co-localization with subcellular markers and dot-blot [109–111][110,111], reinforcing the concept that PrP^C serves as a high-affinity receptor and facilitator of Aβ uptake.

In our study, by employing quantitative approach and expanding our investigation to include Aβ1-40, I provided evidence of PrP^C pivotal role in facilitating Aβ internalization by the cell, implying that it may serve as key player in the process by which intracellular Aβ accumulates. This Intracellular accumulation of Aβ it is believed to play an early role in AD pathogenesis. [112–114] Therefore, PrP^C might be a crucial target candidate in AD therapeutics.

2. In *vivo* studies of PrP^C-mediated toxicity of Aβ

2.1. Establishment of an in vivo model to study the role of PrP^C in AD

In this project, I aimed to shed light on the role of PrP^C in AD in *vivo*. To address this, I employed different mice models with differing PrP^C expression levels, both with and without 5xFAD mutations. WB analyses of brain homogenates were conducted to validate the generation of specific mouse models at protein level, which had been previously confirmed via PCR. Mice with normal physiological PrP^C expression (WT and 5xFADPrnp$^{+/+}$) displayed strong PrP^C bands, while heterozygotes for PrP^C (Prnp$^{-/+}$and 5xFADPrnp$^{-/+}$) exhibited a noticeable decrease in band signal. PrP^C knockout mice (Prnp$^{-/-}$ and 5xFADPrnp$^{-/-}$) showed a complete absence of bands. Mice carrying the 5xFAD mutations (5xFADPrnp$^{+/+}$, 5xFADPrnp$^{-/+}$, and 5xFADPrnp$^{-/-}$) showed a significant increase in APP expression in comparison to mice without the 5xFAD mutations (WT, Prnp$^{-/+}$, and Prnp$^{-/-}$). This characterization of the mice lines ensures that the intended genetic modifications have been accurately introduced into the mice, providing confidence in the reliability and validity of subsequent experiments.

2.2. Expression level of PrP^C in 5xFAD mice depending on aging

2.2.1. PrP^C expression decreased in heterozygotes and remains unaffected by aging and 5xFAD mutations in mice models

To quantify the PrP^C expression differences between animals exhibiting the normal physiological levels of PrP^C and those with heterozygous for PrP^C expression, I utilized an ELISA assay. The ELISA analyses demonstrated a significant decrease in the PrP^C

expression in heterozygous groups (Prnp$^{-/+}$ and 5xFADPrnp$^{-/+}$), compared to the wild type groups for PrP^{C} (WT and 5xFADPrnp$^{+/+}$). This analysis did not show any significant difference in PrP^{C} expression between the WT mice and 5xFADPrnp$^{+/+}$, and between Prnp$^{-/+}$ and 5xFADPrnp$^{-/+}$. Investigating the association between PrP^{C} levels and aging revealed that in both 5xFADPrnp$^{+/+}$ and 5xFADPrnp$^{-/+}$ groups, there was no significant correlation between the PrP^{C} levels and age. The PrP^{C} levels remained constant during the aging process. Indicating that age has no substantial impact on the PrP^{C} expression in these mice models.

These findings suggest that the presence of the 5xFAD mutations alone does not significantly affect PrP^{C} levels. There is some inconsistency in studies investigating PrP^{C} expression levels in AD. Some research in mice indicates an initial increase in PrP^{C} expression during early AD stages followed by a decrease in later stages.[115] Other studies in humans, suggested a tendency toward lower PrP^{C} expression in AD compared to healthy individuals.[116,117] In contrast, there are studies that find no significant differences in PrP^{C} expression between AD patients and healthy controls.[118–120] Interestingly, our data is in accordance with a study that found no altered PrP^{C} expression in familiar AD patients.[117] The variation in these studies could be attributed to many factors as limitations in the assay specificity for the prion protein, and the presence of post-translational modifications of PrP^{C} that may interfere with accurate PrP^{C} quantification.[121]

Similar to our results, other studies found that PrP^{C} levels tend to remain constant during aging in mice.[122–124] However, contradictive reports have suggested that aging may indeed impact PrP^{C} expression and degradation in mice. These reports propose that PrP^{C} expression rises with age while its degradation declines.[125] It has been noted that these results discrepancies could be attributed to the absence of proper normalization procedures, and comprehensive statistical analyses.[126]

2.2.2. Age-related Aβ levels in mice carrying 5xFAD mutations dependent of PrP^{C}

The accumulation of Aβ in the brain is a central pathological hallmark of AD. In this study, I conducted ELISA assays on mice brain homogenates to access the influence

of PrP^C in Aβ levels in 5xFADPrnp$^{+/+}$, 5xFADPrnp$^{-/+}$, and 5xFADPrnp$^{-/-}$ mice groups during aging. Our findings revealed a strong positive correlation between Aβ1-40 and Aβ1-42 levels and aging in all three groups. Notably, the different levels of PrP^C did not influence the correlation between aging and Aβ levels in these mice brains. In order to investigate potential differences in Aβ levels among the three distinct groups, I selected the 9 months old animals as the subjects for comparing their Aβ1-40 and Aβ1-42 levels. Interestingly, 5xFADPrnp$^{-/-}$ group, lacking PrP^C demonstrated a significant decrease (around 50% less) in both Aβ1-40 and Aβ1-42 levels compared to the groups expressing normal physiological levels of PrP^C. These findings indicate a potential role of PrP^C in Aβ generation. In a recent study focusing on prostate and colon cancer, it was found that PrP^C plays a significant role in controlling the levels of Aβ in these cancer cells. The study revealed that PrP^C influences the expression of APP mRNA and BACE1 mRNA, resulting in an increase in the production of Aβ.[127] Additionally, other study reported that overexpressing PrP^C resulted in increased cleavage of APP.[128] However, the role of PrP^C in increasing Aβ levels is still a topic of debate, as several studies in mice and humans have reported a negative correlation between PrP^C and Aβ levels.[129–132] Nevertheless, our data aligns with the notion that PrP^C contributes to increased Aβ production.

2.3. Lifespan and the grade of Aβ-induced behavioral deficits correlate with the concentration of PrP^C

2.3.1. PrP^C expression reduces the lifespan in mice carrying 5xFAD mutations

To explore the impact of PrP^C on the longevity of mice, I monitored their survival of WT, 5xFADPrnp$^{+/+}$, Prnp$^{-/+}$, 5xFADPrnp$^{-/+}$, Prnp$^{-/-}$, and 5xFADPrnp$^{-/-}$ for more than 2 years. The lifespan measurements revealed significant differences among the various mouse strains. WT mice displayed a median lifespan of 826 days, which served as the baseline for comparison with 5xFADPrnp$^{+/+}$ group. The median lifespan of 5xFADPrnp$^{+/+}$ decreased by approximately 57% compared to WT mice. Median lifespan of 5xFADPrnp$^{-/+}$ was 35% decreased in comparison with Prnp$^{-/+}$ mice. The median lifespan of 5xFADPrnp$^{-/-}$ was approximate 16% reduced compared to Prnp$^{-/-}$.

Our findings show that as the levels of PrP^C increase in conjunction with the 5xFAD mutations, the lifespan of these mice decreases significantly. This suggests that there is a direct relationship between higher PrP^C expression and reduced lifespan in the presence of 5XFAD mutations. Several studies utilizing various mouse models for AD have yielded conflicting results. On one hand, research reported that the ablation of PrP^C in AD mice (J20 and TgCRND8 mice lines) did not prevent shortened lifespan[133,134] and on the other hand, studies report that AD transgenic mice lacking PrP^C (APPswe/PSen1dE9) show normal survival.[135,136] Moreover, in recent findings, it has been demonstrated that the co-expression of PrP^C and Aβ contributes to a reduced lifespan in Drosophila. [137] These discrepancies in the results obtained from studies on the role of PrP^C in lifespan in AD mouse models could be attributed to various factors, including different backgrounds of the experimental models. However, our findings do not align completely with either of the existing theories. While the ablation of PrP^C did not fully restore the lifespan to normal, it did show a significant increase compared with mice co-expressing PrP^C and the 5XFAD mutations (5xFADPrnp^{+}/$^{+}$ and 5xFADPrnp^{-}/$^{+}$). Our findings indicate a dose-dependent relationship between PrP^C levels and lifespan in the context of AD. Mice with lower expression of PrP^C exhibit a longer lifespan compared to those with higher PrP^C expression.

2.3.2. Reduced PrP^C levels significantly delays behavior impairments in 5xFAD mice

Alzheimer's disease is a progressive neurodegenerative disorder characterized by the gradual deterioration of cognitive functions. In the present study, several behavior tests, including locomotor activity, motor function, anxiety-related behavior, and associative learning, were conducted to evaluate the influence of PrP^C in mice carrying 5xFAD mutations.

In early age, specifically at 3 months of age, all groups showed no significant behavior deficits. After 9 months, 5xFADPrnp^{+}/$^{+}$ mice had reduced locomotor activity, motor function and anxiety-related behavior compared with WT, while 5xFADPrnp^{-}/$^{+}$ and 5xFADPrnp^{-}/$^{-}$ behaved similar to their controls. In associative learning, both 5xFADPrnp^{+}/$^{+}$ and 5xFADPrnp^{-}/$^{+}$ mice displayed a significant decline at 9 months, with no difference between 5xFADPrnp^{-}/$^{-}$ and Prnp^{-}/$^{-}$ mice. At 12 months, 5xFADPrnp^{-}/$^{+}$

exhibited a decrease in locomotor activity, motor function, anxiety-related behavior, while no significant differences were observed in 5xFADPrnp$^{-/-}$ compared with their respective control. In associative learning, 5xFADPrnp$^{-/+}$ and 5xFADPrnp$^{-/-}$ mice exhibit a decline at 12 months. Remarkably, at 14 months of age, 5xFADPrnp$^{-/-}$ mice showed a decline in motor function and anxiety-related behavior, however, they did not present significant decrease of their locomotor activity compared to Prnp$^{-/-}$ mice.

Our investigation revealed that in addition to associative learning impairment, these mice also exhibit a decrease in locomotor activity, motor function, and anxiety-related behavior. The symptoms show a progressive onset across the different groups, generally, they manifest earlier in 5xFADPrnp$^{+/+}$, subsequently in 5xFADPrnp$^{-/+}$, and later on in 5xFADPrnp$^{-/-}$. This suggests that the severity and timing of these symptoms are influenced by the presence of PrP^{C}, with the most pronounced effects in mice expressing normal physiological PrP^{C}.

The majority of the research conducted to investigate the consequences of PrP^{C} ablation or blocking in AD mice models has primarily focused on assessing learning and memory-related behaviors in other AD models, such as J20 and APPswe/PSen1dE9. [75,133,135,138,139] Our study encompasses not only associative learning but also motor function, anxiety-related behavior, and locomotor activity, providing a more comprehensive understanding of the extension of the PrP^{C} influence in 5xFAD mutation carriers.

Divergent results were observed across different AD mice models. In the APPswe/PSen1dE9 model, both PrP^{C} ablation and antibody blocking led to the reversal of cognitive deficits. [135,139] Conversely, in the J20 model, the ablation of PrP^{C} did not lead to the restoration of memory impairments. [133] A different research investigation, which involved the injection of synthetic Aβ oligomers into mice, concluded that mice lacking PrP^{C} were equally susceptible to Aβ induced toxicity compared to mice expressing PrP^{C}.[75]

The divergent outcomes observed in these studies could be attributed to the distinctive characteristics of these mice lines, as the pace and aggressiveness of AD-like pathology they exhibit. 5xFAD mice exhibit aggressive Aβ pathology and severe cognitive deficits at an early age in comparison with J20 and APPswe/PSen1dE9 mice lines. [140] Other crucial factor that may contribute to the differing findings is the single time point assessment, which potentially overlooks the progressive nature of the

disease. Thus, our assessments range from 3 to 14 months of age, depending on the genotype, allowing us to explore how PrP^C influences the progression of AD-related pathology. Moreover, it's crucial to emphasize the evaluation of mice's motor condition, especially when conducting tests like Morris Water Maze (MWM) that required good motor function. Motor disabilities can lead to potential misleading results, as it might appear that the mouse is experiencing memory deficits when the primary issue is, in fact, motor impairment. Thus, mice exhibiting exceptionally low locomotor activity were excluded from our study to maintain the reliability of the data. As result, 5xFADPrnp^{+}/$^{+}$ mice were included in the study until 9 months of age, 5xFADPrnp^{-}/$^{+}$ until 12 months and 5xFADPrnp^{-}/$^{-}$ up to 14 months.

Overall, in our study, mice with lower levels of PrP^C or those lacking PrP^C tend to demonstrate a postponed onset of impairment caused by 5xFAD mutations. Interestingly, it appears that the severity of the impairment in behavior is PrP^C dose-dependent in these mice. However, it's important to note that PrP^C knockout mice do not fully recover. Even though PrP^C levels appear to play a role in influencing behavior decline in AD, they do not represent a solo determinant.

2.3.3. Aβ levels do not correlate with behavioral deficits in the absence of PrP^C

After conducting the behavioral tests, I examined the potential connection between Aβ1-40 and Aβ1-42 levels and the performance of the mice across these tests. Our intention was to explore whether variations in Aβ1-40 and Aβ1-42 levels could shed light on the mice's behavior.

No significant correlations were found between Aβ1-40 and Aβ1-42 levels and locomotor activity in any of the mice groups. In the EPM test, 5xFADPrnp^{+}/$^{+}$ and 5xFADPrnp^{-}/$^{+}$ showed a significant negative correlation between higher levels of Aβ1-40 and decreased anxiety-related behavior, as well as higher Aβ1-42 levels and decreased anxiety-related behavior in 5xFADPrnp^{+}/$^{+}$. In terms of motor function, all three mice models exhibited significant negative correlation between Aβ1-40 levels and motor performance, as well as high Aβ1-42 levels and motor impairment in 5xFADPrnp^{+}/$^{+}$ and 5xFADPrnp^{-}/$^{+}$. In terms of associative learning skills, in 5xFADPrnp^{+}/$^{+}$ mice, I observed a significant negative correlation between Aβ1-40 and

Aβ1-42 levels and the associative learning skills. In 5xFADPrnp$^{-/+}$ and 5xFADPrnp$^{-/-}$ mice, I did not find any significant correlation between Aβ1-40 and Aβ1-42 levels and associative learning abilities.

Our findings point to a link between the levels of Aβ1-40 and Aβ1-42 and the compromised performance of the mice in the conducted tests. Suggesting that the high quantities of Aβ1-40 and Aβ1-42 present in the brain may indeed contribute to impairments observed in the mice's test performance. However, this correlation is depending on PrP^{C}. It appears that the extent of correlation between Aβ1-40, Aβ1-42, and behavior impairments is influenced by the presence of PrP^{C}. When PrP^{C} levels are low or inexistent, the correlation between Aβ1-40, Aβ1-42, and behavioral impairments diminishes. Its presence or absence plays a pivotal role in determining the strength of association between Aβ levels and behavioral outcomes.

A study conducted in Tg2576 model of AD found that there was no clear relationship between memory and insoluble Aβ levels when considering a group of animals with varying ages. This relationship only could be observed when the mice were separated into age-based subgroups. [141] In another study using APP/PS1 model of AD, it was found that the extent of Aβ pathology at various ages did not show any connection with cognitive deficits, implying that Aβ levels do not serve as an indicator of memory decline. [142] A systematic review study conclude that mice intentionally bred to exhibit higher levels of Aβ do not exhibit significant poorer performance in cognitive tests compared to mice that do not have elevated Aβ levels.[143] In humans, Aβ levels are frequently elevated in AD patients, but these levels are not a reliable indicator of the advancement and progression of clinical AD among individuals.[144] An explanatory hypothesis for this is that the cognitive impairments in AD are linked to the presence of the qualitative high levels of Aβ but not influenced by the specific quantities of Aβ.[143]

In fact, in our 5xFAD mice model, I identified a negative correlation between Aβ levels and behavior impairments. Still, this correlation seems to be dependent on PrP^{C}. However, in absence of PrP^{C}, mice still exhibit behavior impairments at later age, although these impairments are not directly associated with the Aβ levels. This could be attributed to the existence of a specific Aβ conformation that interacts with other receptors, exerting a substantial influence than solely the levels of Aβ, in absence of PrP^{C}.

2.3.4. PrP^C expression correlates with elevated Aβ plaque load in mice

In the present study, I used light sheet microscopy in conjunction with QUINT workflow to investigate the distribution of Aβ deposition within various brain regions. This approached allowed for both visualization and quantitative analysis of these structures in a three-dimensional context in two different mouse models, namely the 5xFADPrnp$^{+/+}$ and 5xFADPrnp$^{-/-}$ mice. The analysis of the Aβ plaque distribution revealed a widespread deposition of Aβ plaques across diverse brain areas, in both 5xFADPrnp$^{+/+}$ and 5xFADPrnp$^{-/-}$ mice. Among these regions, the cortex, olfactory area, and hippocampus exhibited the highest Aβ plaque load in both mouse models. However, the cortex Aβ plaques load was significantly higher in 5xFADPrnp$^{+/+}$ compared with 5xFADPrnp$^{-/-}$. Similar trends were observed in all the other regions, though without statistical significance. The elevated Aβ plaque load in these areas suggested that Aβ pathology could significantly impact these cognitive and motor functions. This aligns with the impairments that I observed in the behavior testing. Another interesting observation is the generalized higher load of Aβ plaque in the brain of 5xFADPrnp$^{+/+}$ compared to 5xFADPrnp$^{-/-}$. This highlights the potential role of PrP^C in modulating Aβ plaque load or it may influence the spreading of Aβ pathology within the brain.

AD is characterized by the accumulation of Aβ in the brain, leading to cognitive and behavioral impairments.[145] Understanding specific brain regions affected is essential for understanding the disease progression and its impact on the mice behavior. Brain regions as cortex, olfactory area and hippocampus are crucial for cognitive processes including memory, learning, voluntary movements, and sensory perception in mice.[146–150] In fact, in other study involving sHaPrP Tg7 mice expressing APPSwed+Ind and having an overexpression of PrP^C, it was observed that the mice cortex had a significantly higher load of Aβ plaques compared to mice with APPSwed+Ind mutation and with normal physiological levels of PrP^C.[151] In a more recent investigation using TgAD mice, researchers observed increased levels of Aβ plaques in mice expressing PrP^C when compared to mice that lacked PrP^C. [152]

Our study utilized advanced imaging technique to explore the distribution and the load of Aβ plaques in a 3D context. This approach enabled us for the first time to

precisely pinpoint the special location of these plaques and conduct a comprehensive quantitative assessment across the entire brain.

3. Further protein in the PrP^C mediated uptake of Aβ

3.1. Caveolin-1 directly interacts with PrP^C, Aβ1-40, and Aβ1-42

Research findings suggest that PrP^C is enriched in caveolae or caveolae-like domains with caveolin-1 (Cav-1), and together participate in Fyn recruitment for signaling transduction.[153,154]Additionally, there is substantial evidence supporting the connection between caveolin-1 and AD, as elevated levels of caveolin-1 have been confirmed in the brain tissue of AD patients.[155]

Therefore, I employed SPR to explore the interaction between Cav-1 and PrP^C, Aβ1-40, and Aβ1-42. The results of this study suggest that Cav-1 interact with PrP^C in a significant and strong manner, presented by a specific and stable binding in SPR (KD= 1.41E-08 M). Interestingly, I also found a direct interaction between Cav-1 and Aβ1-40 (KD= 1.14E-08 M), and Aβ1-42 (KD= 1.30E-08 M).

A previous study, found that PrP^C and Cav-1 colocalize, also that PrP^C octarepeats region interacts with Cav-1 which supports our observations.[156] Interestingly, I also found a direct interaction between Cav-1 and Aβ1-40, and Aβ1-42. Other studies found that Cav-1 interacts with APP C-terminal, and that Cav-1 regulates APP cleavage by gamma-secretase.[157,158] However, it's worth noting that the literature has not previously documented the interaction between Cav-1 and Aβ1-40, as well as Aβ1-42. I consider the results of our interaction study as a relevant indicator for the involvement of Cav-1 in PrP^C promoted uptake of Aβ, raising the question whether a knock-out of Cav-1 may inhibit the uptake of Aβ, which provides new insights into a new potential molecular mechanism in AD.

3.2. Cav-1 knockout neurons exhibit reduced Aβ internalization

In order to investigate whether a knockout of Cav-1 influences the internalization of Aβ, I treated primary cortical neurons from both WT and Cav-1 KO mice with Aβ1-40

and Aβ1-42 oligomers for an overnight incubation period. Utilizing Aβ1-40 and Aβ1-42 ELISAS, I quantified the Aβ levels within these neuronal cultures. Our results demonstrate a substantial reduction in Aβ1-40 levels by approximately 65% and a notable decrease in Aβ1-42 levels by around 25% in Cav-1 KO neurons compared with WT neurons. These findings indicate an influence of Cav-1 on the internalization of PrP^C 1-40 and Aβ1-42 oligomers within neurons suggesting a novel role of Cav-1 and caveolae in the PrP^C mediated uptake of Aβ.

There is limited literature available on the effect of Cav-1 and PrP^C interaction. Existing reports suggest that this interaction can trigger the activation of Fyn. Additionally, it has been reported that PrP^C binding to Cav-1 facilitates the internalization of PrP^C, [154,159,160] which can mean that the protein complexes of PrP^C and Aβ may be internalized through building a complex with Cav-1 via caveolae. This can be the new pathophysiological mechanism and a new diagnostic target in AD which may explain the toxic function of PrP^C in AD.

A link between PrP^C and Cav-1 has been already described in prostate and colon cancer. Here, PrP^C and CAV-1 were found to be co-localized in MDST8 cells evidenced by Proximity Ligation Assay. Moreover, PrP^C overexpressing LoVo cells showed an upregulation of Cav-1 mRNA, while PrP^C knockout MDST8 cells had a reduction in Cav-1 mRNA suggesting an association between both proteins at transcriptomic and proteomic level.[127,154,159,160]

A potential physiological mechanism might be that PrP^C- Aβ binding and Cav-1 interaction leads to the activation of Fyn leading to the hyperphosphorylation of Tau.[156,161] Based on our results and on the available literature, I hypothesize, that besides the Fyn activation, PrP^C when bound to Aβ, undergoes internalization through caveolea, mediated by Cav-1 leading to an increase of intracellular Aβ (Figure 34) which may result in several intracellular dysfunctions, such as increased cellular stress and apoptosis.

While our study has shed light on the influence of Cav-1 on internalization of Aβ in primary cortical neurons, it is important to acknowledge the limitations of our research and chart a path for future investigations. One limitation of our study is the relatively narrow focus on the effect of Cav-1 knockout on the Aβ levels within the neurons, to further understand the dynamics of Cav-1 and PrP^C interactions in the context of AD,

more research is needed, as exploring the downstream signaling pathway, exploring the Aβ-PrP^{C}-Cav1 complex in *vivo* models (e.g., PrP^{C} and Cav-1 double knockout mice), and possibly in human samples. Future studies can build upon our findings, exploring broader molecular and cellular mechanisms underlying these interactions, with the ultimate goal of contributing to a deeper understanding of AD and potential therapeutic targets.

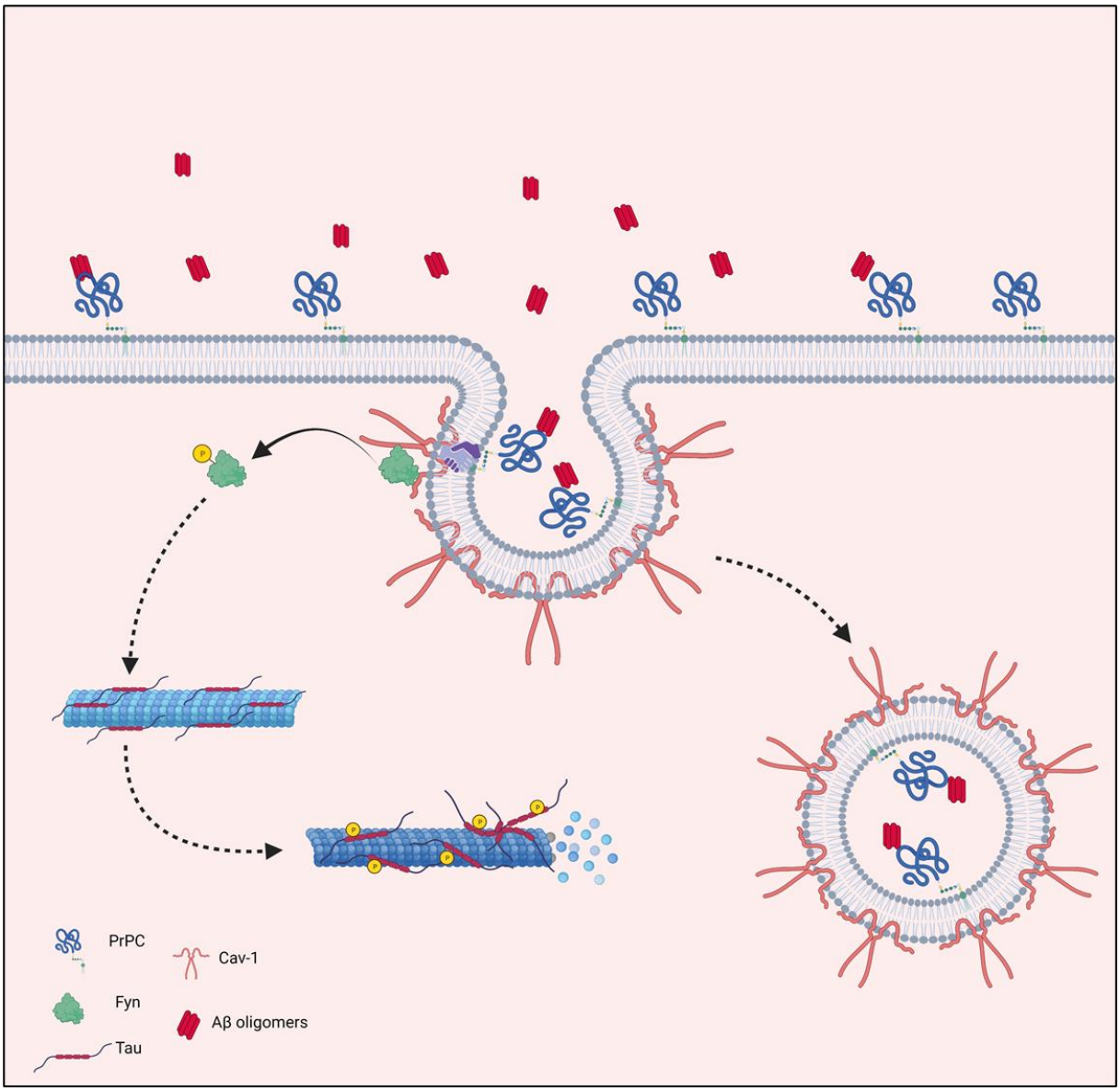

Figure 34 - Proposed models of PrP^{C} – Cav-1 interactions. The binding of PrP^{C}- Aβ leads to Fyn kinase activation through Cav-1. The activation of Fyn leads to excessive phosphorylation of Tau, causing it to detach from the microtubules. In addition, PrP^{C}- Aβ complexes may undergo internalization facilitated by the interaction of PrP^{C} with Cav-1. This internalization mechanism may contribute to increased intracellular Aβ levels. Figure created with BioRender.com.

VII. Conclusion

Alzheimer's disease poses a substantial and increasing challenge, particularly due to our aging population. While pathophysiological mechanisms are still under debate, there is a focus on the Aβ, which is thought to be the central pathogenic event in AD. Our data indicated PrP^C as a major player in this process and provided valuable insights into the pathophysiological function of PrP^C in this context.

The *in vitro* experiments revealed a direct and stable interaction not only between PrP^C and Aβ1-42, but also with Aβ1-40, showing that the binding ofPrP^C is not restricted to one form of Aβ.

In SH-SY5Y cells, our findings revealed PrP^C's role as a key facilitator of Aβ oligomer internalization suggesting that PrP^C may play an early role in AD pathogenesis and in the spreading of Aβ pathology.

In vivo, our study revealed a correlation between PrP^C levels and the reduction of the lifespan and behaviour deficits of 5xFAD mice. While PrP^C ablation has a discernible impact, it does not restore the Aβ-induced reduction of lifespan or entirely reverse the observed behavior impairments. Additionally, our study revealed a direct correlation between Aβ1-40 and Aβ1-42 and behavioral impairments in a presence of PrP^C. In PrP^C knockout mice, behavioral deficits did not correlate with the Aβ concertation, suggesting other Aβ conformations, rather than its total levels, may play a role in the Aβ induced toxicity. Moreover, I found that PrP^C influences the plaque burden rather than the spatial distribution of Aβ in different brain regions, which might indicate a regulatory role of PrP^C on Aβ expression.

In addition, our study provided the first evidence that Cav-1 may play a relevant role on the PrP^C and Aβ internalization , which may be a pivotal mechanism in Aβ-provoked toxicity in AD.

Overall, our research highlights the important role of PrP^C and Cav-1 in complex processes related with Aβ mediated pathophysiology of the disease.

VIII. Bibliography

1. Anderson ED. *Dementia: A Comprehensive Guide to Understanding, Diagnosis, and Treatment*.; 2023.
2. International D. World Alzheimer Report 2018 - The state of the art of dementia research: New frontiers; World Alzheimer Report 2018 - The state of the art of dementia research: New frontiers.
3. Gale SA, Acar D, Daffner KR. Dementia. *Am J Med*. 2018;131(10):1161-1169. doi:10.1016/J.AMJMED.2018.01.022
4. Livingston G, Huntley J, Sommerlad A, et al. Dementia prevention, intervention, and care: 2020 report of the Lancet Commission. *Lancet*. 2020;396(10248):413. doi:10.1016/S0140-6736(20)30367-6
5. Josephs KA, Ahlskog JE, Parisi JE, et al. Rapidly Progressive Neurodegenerative Dementias. *Arch Neurol*. 2009;66(2):201-207. doi:10.1001/ARCHNEUROL.2008.534
6. Stelzmann RA, Norman Schnitzlein H, Reed Murtagh F. An english translation of alzheimer's 1907 paper, "über eine eigenartige erkankung der hirnrinde." *Clinical Anatomy*. 1995;8(6):429-431. doi:10.1002/CA.980080612
7. López OL, DeKosky ST. Clinical symptoms in Alzheimer's disease. *Handb Clin Neurol*. 2008;89:207-216. doi:10.1016/S0072-9752(07)01219-5
8. Brody H, Grayson M, Mandavilli A, Scully T, Haines N. Alzheimer's Disease. *Nature*. 2011;475(7355 SUPPL.). doi:10.1038/475S1A
9. WHO. Dementia. Accessed July 4, 2023. https://www.who.int/news-room/fact-sheets/detail/dementia
10. Li X, Feng X, Sun X, Hou N, Han F, Liu Y. Global, regional, and national burden of Alzheimer's disease and other dementias, 1990–2019. *Front Aging Neurosci*. 2022;14:937486. doi:10.3389/FNAGI.2022.937486/BIBTEX
11. Livingston G, Huntley J, Sommerlad A, et al. Dementia prevention, intervention, and care: 2020 report of the Lancet Commission. *The Lancet*.

2020;396(10248):413-446. doi:10.1016/S0140-6736(20)30367-6/ATTACHMENT/5F8C54CB-A837-4EBA-AC5D-9F2EF488E625/MMC1.PDF

12. Deture MA, Dickson DW. The neuropathological diagnosis of Alzheimer's disease. *Molecular Neurodegeneration 2019 14:1*. 2019;14(1):1-18. doi:10.1186/S13024-019-0333-5

13. Martins RN, Brennan CS, Fernando WMADB, Brennan MA, Fuller SJ. *Neurodegeneration and Alzheimer's Disease: The Role of Diabetes, Genetics, Hormones, and Lifestyle*.; 2019. doi:10.1002/9781119356752

14. Glenner GG, Wong CW. Alzheimer's disease: Initial report of the purification and characterization of a novel cerebrovascular amyloid protein. *Biochem Biophys Res Commun*. 1984;120(3):885-890. doi:10.1016/S0006-291X(84)80190-4

15. Pfaff DW. *Neuroscience in the 21st Century: From Basic to Clinical*. Springer New York; 2013. doi:10.1007/978-1-4614-1997-6/COVER

16. Piaceri I, Nacmias B, Sorbi S. Genetics of familial and sporadic Alzheimer's disease. *Frontiers in Bioscience - Elite*. 2013;5 E(1):167-177. doi:10.2741/E605

17. Wirths O, Bouter Y, Bayer TA. Alzheimer's Disease. In: *Neuroscience in the 21st Century*. Springer International Publishing; 2022:4323-4344. doi:10.1007/978-3-030-88832-9_114

18. Duthey B. Background Paper 6.11 Alzheimer Disease and other Dementias. Published online 2013.

19. Cruts M, Backhovens H, Wang SY, et al. Molecular genetic analysis of familial early-onset alzheimer's disease linked to chromosome 14q24.3. *Hum Mol Genet*. 1995;4(12). doi:10.1093/hmg/4.12.2363

20. Campion D, Flaman JM, Brice A, et al. Mutations of the presenilin I gene in families with early-onset alzheimer's disease. *Hum Mol Genet*. 1995;4(12). doi:10.1093/hmg/4.12.2373

21. Sherrington R, Froelich S, Sorbi S, et al. Alzheimer's disease associated with mutations in presenilin 2 is rare and variably penetrant. *Hum Mol Genet*. 1996;5(7). doi:10.1093/hmg/5.7.985

22. Goate A, Chartier-Harlin MC, Mullan M, et al. Segregation of a missense mutation in the amyloid precursor protein gene with familial Alzheimer's disease. *Nature*. 1991;349(6311). doi:10.1038/349704a0

23. Wu L, Rosa-Neto P, Hsiung GYR, et al. Early-Onset Familial Alzheimer's Disease (EOFAD). *Can J Neurol Sci*. 2012;39:436-445. doi:10.1017/S0317167100013949

24. Evin G, Weidemann A. Biogenesis and metabolism of Alzheimer's disease Aβ amyloid peptides. *Peptides (NY)*. 2002;23(7):1285-1297. doi:10.1016/S0196-9781(02)00063-3

25. Hardy JA, Higgins GA. Alzheimer's disease: The amyloid cascade hypothesis. *Science (1979)*. 1992;256(5054):184-185. doi:10.1126/SCIENCE.1566067/ASSET/74A758CB-215F-4A8E-9AAA-05F4D89DA62A/ASSETS/SCIENCE.1566067.FP.PNG

26. Barage SH, Sonawane KD. Amyloid cascade hypothesis: Pathogenesis and therapeutic strategies in Alzheimer's disease. *Neuropeptides*. 2015;52. doi:10.1016/j.npep.2015.06.008

27. Rogers J, Webster S, Lue LF, et al. Inflammation and Alzheimer's disease pathogenesis. *Neurobiol Aging*. 1996;17(5):681-686. doi:10.1016/0197-4580(96)00115-7

28. McGeer PL, McGeer EG. The inflammatory response system of brain: implications for therapy of Alzheimer and other neurodegenerative diseases. *Brain Res Rev*. 1995;21(2):195-218. doi:10.1016/0165-0173(95)00011-9

29. Eikelenboom P, Zhan SS, van Gool WA, Allsop D. Inflammatory mechanisms in Alzheimer's disease. *Trends Pharmacol Sci*. 1994;15(12):447-450. doi:10.1016/0165-6147(94)90057-4

30. Wildsmith KR, Holley M, Savage JC, Skerrett R, Landreth GE. Evidence for impaired amyloid β clearance in Alzheimer's disease. *Alzheimers Res Ther*. 2013;5(4):1-6. doi:10.1186/ALZRT187/FIGURES/1

31. Carter DB, Dunn E, McKinley DD, et al. Human apolipoprotein E4 accelerates β-amyloid deposition in APPsw transgenic mouse brain. *Ann Neurol*. 2001;50(4):468-475. doi:10.1002/ANA.1134

32. Henstridge CM, Hyman BT, Spires-Jones TL. Beyond the neuron–cellular interactions early in Alzheimer disease pathogenesis. *Nature Reviews Neuroscience 2018 20:2*. 2019;20(2):94-108. doi:10.1038/s41583-018-0113-1

33. Park J, Wetzel I, Marriott I, et al. A 3D human triculture system modeling neurodegeneration and neuroinflammation in Alzheimer's disease. *Nature Neuroscience 2018 21:7*. 2018;21(7):941-951. doi:10.1038/s41593-018-0175-4

34. Qian J, Zhang Y, Betensky RA, Hyman BT, Serrano-Pozo A. Neuropathology-Independent Association between APOE Genotype and Cognitive Decline Rate in the Normal Aging-Early Alzheimer Continuum. *Neurol Genet*. 2023;9(1). doi:10.1212/NXG.0000000000200055

35. Nelson PT, Alafuzoff I, Bigio EH, et al. Correlation of alzheimer disease neuropathologic changes with cognitive status: A review of the literature. *J Neuropathol Exp Neurol*. 2012;71(5). doi:10.1097/NEN.0b013e31825018f7

36. Muller-Hill B, Beyreuther K. Molecular biology of Alzheimer's disease. *Annu Rev Biochem*. 1989;58. doi:10.1146/annurev.bi.58.070189.001443

37. Zheng H, Koo EH. Molecular Neurodegeneration The amyloid precursor protein: beyond amyloid. *Mol Neurodegener*. 2006;1.

38. Wilkins HM, Swerdlow RH. Amyloid Precursor Protein Processing and Bioenergetics. *Brain Res Bull*. 2017;133:71. doi:10.1016/J.BRAINRESBULL.2016.08.009

39. De Strooper B, Annaert W. Proteolytic processing and cell biological functions of the amyloid precursor protein. *J Cell Sci*. 2000;113(11). doi:10.1242/jcs.113.11.1857

40. Selkoe DJ. Alzheimer's disease: Genes, proteins, and therapy. *Physiol Rev*. 2001;81(2). doi:10.1152/physrev.2001.81.2.741

41. Jiang S, Li Y, Zhang X, Bu G, Xu H, Zhang YW. Trafficking regulation of proteins in Alzheimer's disease. *Mol Neurodegener*. 2014;9(1). doi:10.1186/1750-1326-9-6

42. Yuksel M, Tacal O. Trafficking and proteolytic processing of amyloid precursor protein and secretases in Alzheimer's disease development: An up-to-date review. *Eur J Pharmacol*. 2019;856. doi:10.1016/j.ejphar.2019.172415

43. Thinakaran G, Koo EH. Amyloid precursor protein trafficking, processing, and function. *Journal of Biological Chemistry*. 2008;283(44). doi:10.1074/jbc.R800019200

44. Wilson CA, Doms RW, Lee VMY. Intracellular APP Processing and Aβ Production in Alzheimer Disease. *J Neuropathol Exp Neurol*. 1999;58(8):787-794. doi:10.1097/00005072-199908000-00001

45. SISODIA SS. Secretion of the beta-amyloid precursor protein. *Ann N Y Acad Sci*. 1992;674(1):53-57. doi:10.1111/J.1749-6632.1992.TB27476.X

46. Anderson JP, Esch FS, Keim PS, Sambamurti K, Lieberburg I, Robakis NK. Exact cleavage site of Alzheimer amyloid precursor in neuronal PC-12 cells. *Neurosci Lett*. 1991;128(1):126-128. doi:10.1016/0304-3940(91)90775-O

47. Zhao J, Liu X, Xia W, Zhang Y, Wang C. Targeting Amyloidogenic Processing of APP in Alzheimer's Disease. *Front Mol Neurosci*. 2020;13. doi:10.3389/FNMOL.2020.00137

48. Jeong H, Shin H, Hong S, Kim YS. Physiological Roles of Monomeric Amyloid-β and Implications for Alzheimer's Disease Therapeutics. *Exp Neurobiol*. 2022;31(2):65. doi:10.5607/EN22004

49. Plant LD, Boyle JP, Smith IF, Peers C, Pearson HA. The Production of Amyloid β Peptide Is a Critical Requirement for the Viability of Central Neurons. *The Journal of Neuroscience*. 2003;23(13):5531. doi:10.1523/JNEUROSCI.23-13-05531.2003

50. Giuffrida ML, Giuffrida ML, Caraci F, et al. The Monomer State of Beta-Amyloid: Where the Alzheimer's Disease Protein Meets Physiology. *Rev Neurosci*. 2010;21(2):83-94. doi:10.1515/REVNEURO.2010.21.2.83/MACHINEREADABLECITATION/RIS

51. Giuffrida ML, Tomasello F, Caraci F, Chiechio S, Nicoletti F, Copani A. Beta-amyloid monomer and insulin/IGF-1 signaling in Alzheimer's disease. *Mol Neurobiol*. 2012;46(3):605-613. doi:10.1007/S12035-012-8313-6

52. Brody DL, Magnoni S, Schwetye KE, et al. Amyloid-beta dynamics correlate with neurological status in the injured human brain. *Science*. 2008;321(5893):1221-1224. doi:10.1126/SCIENCE.1161591

53. Chen GF, Xu TH, Yan Y, et al. Amyloid beta: structure, biology and structure-based therapeutic development. *Acta Pharmacologica Sinica 2017 38:9*. 2017;38(9):1205-1235. doi:10.1038/aps.2017.28

54. Ono K, Watanabe-Nakayama T. Aggregation and structure of amyloid β-protein. *Neurochem Int*. 2021;151:105208. doi:10.1016/J.NEUINT.2021.105208

55. Cline EN, Assunç˜ A, Bicca A, Viola KL, Klein WL, Klein W. The Amyloid-Oligomer Hypothesis: Beginning of the Third Decade the Creative Commons Attribution Non-Commercial License (CC BY-NC 4.0). *Journal of Alzheimer's Disease*. 2018;64:567-610. doi:10.3233/JAD-179941

56. Ding Y, Zhao J, Zhang X, et al. Amyloid Beta Oligomers Target to Extracellular and Intracellular Neuronal Synaptic Proteins in Alzheimer's Disease. *Front Neurol*. 2019;10:484223. doi:10.3389/FNEUR.2019.01140/BIBTEX

57. Liu P, Reed MN, Kotilinek LA, et al. Quaternary structure defines a large class of amyloid-β oligomers neutralized by sequestration. *Cell Rep*. 2015;11(11):1760. doi:10.1016/J.CELREP.2015.05.021

58. Ashe KH. The biogenesis and biology of amyloid β oligomers in the brain. *Alzheimer's & Dementia*. 2020;16(11):1561. doi:10.1002/ALZ.12084

59. Uversky VN, Lyubchenko Y. Bio-Nanoimaging : Protein Misfolding & Aggregation. :526.

60. Naiki H, Gejyo F. Kinetic analysis of amyloid fibril formation. *Methods Enzymol*. 1999;309:305-318. doi:10.1016/S0076-6879(99)09022-9

61. Lomakin A, Teplow DB, Kirschner DA, Benedeki GB. Kinetic theory of fibrillogenesis of amyloid β-protein. *Proc Natl Acad Sci U S A*. 1997;94(15):7942-7947. doi:10.1073/PNAS.94.15.7942/ASSET/DDBA7DC9-BEF0-4A4D-A477-62A2126921F7/ASSETS/GRAPHIC/PQ1571602004.JPEG

62. Jarrett JT, Lansbury PT. Seeding “one-dimensional crystallization” of amyloid: A pathogenic mechanism in Alzheimer’s disease and scrapie? *Cell*. 1993;73(6):1055-1058. doi:10.1016/0092-8674(93)90635-4

63. Cohen SIA, Linse S, Luheshi LM, et al. Proliferation of amyloid-β42 aggregates occurs through a secondary nucleation mechanism. *Proc Natl Acad Sci U S A*. 2013;110(24). doi:10.1073/pnas.1218402110

64. Brody DL, Jiang H, Wildburger N, Esparza TJ. Non-canonical soluble amyloid-beta aggregates and plaque buffering: controversies and future directions for target discovery in Alzheimer’s disease. *Alzheimers Res Ther*. 2017;9(1). doi:10.1186/S13195-017-0293-3

65. Jarosz-Griffiths HH, Noble E, Rushworth J V., Hooper NM. Amyloid-β receptors: The good, the bad, and the prion protein. *Journal of Biological Chemistry*. 2016;291(7):3174-3183. doi:10.1074/JBC.R115.702704/ATTACHMENT/3739861F-CA6A-448E-80AC-3B0FE022855F/MMC6.PDF

66. Mroczko B, Groblewska M, Litman-Zawadzka A, Kornhuber J, Lewczuk P. Cellular Receptors of Amyloid β Oligomers (AβOs) in Alzheimer’s Disease. *Int J Mol Sci*. 2018;19(7). doi:10.3390/IJMS19071884

67. Sepulveda FJ, Parodi J, Peoples RW, Opazo C, Aguayo LG. Synaptotoxicity of Alzheimer Beta Amyloid Can Be Explained by Its Membrane Perforating Property. *PLoS One*. 2010;5(7):11820. doi:10.1371/JOURNAL.PONE.0011820

68. Laurén J, Gimbel DA, Nygaard HB, Gilbert JW, Strittmatter SM. Cellular Prion Protein Mediates Impairment of Synaptic Plasticity by Amyloid-β Oligomers. *Nature*. 2009;457(7233):1128. doi:10.1038/NATURE07761

69. Kudo W, Lee HP, Zou WQ, et al. Cellular prion protein is essential for oligomeric amyloid-β-induced neuronal cell death. *Hum Mol Genet*. 2012;21(5):1138. doi:10.1093/HMG/DDR542

70. Cox TO, Gunther EC, Brody AH, et al. Anti-PrPC antibody rescues cognition and synapses in transgenic alzheimer mice. *Ann Clin Transl Neurol*. 2019;6(3):554-574. doi:10.1002/ACN3.730

71. Zhang Y, Zhao Y, Zhang L, Yu W, Wang Y, Chang W. Cellular Prion Protein as a Receptor of Toxic Amyloid-β42 Oligomers Is Important for Alzheimer's Disease. *Front Cell Neurosci*. 2019;13. doi:10.3389/FNCEL.2019.00339

72. Larson M, Sherman MA, Amar F, et al. The Complex PrPc-Fyn Couples Human Oligomeric Aβ with Pathological Tau Changes in Alzheimer's Disease. *The Journal of Neuroscience*. 2012;32(47):16857. doi:10.1523/JNEUROSCI.1858-12.2012

73. Schwarze-Eicker K, Keyvani K, Görtz N, Westaway D, Sachser N, Paulus W. Prion protein (PrPc) promotes β-amyloid plaque formation. *Neurobiol Aging*. 2005;26(8):1177-1182. doi:10.1016/J.NEUROBIOLAGING.2004.10.004

74. Rial D, Piermartiri TC, Duarte FS, Tasca CI, Walz R, Prediger RD. Overexpression of cellular prion protein (PrP(C)) prevents cognitive dysfunction and apoptotic neuronal cell death induced by amyloid-β ($A\beta_{1-40}$) administration in mice. *Neuroscience*. 2012;215:79-89. doi:10.1016/J.NEUROSCIENCE.2012.04.034

75. Balducci C, Beeg M, Stravalaci M, et al. Synthetic amyloid-β oligomers impair long-term memory independently of cellular prion protein. *Proc Natl Acad Sci U S A*. 2010;107(5):2295. doi:10.1073/PNAS.0911829107

76. Wilcox KC, Marunde MR, Das A, et al. Nanoscale Synaptic Membrane Mimetic Allows Unbiased High Throughput Screen That Targets Binding Sites for Alzheimer's-Associated Aβ Oligomers. *PLoS One*. 2015;10(4). doi:10.1371/JOURNAL.PONE.0125263

77. Sparkes RS, Simon M, Cohn VH, et al. Assignment of the human and mouse prion protein genes to homologous chromosomes. *Proc Natl Acad Sci U S A*. 1986;83(19):7358-7362. doi:10.1073/PNAS.83.19.7358

78. Stahl N, Borchelt DR, Hsiao K, Prusiner SB. Scrapie prion protein contains a phosphatidylinositol glycolipid. *Cell*. 1987;51(2):229-240. doi:10.1016/0092-8674(87)90150-4

79. Knaus KJ, Morillas M, Swietnicki W, Malone M, Surewicz WK, Yee VC. Crystal structure of the human prion protein reveals a mechanism for oligomerization.

Nature Structural Biology 2001 8:9. 2001;8(9):770-774. doi:10.1038/nsb0901-770

80. Riek R, Hornemann S, Wider G, Glockshuber R, Wüthrich K. NMR characterization of the full-length recombinant murine prion protein, mPrP(23-231). *FEBS Lett*. 1997;413(2):282-288. doi:10.1016/S0014-5793(97)00920-4

81. Riesner D. Biochemistry and structure of PrPC and PrPSc. *Br Med Bull*. 2003;66. doi:10.1093/bmb/66.1.21

82. Ning ZY, Zhao DM, Yang JM, et al. Quantification of prion gene expression in brain and peripheral organs of golden hamster by real-time RT-PCR. *Anim Biotechnol*. 2005;16(1). doi:10.1081/ABIO-200053404

83. Schmitz M, Zafar S, Silva CJ, Zerr I. Behavioral abnormalities in prion protein knockout mice and the potential relevance of PrPC for the cytoskeleton. *Prion*. 2014;8(6):381. doi:10.4161/19336896.2014.983746

84. Brown DR. Prion and prejudice: normal protein and the synapse. *Trends Neurosci*. 2001;24(2):85-90. doi:10.1016/S0166-2236(00)01689-1

85. Tobler I, Gaus SE, Deboer T, et al. Altered circadian activity rhythms and sleep in mice devoid of prion protein. *Nature*. 1996;380(6575):639-642. doi:10.1038/380639A0

86. Roucou X, Guo Q, Zhang Y, Goodyer CG, LeBlanc AC. Cytosolic prion protein is not toxic and protects against Bax-mediated cell death in human primary neurons. *J Biol Chem*. 2003;278(42):40877-40881. doi:10.1074/JBC.M306177200

87. Kim BH, Lee HG, Choi JK, et al. The cellular prion protein (PrPC) prevents apoptotic neuronal cell death and mitochondrial dysfunction induced by serum deprivation. *Molecular Brain Research*. 2004;124(1):40-50. doi:10.1016/j.molbrainres.2004.02.005

88. Diarra-Mehrpour M, Arrabal S, Jalil A, et al. Prion protein prevents human breast carcinoma cell line from tumor necrosis factor alpha-induced cell death. *Cancer Res*. 2004;64(2):719-727. doi:10.1158/0008-5472.CAN-03-1735

89. Milhavet O, Lehmann S. Oxidative stress and the prion protein in transmissible spongiform encephalopathies. *Brain Res Rev*. 2002;38(3):328-339. doi:10.1016/S0165-0173(01)00150-3

90. Ryan DA, Narrow WC, Federoff HJ, Bowers WJ. An Improved Method for Generating Consistent Soluble Amyloid-beta Oligomer Preparations for In Vitro Neurotoxicity Studies. *J Neurosci Methods*. 2010;190(2):171. doi:10.1016/J.JNEUMETH.2010.05.001

91. Fa M, Orozco IJ, Francis YI, Saeed F, Gong Y, Arancio O. Preparation of oligomeric beta-amyloid 1-42 and induction of synaptic plasticity impairment on hippocampal slices. *J Vis Exp*. 2010;(41). doi:10.3791/1884

92. Da Silva Correia SM, Schmitz M, Fischer A, Hermann P, Zerr I. Role of different recombinant PrP substrates in the diagnostic accuracy of the CSF RT-QuIC assay in Creutzfeldt-Jakob disease. *Cell Tissue Res*. 2023;392(1):301-306. doi:10.1007/S00441-022-03715-9

93. Renier N, Wu Z, Simon DJ, Yang J, Ariel P, Tessier-Lavigne M. iDISCO: a simple, rapid method to immunolabel large tissue samples for volume imaging. *Cell*. 2014;159(4):896-910. doi:10.1016/J.CELL.2014.10.010

94. iDISCO+. iDISCO+ protocol Recommendations for sample handling. Published 2016. Accessed July 16, 2023. https://idisco.info/

95. Yates SC, Groeneboom NE, Coello C, et al. QUINT: Workflow for Quantification and Spatial Analysis of Features in Histological Images From Rodent Brain. *Front Neuroinform*. 2019;13:453735. doi:10.3389/FNINF.2019.00075/BIBTEX

96. Harmey JH, Doyle D, Brown V, Rogers MS. The cellular isoform of the prion protein, PrPc, is associated with caveolae in mouse neuroblastoma (N2a) cells. *Biochem Biophys Res Commun*. 1995;210(3):753-759. doi:10.1006/BBRC.1995.1723

97. Rothberg KG, Heuser JE, Donzell WC, Ying YS, Glenney JR, Anderson RGW. Caveolin, a Protein Component of Caveolae Membrane Coats. *Cell*. 1992;68:673-682.

98. Prevalence of dementia in Europe | Alzheimer Europe. Accessed September 7, 2023. https://www.alzheimer-europe.org/dementia/prevalence-dementia-europe

99. THE PATIENT JOURNEY IN AN ERA OF NEW TREATMENTS. doi:10.1002/alz.13016

100. Iwatsubo T, Odaka A, Suzuki N, Mizusawa H, Nukina N, Ihara Y. Visualization of Aβ42(43) and Aβ40 in senile plaques with end-specific Aβ monoclonals: Evidence that an initially deposited species is Aβ42(43). *Neuron*. 1994;13(1):45-53. doi:10.1016/0896-6273(94)90458-8

101. Selkoe DJ. Alzheimer's disease: genes, proteins, and therapy. *Physiol Rev*. 2001;81(2):741-766. doi:10.1152/PHYSREV.2001.81.2.741

102. Smith LM, Kostylev MA, Lee S, Strittmatter SM. Systematic and standardized comparison of reported amyloid-β receptors for sufficiency, affinity, and Alzheimer's disease relevance. *Journal of Biological Chemistry*. 2019;294(15):6042-6053. doi:10.1074/JBC.RA118.006252

103. Freir DB, Nicoll AJ, Klyubin I, et al. Interaction between prion protein and toxic amyloid β assemblies can be therapeutically targeted at multiple sites. *Nat Commun*. 2011;2(1):336. doi:10.1038/NCOMMS1341

104. Kessels HW, Nguyen LN, Nabavi S, Malinow R. The prion protein as a receptor for amyloid-β. *Nature*. 2010;466(7308):E3. doi:10.1038/NATURE09217

105. Chen S, Yadav SP, Surewicz WK. Interaction between Human Prion Protein and Amyloid-β (Aβ) Oligomers. *Journal of Biological Chemistry*. 2010;285(34):26377-26383. doi:10.1074/jbc.M110.145516

106. Jarrett JT, Berger EP, Lansbury PT. The carboxy terminus of the beta amyloid protein is critical for the seeding of amyloid formation: implications for the pathogenesis of Alzheimer's disease. *Biochemistry*. 1993;32(18):4693-4697. doi:10.1021/BI00069A001

107. Jarrett JT, Lansbury PT. Seeding "one-dimensional crystallization" of amyloid: A pathogenic mechanism in Alzheimer's disease and scrapie? *Cell*. 1993;73(6):1055-1058. doi:10.1016/0092-8674(93)90635-4

108. Laurén J, Gimbel DA, Nygaard HB, Gilbert JW, Strittmatter SM. Cellular prion protein mediates impairment of synaptic plasticity by amyloid-β oligomers. *Nature*. 2009;457(7233):1128-1132. doi:10.1038/nature07761

109. Rushworth J V., Griffiths HH, Watt NT, Hooper NM. Prion Protein-mediated Toxicity of Amyloid-β Oligomers Requires Lipid Rafts and the Transmembrane LRP1. *Journal of Biological Chemistry*. 2013;288(13):8935-8951. doi:10.1074/jbc.M112.400358

110. Boroujeni ER, Hosseini SM, Fani G, Cecchi C, Chiti F. Soluble Prion Peptide 107–120 Protects Neuroblastoma SH-SY5Y Cells against Oligomers Associated with Alzheimer's Disease. *Int J Mol Sci*. 2020;21(19):1-21. doi:10.3390/IJMS21197273

111. Foley AR, Roseman GP, Chan K, et al. Evidence for aggregation-independent, PrPC-mediated Aβ cellular internalization. *Proc Natl Acad Sci U S A*. 2020;117(46):28625-28631. doi:10.1073/PNAS.2009238117/-/DCSUPPLEMENTAL

112. Oddo S, Caccamo A, Shepherd JD, et al. Triple-transgenic model of Alzheimer's Disease with plaques and tangles: Intracellular Aβ and synaptic dysfunction. *Neuron*. 2003;39(3):409-421. doi:10.1016/S0896-6273(03)00434-3

113. LaFerla FM, Green KN, Oddo S. Intracellular amyloid-beta in Alzheimer's disease. *Nat Rev Neurosci*. 2007;8(7):499-509. doi:10.1038/NRN2168

114. Gouras GK, Tsai J, Naslund J, et al. Intraneuronal Aβ42 Accumulation in Human Brain. *Am J Pathol*. 2000;156(1):15. doi:10.1016/S0002-9440(10)64700-1

115. Vergara C, Ordóñez-Gutiérrez L, Wandosell F, Ferrer I, del Río JA, Gavín R. Role of PrP(C) Expression in Tau Protein Levels and Phosphorylation in Alzheimer's Disease Evolution. *Mol Neurobiol*. 2015;51(3):1206-1220. doi:10.1007/S12035-014-8793-7

116. Velayos JL, Irujo A, Cuadrado-Tejedor M, Paternain B, Moleres FJ, Ferrer V. The cellular prion protein and its role in Alzheimer disease. *http://dx.doi.org/104161/pri329135*. 2009;3(2):110-117. doi:10.4161/PRI.3.2.9135

117. Whitehouse IJ, Jackson C, Turner AJ, Hooper NM. Prion Protein is Reduced in Aging and in Sporadic but not in Familial Alzheimer's Disease. *Journal of Alzheimer's Disease*. 2010;22(3):1023-1031. doi:10.3233/JAD-2010-101071

118. Abu Rumeileh S, Lattanzio F, Stanzani Maserati M, Rizzi R, Capellari S, Parchi P. Diagnostic Accuracy of a Combined Analysis of Cerebrospinal Fluid t-PrP, t-tau, p-tau, and Aβ 42 in the Differential Diagnosis of Creutzfeldt-Jakob Disease from Alzheimer's Disease with Emphasis on Atypical Disease Variants. *Journal of Alzheimer's Disease*. 2017;55(4):1471-1480. doi:10.3233/JAD-160740

119. Dohler F, Sepulveda-Falla D, Krasemann S, et al. High molecular mass assemblies of amyloid-β oligomers bind prion protein in patients with Alzheimer's disease. *Brain*. 2014;137(3):873-886. doi:10.1093/BRAIN/AWT375

120. Saijo E, Scheff SW, Telling GC. Unaltered prion protein expression in Alzheimer disease patients. *http://dx.doi.org/104161/pri5216355*. 2011;5(2):109-116. doi:10.4161/PRI.5.2.16355

121. Zhang Y, Zhao Y, Zhang L, Yu W, Wang Y, Chang W. Cellular Prion Protein as a Receptor of Toxic Amyloid-β42 Oligomers Is Important for Alzheimer's Disease. *Front Cell Neurosci*. 2019;13. doi:10.3389/fncel.2019.00339

122. Agostini F, Dotti CG, Pérez-Cañamás A, Ledesma MD, Benetti F, Legname G. Prion Protein Accumulation in Lipid Rafts of Mouse Aging Brain. *PLoS One*. 2013;8(9):74244. doi:10.1371/JOURNAL.PONE.0074244

123. Salès N, Hässig R, Rodolfo K, et al. Developmental expression of the cellular prion protein in elongating axons. *Eur J Neurosci*. 2002;15(7):1163-1177. doi:10.1046/J.1460-9568.2002.01953.X

124. Benvegnù S, Poggiolini I, Legname G. Neurodevelopmental expression and localization of the cellular prion protein in the central nervous system of the mouse. *J Comp Neurol*. 2010;518(11):1879-1891. doi:10.1002/CNE.22357

125. Williams WM, Stadtman ER, Moskovitz J. Ageing and exposure to oxidative stress in vivo differentially affect cellular levels of PrPc in mouse cerebral microvessels and brain parenchyma. *Neuropathol Appl Neurobiol*. 2004;30(2):161-168. doi:10.1111/J.1365-2990.2003.00523.X

126. Gasperini L, Legname G. Prion protein and aging. *Front Cell Dev Biol*. 2014;2. doi:10.3389/fcell.2014.00044

127. Mouillet-Richard S, Martin-Lannerée S, Le Corre D, et al. A proof of concept for targeting the PrPC - Amyloid β peptide interaction in basal prostate cancer and

mesenchymal colon cancer. *Oncogene*. 2022;41(38):4397-4404. doi:10.1038/s41388-022-02430-7

128. McHugh PC, Wright JA, Williams RJ, Brown DR. Prion protein expression alters APP cleavage without interaction with BACE-1. *Neurochem Int*. 2012;61(5):672-680. doi:10.1016/j.neuint.2012.07.002

129. Whitehouse IJ, Brown D, Baybutt H, et al. Ablation of Prion Protein in Wild Type Human Amyloid Precursor Protein (APP) Transgenic Mice Does Not Alter The Proteolysis of APP, Levels of Amyloid-β or Pathologic Phenotype. *PLoS One*. 2016;11(7):e0159119. doi:10.1371/journal.pone.0159119

130. Whitehouse IJ, Miners JS, Glennon EBC, et al. Prion Protein Is Decreased in Alzheimer's Brain and Inversely Correlates with BACE1 Activity, Amyloid-β Levels and Braak Stage. *PLoS One*. 2013;8(4):e59554. doi:10.1371/journal.pone.0059554

131. Griffiths HH, Whitehouse IJ, Baybutt H, et al. Prion Protein Interacts with BACE1 Protein and Differentially Regulates Its Activity toward Wild Type and Swedish Mutant Amyloid Precursor Protein. *Journal of Biological Chemistry*. 2011;286(38):33489-33500. doi:10.1074/jbc.M111.278556

132. Parkin ET, Watt NT, Hussain I, et al. Cellular prion protein regulates β-secretase cleavage of the Alzheimer's amyloid precursor protein. *Proceedings of the National Academy of Sciences*. 2007;104(26):11062-11067. doi:10.1073/pnas.0609621104

133. Cissé M, Sanchez PE, Kim DH, Ho K, Yu GQ, Mucke L. Ablation of Cellular Prion Protein Does Not Ameliorate Abnormal Neural Network Activity or Cognitive Dysfunction in the J20 Line of Human Amyloid Precursor Protein Transgenic Mice. *The Journal of Neuroscience*. 2011;31(29):10427. doi:10.1523/JNEUROSCI.1459-11.2011

134. Westaway D, Jhamandas JH. The P's and Q's of cellular PrP-Aβ interactions. *Prion*. 2012;6(4):359-363. doi:10.4161/pri.20675

135. Gimbel DA, Nygaard HB, Coffey EE, et al. Memory Impairment in Transgenic Alzheimer Mice Requires Cellular Prion Protein. *The Journal of Neuroscience*. 2010;30(18):6367-6374. doi:10.1523/JNEUROSCI.0395-10.2010

136. Um JW, Nygaard HB, Heiss JK, et al. Alzheimer Amyloid-β Oligomer Bound to Post-Synaptic Prion Protein Activates Fyn to Impair Neurons. *Nat Neurosci*. 2012;15(9):1227. doi:10.1038/NN.3178

137. Younan ND, Chen KF, Rose RS, Crowther DC, Viles JH. Prion protein stabilizes amyloid-β (Aβ) oligomers and enhances Aβ neurotoxicity in a Drosophila model of Alzheimer's disease. *Journal of Biological Chemistry*. 2018;293(34):13090-13099. doi:10.1074/jbc.RA118.003319

138. Gunther EC, Smith LM, Kostylev MA, et al. Rescue of Transgenic Alzheimer's Pathophysiology by Polymeric Cellular Prion Protein Antagonists. *Cell Rep*. 2019;26(1):145-158.e8. doi:10.1016/j.celrep.2018.12.021

139. Chung E, Ji Y, Sun Y, et al. Anti-PrPC monoclonal antibody infusion as a novel treatment for cognitive deficits in an alzheimer's disease model mouse. *BMC Neurosci*. 2010;11(1):130. doi:10.1186/1471-2202-11-130

140. Oakley H, Cole SL, Logan S, et al. Intraneuronal β-Amyloid Aggregates, Neurodegeneration, and Neuron Loss in Transgenic Mice with Five Familial Alzheimer's Disease Mutations: Potential Factors in Amyloid Plaque Formation. *The Journal of Neuroscience*. 2006;26(40):10129-10140. doi:10.1523/JNEUROSCI.1202-06.2006

141. Westerman MA, Cooper-Blacketer D, Mariash A, et al. The Relationship between Aβ and Memory in the Tg2576 Mouse Model of Alzheimer's Disease. *The Journal of Neuroscience*. 2002;22(5):1858-1867. doi:10.1523/JNEUROSCI.22-05-01858.2002

142. Trinchese F, Liu S, Battaglia F, Walter S, Mathews PM, Arancio O. Progressive age-related development of Alzheimer-like pathology in APP/PS1 mice. *Ann Neurol*. 2004;55(6):801-814. doi:10.1002/ana.20101

143. Foley AM, Ammar ZM, Lee RH, Mitchell CS. Systematic Review of the Relationship between Amyloid-β Levels and Measures of Transgenic Mouse Cognitive Deficit in Alzheimer's Disease. *Journal of Alzheimer's Disease*. 2015;44(3):787-795. doi:10.3233/JAD-142208

144. Hardy J, Selkoe DJ. The Amyloid Hypothesis of Alzheimer's Disease: Progress and Problems on the Road to Therapeutics. *Science (1979)*. 2002;297(5580):353-356. doi:10.1126/science.1072994

145. Bloom GS. Amyloid-β and Tau: The Trigger and Bullet in Alzheimer Disease Pathogenesis. *JAMA Neurol*. 2014;71(4):505-508. doi:10.1001/JAMANEUROL.2013.5847

146. Schröder H, Moser N, Huggenberger S. The Mouse Olfactory System. In: *Neuroanatomy of the Mouse*. Springer International Publishing; 2020:319-331. doi:10.1007/978-3-030-19898-5_14

147. Schröder H, Moser N, Huggenberger S. The Mouse Hippocampus. In: *Neuroanatomy of the Mouse*. Springer International Publishing; 2020:267-288. doi:10.1007/978-3-030-19898-5_11

148. Schröder H, Moser N, Huggenberger S. The Mouse Hypothalamus. In: *Neuroanatomy of the Mouse*. Springer International Publishing; 2020:205-230. doi:10.1007/978-3-030-19898-5_9

149. Schröder H, Moser N, Huggenberger S. The Mouse Thalamus. In: *Neuroanatomy of the Mouse*. Springer International Publishing; 2020:171-203. doi:10.1007/978-3-030-19898-5_8

150. Schröder H, Moser N, Huggenberger S. The Mouse Cerebral Cortex. In: *Neuroanatomy of the Mouse*. Springer International Publishing; 2020:231-265. doi:10.1007/978-3-030-19898-5_10

151. Schwarze-Eicker K, Keyvani K, Görtz N, Westaway D, Sachser N, Paulus W. Prion protein (PrPc) promotes β-amyloid plaque formation. *Neurobiol Aging*. 2005;26(8):1177-1182. doi:10.1016/j.neurobiolaging.2004.10.004

152. Qin K, Zhao L, Gregory C, Solanki A, Mastrianni JA. "Dual Disease" TgAD/GSS mice exhibit enhanced Alzheimer's disease pathology and reveal PrPC-dependent secretion of Aβ. *Sci Rep*. 2019;9(1):8524. doi:10.1038/s41598-019-44317-w

153. Harmey JH, Doyle D, Brown V, Rogers MS. The cellular isoform of the prion protein, PrPc, is associated with caveolae in mouse neuroblastoma (N2a) cells.

Biochem Biophys Res Commun. 1995;210(3):753-759. doi:10.1006/BBRC.1995.1723

154. Mouillet-Richard S, Ermonval M, Chebassier C, et al. Signal Transduction Through Prion Protein. *Science (1979)*. 2000;289(5486):1925-1928. doi:10.1126/science.289.5486.1925

155. Gaudreault SB, Dea D, Poirier J. Increased caveolin-1 expression in Alzheimer's disease brain. *Neurobiol Aging*. 2004;25(6):753-759. doi:10.1016/J.NEUROBIOLAGING.2003.07.004

156. Shi Q, Jing YY, Wang SB, et al. PrP octarepeats region determined the interaction with caveolin-1 and phosphorylation of caveolin-1 and Fyn. *Med Microbiol Immunol*. 2013;202(3):215-227. doi:10.1007/s00430-012-0284-8

157. Ikezu T, Trapp BD, Song KS, Schlegel A, Lisanti MP, Okamoto T. Caveolae, plasma membrane microdomains for alpha-secretase-mediated processing of the amyloid precursor protein. *J Biol Chem*. 1998;273(17):10485-10495. doi:10.1074/JBC.273.17.10485

158. Ikezu T, Trapp BD, Song KS, Schlegel A, Lisanti MP, Okamoto T. Caveolae, plasma membrane microdomains for alpha-secretase-mediated processing of the amyloid precursor protein. *J Biol Chem*. 1998;273(17):10485-10495. doi:10.1074/JBC.273.17.10485

159. Peters PJ, Mironov A, Peretz D, et al. Trafficking of prion proteins through a caveolae-mediated endosomal pathway. *J Cell Biol*. 2003;162(4):703-717. doi:10.1083/JCB.200304140

160. Toni M, Spisni E, Griffoni C, et al. Cellular prion protein and caveolin-1 interaction in a neuronal cell line precedes Fyn/Erk 1/2 signal transduction. *J Biomed Biotechnol*. 2006;2006(5). doi:10.1155/JBB/2006/69469

161. Larson M, Sherman MA, Amar F, et al. The Complex PrP ^{c} -Fyn Couples Human Oligomeric Aβ with Pathological Tau Changes in Alzheimer's Disease. *The Journal of Neuroscience*. 2012;32(47):16857-16871. doi:10.1523/JNEUROSCI.1858-12.2012

IX. Acknowledgments

I would to express my heartfelt gratitude to the following individuals, whose contributions have been pivotal in both academic journey and personal life:

I am deeply thankful to Prof. Dr. Inga Zerr, for her support throughout my academic journey as my group leader and supervisor. Her expertise and mentorship have been instrumental in shaping my research and career.

I would like to extend my sincere appreciation to PD. Dr. Matthias Schmitz, whose contributions to my academic and personal growth go beyond the role of a project supervisor. His valuable insights, support and friendship have added a unique dimension to my academic pursuits.

To my sister and esteemed colleague, Dr. Susana da Silva Correia, I am grateful for your constant support and partnership. Your presence has been instrumental in helping me navigating the challenges of both academia and life.

To my dear colleagues, Anna-Lisa Fischer, Sezgi Canaslan, and Tayyaba Saleem, I want to thank you for your camaraderie, collaboration, and friendship. Your contributions and camaraderie have made the research environment vibrant and fulfilling.

Last but certainly not least, I want to express my deep appreciation to my family, my mother Madalena, my daughter Ariana and, my uncle João and friends for the encouragement and love that have been pillars of my personal and academic life. Your support has been immeasurable, and I am profoundly grateful for each one of you.